NUCLEAR ACTIVATION STUDIES IN FUSION SYSTEMS: NEW METHODS AND ALGORITHMS

By

PRITI KANTH

ENGG06201504009

Institute for Plasma Research, Gandhinagar

A thesis submitted to the

Board of Studies in Engineering Sciences

In partial fulfillment of requirements

For the Degree of

DOCTOR OF PHILOSOPHY

of

HOMI BHABHA NATIONAL INSTITUTE

February, 2020

Homi Bhabha National Institute

Recommendations of the Viva Voce Board

As members of the Viva Voce Board, we certify that we have read the dissertation prepared by **Priti Kanth** entitled **"Nuclear Activation Studies in Fusion Systems: New Methods and Algorithms"** and recommend that it may be accepted as fulfilling the dissertation requirement for the Degree of Doctor of Philosophy.

Date: 4/9/2020

Chair - Prof Shishir Deshpande

Date: 31/8/2020

Guide/Convener - Dr. P.V. Subhash

Date: 3/9/2020

Co-guide - Dr. R. Srinivasan

Amitava Gupta

Date: 31st August 2020

External Examiner - Prof. Dr. Amitava Gupta

Date: 31/8/2020

Member 1 - Dr. Vinay Kumar

Date: 3/9/2020

Member 2 - Dr. Mainak Bandyopadhyay

Final approval and acceptance of this dissertation is contingent upon the candidate's submission of the final copies of the dissertation to HBNI.

I hereby certify that I have read this dissertation prepared under my direction and recommend that it may be accepted as fulfilling the dissertation requirement.

Date: 08/09/20

Place: Gandhinagar

Dr. R. Srinivasan
Co-Guide

Dr. P.V. Subhash
Guide

CERTIFICATION ON ACADEMIC INTEGRITY

1. I Priti Kanth HBNI Enrolment No. ENGG06201504009 hereby undertake that, the Thesis titled "***Nuclear Activation Studies in Fusion Systems: New Methods and Algorithms***" is prepared by me and is the original work undertaken by me and free of any plagiarism. That the document has been duly checked through a plagiarism detection tool and the document is plagiarism free.

2. I am aware and undertake that if plagiarism is detected in my thesis at any stage in future, suitable penatlty will be imposed as per the applicable guidelines of the Institute/UGC.

Priti Kanth

Signature of Student

Endorsed by the thesis Supervisor:
(I certify that the work done by the Researcher is plagiarism free)

Signature

Name: Dr. P.V. Subhash
Designation: Scientific Officer- F
Department/Centre: Diagnostics Group, Iter-India
Name of CI/OCC: Institute for Plasma Research, Gandhinagar

STATEMENT BY AUTHOR

This dissertation has been submitted in partial fulfillment of requirements for an advanced degree at Homi Bhabha National Institute (HBNI) and is deposited in the Library to be made available to borrowers under rules of the HBNI.

Brief quotations from this dissertation are allowable without special permission, provided that accurate acknowledgment of source is made. Requests for permission for extended quotation from or reproduction of this manuscript in whole or in part may be granted by the Competent Authority of HBNI when in his or her judgment the proposed use of the material is in the interests of scholarship. In all other instances, however, permission must be obtained from the author.

Priti Kanth

Priti Kanth

DECLARATION

I, hereby declare that the investigation presented in the thesis has been carried out by me. The work is original and has not been submitted earlier as a whole or in part for a degree / diploma at this or any other Institution / University.

Priti Kanth

List of Publications arising from the thesis

Journal

1. Priti Kanth, Sai Chaitanya Tadepalli, P.V. Subhash, Composition Optimization Strategy Based on Multiple Radiological Responses for Materials in Spatially and Temporally Varying Neutron Fields, *Nuclear Fusion, 58(12):126019, 2018.*

2. Priti Kanth, P. Subhash, ACTYS-ASG, tool for coupling ACTYS-1-GO with ATTILA, *Fusion Engineering and Design, 129:196-201, 2018.*

3. Priti Kanth, S. C. Tadepalli, R. Srinivasan, P. V. Subhash, ACTYS-1-GO: Faster and accurate algorithm for multipoint nuclear activation calculation, *Fusion Engineering and Design, 122:154 - 162, 2017.*

4. S. C. Tadepalli, Priti Kanth, and P.V. Subhash, Parent Isotopic and Elemental Contributing Factors to Minimize Nuclear Radiological Responses and Optimize Material Composition, *Nuclear Science and Engineering, 188(03):282 - 293,2017.*

5. S. C. Tadepalli, Priti Kanth, G. Indauliya, S. P. Deshpande, P.V. Subhash, Development and Validation of ACTYS, an Activation Analysis code, *Annals of Nuclear Energy, 107C:71-81, 2017.*

6. P.V. Subhash, G. Indauliya, T. S. Chaitanya, Priti Kanth, S. Jakhar, Sanjeev Varshney, Siddharth Kumar, K. Raja Krishna, Nirav Bhaliya, Sapna Mishra, P. Shrishail and Vinay Kumar, Activation and Radwaste Analysis for Survey X-Ray Crystal Spectrometer of ITER, *Fusion Science and Technology, 71(2):215-224, 2017.*

Conferences

1. Priti Kanth, P.V. Subhash,"Nuclear Activation Code Development for Fusion Systems", *22nd National Symposium on Radiation Physics, held at Delhi, India on November 8-10, 2019*
2. Priti Kanth, T.S. Chaitanya, P.V. Subhash,"A Multi-Parameter Optimization technique considering temporal and spatial variation in nuclear response of materials in Fusion devices", *27th IAEA Fusion Energy Conference, held at Gandhinagar, India on 22-28 October 2018*
3. Priti Kanth, T.S. Chaitanya, P.V. Subhash, "Material optimization technique to minimize radiological responses in fusion reactors", *30th Symposium on Fusion Technology (SOFT-2018), held at Giardini Naxos on 16-21 September 2018.*
4. Priti Kanth, Sai Chaitanya Tadepalli, P.V. Subhash, Visualization Technique for Nuclear Materials using ACTYS, *Proceedings of the DAE Symposium on Nuclear Physics 62 (2017)*
5. Priti Kanth, T.S. Chaitanya, R. Srinivasan, P.V. Subhash, Development and Validation of ACTYS-1-GO: A Multipoint Nuclear Activation Code, *26th International Toki Conference (ITC-26) and the 11th Asia Plasma and Fusion Association Conference (APFA) was hosted by at NIFS, Gifu, Japan, (2017)*
6. Priti Kanth, T.S. Chaitanya, R. Srinivasan, P.V. Subhash, Development and Validation of Multipoint Analysis Code ACTYS-1-GO and Coupling with ATTILA, *The 32nd National Symposium on Plasma Science and Technology was hosted by Institute for Plasma Research, Gandhinagar, India, 2017*
7. Priti Kanth, T.S. Chaitanya, R. Srinivasan, P.V. Subhash, Development of Multipoint Nuclear Activation Code for Fusion Devices, *International Conference on High Energy Radiation and Applications, held at Baroda, India, 2017*

Priti Kanth

Priti Kanth

ACKNOWLEDGMENTS

I express my sincere gratitude towards Dr. P.V. Subhash, for his constant support, encouragement, invaluable guidance and for our countless hours of discussions and brainstorming sessions. I am very thankful to my doctoral committee members Prof Shishir Deshpande, Dr. Mainak Bandyopadhyay, Dr. Vinay Kumar and Dr. R. Srinivasan for their continuous encouragement, constructive suggestions, and advice. I would like to thank Prof. Sudip and Prof. S. Mukherjee for their friendly support and advice in academic affairs.

I am thankful to my dear friends Arun, Mayank, Arnab, Neeraj, Piyush, Garima, Srimaonto for their care and support throughout my stay in the hostel. I will always cherish our long, sometimes pointless, discussions at 2 in the mornings. I am also thankful to my seniors and postdoctoral fellow for their invaluable advice and discussions. I thank my family for their constant love, support, strength, and patience.

Contents

List of Figures

List of Tables

Chapter 7

Conclusion and Future works

As discussed in section 1.1.3, activation due to fusion neutrons is one of the major obstacles in the design and construction of fusion reactors. The present work aims at addressing some of the issues that will be faced by fusion materials and tries to solve them. This thesis aims at developing various methods to simulate neutron-induced activation more accurately, to develop a scheme for direct assessment of neutron-induced damage in fusion materials and methodology to create low activation materials.

In this thesis various methods are developed to 1) read standard decay data library, 2) evaluate contact dose rate, decay heat, gamma spectrum, multi-channel pathways and radwaste classification, 3) to efficiently perform multi-point activation calculation for fusion reactor like geometry, 4) couple transport and activation code for evaluation of shutdown dose rate, 5) visualize enormous data produced during the activation calculation in an easily understandable format, 6) optimize material composition based of multiple parameters to produce a low activation material suitable for fusion environment and, 7) develop diagrams based on optimization scheme for a better design analysis. ACTYS-1-GO with all its modules is a complete code for simultaneously simulating neutron activation for a fusion device. It can directly read the neutron spectrum from neutron transport codes, evaluate fast multipoint activation, generate source file for photon transport, generate

pathways and various visualization techniques for analysis of radiation damage, evaluate contribution factor of each element/isotope towards any radiological quantity and suggest a composition for achieving low activation in fusion materials.

There are many capabilities still lacking in the code, which can be added in the future. Following are some of the future scope:

- **Addition of uncertainty**

  ACTYS-1-GO currently does not have a functional subroutine to evaluate the uncertainty in the quantities due to the uncertainty in the nuclear data available. A method has been developed for uncertainty assessment in the linear chain method and is given in the article [109]. This work could be implemented in ACTYS-1-GO and such an addition would enhance the acceptability of the code on the global platform.

- **Addition of PKA spectra in ACTYS-1-GO**

  Neutron also damages the material by scattering the lattice atoms in the material. PKA or the primary knock-out atoms are generated in the material after the atoms had direct interaction with neutron and underwent a scattering or nuclear reaction. These PKA travel in the material further displacing other atoms from their lattice position, which results in structural damage to the material. This is an important quantity that can be added to ACTYS-1-GO for a complete assessment of neutron-material interaction.

- **Extending the optimization scheme to include thermo-mechanical properties of the material**

  As discussed above, structural damage to the material is caused by PKA generated from neutron-matter interaction. The ECF optimization scheme developed during the thesis can be extended to include damage due to the PKA generated in the material by defining appropriate response functions. This would quantify the damage induced by PKA in the material in terms of initial material composition and neutron

energy. Such a scheme could be used to construct realistic low activation materials.

- **Addition of Fission cross-section and fission yield**

  At present, ACTYS and ACTYS-1-GO can perform activation calculation for fusion materials, which means that they do not perform calculations for multiplying medium (where neutrons are produced in the material during the activation process). ACTYS and ACTYS-1-GO can be extended to include fission cross-section and fission yield to make them suitable for fission core calculations.

SUMMARY

Neutrons interact with material and lead to changes in the elemental composition (transmutation), production of ionizing radiation and generation of defects. The structural and the functional materials in the fusion reactors interact with the neutrons produced from the fusion reaction. The isotopes present in these materials may undergo transmutation and subsequent radioactive decay. This process is known as activation. To evaluate nuclear activation in fusion devices, the modified Bateman equation is solved at each location using the initial material composition, incident neutron spectrum, irradiation scenario, and nuclear data, to obtain the final isotopic inventory in the material. Using final isotopic inventory and radiation decay data as input, radiological quantities like activity, decay heat, gamma dose rate, etc can be evaluated. In this thesis, various methods and tools are developed to evaluate activation in materials placed in a fusion reactor like device. Summary of the work carried out is given below:

1. Various techniques and methods are developed to evaluate radiological quantities like biological dose rate, gamma spectrum, decay heat, multi-channel pathways, and ANDRA radwaste classification. These methods consist of reading the raw data from nuclear data libraries, processing the data in a readable format and developing efficient algorithms for evaluation of these quantities. These are then implemented in the activation code ACTYS. An extensive validation for these methods and ACTYS is performed using standard benchmarking problems including benchmark problems given by the International Atomic Energy Agency (IAEA).

2. Fusion reactors are big devices with large spatial variations of the neutron spectrum. Hence to evaluate activation on the entire reactor/device, the concept of Superlist is developed. This formulation captures the essence of an entire material placed at multiple locations and experiencing different neutron spectrum into a small set of isotopes called the superlist. It is defined uniquely for each material, irradiation scenario and the set of neutron spectrum incident of it. Activation calculation performed on this list alone yields radiological quantities with 99% accuracy in just 1.5% computation time as compared to other conventional methods. This concept of superlist is implemented in code ACTYS-1-GO. Successful benchmarking of the above formulation is performed using standard benchmarking exercises given by IAEA and with the ITER radial buildup model.
3. Shutdown Dose Rate (SDDR) produced by decay gamma emitted from activated materials is evaluated using the Rigorous 2 Step (R2S) Method. In this method, one to one coupling of neutron transport code with activation code is required. A coupler has been developed to perform intermediate activation calculations for the evaluation of SDDR under the R2S scheme. Such a coupler is very useful at a domestic scale as some commercial activation codes do not provide (or provide limited) source code and the nuclear data libraries for activation calculation.
4. Activation may lead to prolonged radioactivity or may cause mechanical failure of materials in fusion devices. All of these may lead to radiation leakage from the material and thus, low activation materials are pre-requisite for fusion reactor development. No tools were available in the literature to directly evaluate the best material composition based on radiological quantities obtained from the activation calculation. Hence, the composition optimization scheme for materials is developed. This formulation evaluates the best composition for a material placed in a spatially and temporally varying neutron field and will have a lower activation. This method requires an upper and lower limit for each element in the material to obtain a realistic material composition. This optimization scheme is also added to ACTYS-1-GO.

Chapter 1

Introduction

Energy production is one of the major concerns for the world today [1, 2]. The U.S. Energy Information Administration (EIA) projects that world energy consumption will grow by nearly 50% between 2018 and 2050 [3]. To cope with the increasing demand created by the increasing population and increasing living standards, a steady source of energy is required. Furthermore, for this source to be sustainable, it should have a minimum carbon footprint on the environment [4]. Renewable energy like solar, wind and geothermal are promising sources of energy. Despite the fact renewable energy has several advantages like unlimited fuel source and lower maintenance requirements; these sources of energy have a higher upfront cost, inefficient energy conversion ratio and most importantly many of these sources are not a steady source of energy year-round. This creates a demand for research in the development of new kinds of energy sources. Hence keeping all factors into account, the most promising energy source satisfying the all above criteria are nuclear reactors, Fission and Fusion [5]. Fission reactors are currently used as a base source of energy in many countries. However, fission reactors have two major disadvantages, 1) limited availability of the fuel, which is the fissile isotope of Uranium ($^{235}_{92}$U) and 2) production of long-lived actinides in the depleted fuel rods [6]. In India, uranium ores are scarcely available. Thus sustaining a fission reactor from imported fuel has limited

capabilities. This scarcity of fission fuels demands that more money and resources are invested in a new branch of nuclear reactors i.e. fusion reactors [7, 8, 9]. Fusion reactors utilize heavy isotopes of Hydrogen isotopes as fuel, which are very abundant in nature or can be bred from abundant elements. Thus, fusion reactors create scope for a clean energy source which is not limited to a great extent on the availability of fuel and thus could be a path towards self-sustainability [10, 11].

Fusion reactors are green sources of energy i.e. they do not produce carbon dioxide as a bi-product, but these reactors are not neutron free [12, 10]. Neutrons produced within the fusion reactor core travel throughout the device interacting with the material in two ways:

1. The materials absorb the incident neutron and undergo transmutation which is the production of new isotopes via nuclear reaction. This changes the elemental composition of the material significantly and also creates radioactive isotopes [13, 14]. The production of radioactive isotopes via transmutation or radioactive decay is known as Activation. These radioactive isotopes emit ionizing radiation leading to radio-toxicity in the material. Thus, the nuclear activation study of structural material in a fusion device is very crucial from an operation, maintenance and safety point of view [15, 16, 17].

2. Incident neutrons scatter off the atoms in the material, producing energetic knock out atoms, which further causes atomic displacements within the materials. This leads to the generation and accumulation of lattice defects, which cause hardening, embrittlement, and irradiation creep, etc [14, 18, 19]. Gaseous (like H and He) transmutants accumulate in these sites causing swelling in the material, which leads to further degradation.

Therefore, it is essential to accurately determine the amount and composition of solid and gaseous transmutants created in the fusion nuclear environment and the corresponding radiological quantities produced by them. This kind of rigorous nuclear activation

calculation can only be achieved by the use of efficient activation codes [20, 21]. These codes simulate neutron-induced reaction and radioactive decay occurring in the materials, placed in a neutron environment. This is the motivation for the present Ph.D. work. A more detailed introduction to neutron interaction with the material, neutron-induced activation, the need for developments of nuclear activation codes for designing fusion reactors, and motivation are given in this chapter.

Section 1.1 gives a brief introduction to basic nuclear physics, fusion reactions and activation in the fusion reactors. In section: 1.2, neutron transport in the reactor is discussed along with various methods that are used to simulate it. Section 1.3, gives details neutron activation, various parameters to describe it and a brief description of the existing codes that are used to calculate neutron activation in the material. Finally, section: 1.4, gives the motivation for current work and section: 1.5 describes the chapter wise thesis structure.

1.1 Nuclear physics to Fusion neutronics

A brief introduction to basic nuclear physics and various aspects of fusion reactors are given in this section. This lays down the requirement of neutron transport and activation codes for fusion reactors. The study of neutron interaction with materials and subsequent production of radioactive isotopes is crucial to understand the effects of radiation on the machinery and living organisms, and material degradation during and after neutron irradiation.

1.1.1 Binding Energy

In an atom, neutrons and protons exist in a bound state held together by the residual strong force also known as nuclear force, and are collectively referred to as ‘nucleons’. Since some energy is required to bring the constituent nucleons together to overcome the

coulomb barrier and form an atomic nucleus, the nucleus exists in a negative energy state as shown in the figure: 1.1a. This also implies that the mass of an atomic nucleus is less than the sum of the masses of its constituent's nucleons. This difference in mass between the atomic nucleus and its constituents is referred to as mass defect and is given by:

$$\Delta = [Zm_p + (A-Z)m_n] - m(A,Z) \tag{1.1}$$

Where Z is the atomic number (number of protons), A is the mass number (number of nucleons), Δ is the mass defect (amu), m_p is the mass of a proton (1.007277 amu) m_n is the mass of a neutron (1.008665 amu) and m(A,Z) is the mass of nuclide ${}^{A}_{Z}X$ (amu). The energy required to disassemble the atomic nuclei into separate particles is known as the binding energy of the nucleus and is given by, $BE = \Delta c^2$, in accordance with Einstein's equation, $E = m*C^2$ [22, 23]. The binding energy is often expressed as binding energy per

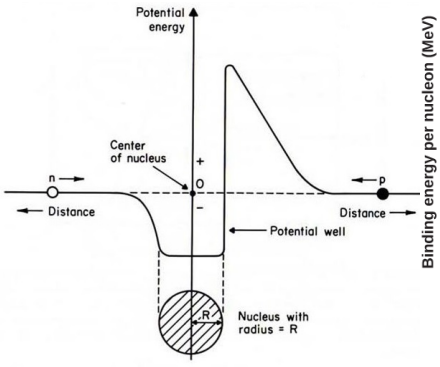

(a) The shape of Potential well, as predicted by Shell Model

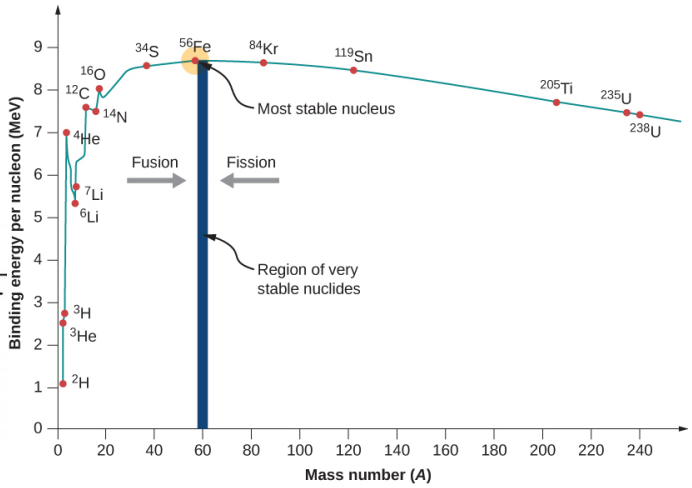

(b) BE/A for different isotopes

nucleon (BE/A), and BE/A as a function of atomic number is shown in the figure: 1.1b. From figure 1.1b, it can be concluded that the BE/A increases with the increase in atomic mass of the nucleus and reaches a maximum for iron and nickel and then decreases again. Since some atomic nucleus has more binding energy per nucleon than others, any process that would result in nuclides being converted into nuclides with more binding energy per nucleon would release energy. Two such processes that can harness this nuclear energy are

Fission and Fusion reactions. Fusion reactions occur when two nuclides with low atomic mass combine to form a nuclide with higher atomic mass. And fission is the process of splitting of nuclides with very high atomic mass to form nuclides of intermediate atomic mass.

1.1.2 Fusion Reaction

During the fusion reaction, nuclei of the low atomic mass combine to form nuclei of higher atomic mass thus increasing the BE/A. The energy released through fusion reactions is the most abundant form of energy in the universe, as all the stars produce energy through it. The atomic nucleus is positively charged and has a natural tendency to repel each other, known as Coulomb repulsion, as seen in figure: 1.1a. For a fusion reaction to occur these nuclei must overcome the Coulomb barrier. Therefore, a certain amount of energy is necessary to felicitate the fusion reaction. The probability of crossing the coulomb barrier for any atomic nuclei is quantified by the 'cross-section' of the reaction, the fusion cross-section for various reactions is given in the table: 1.1.

Reaction	σ at 10 keV (barn)	σ_{max} (barn)	Center-of-mass energy (keV) for σ_{max}	Energy released (Mev)
$D+T \rightarrow {}^4\text{He}+n$	2.72 X 10^{-2}	5.0	64	17.59
$D+D \rightarrow T+p$	2.81 X 10^{-4}	0.096	1250	4.04
$D+D \rightarrow {}^3\text{He}+n$	2.78 X 10^{-4}	0.11	1750	3.27
$T+T \rightarrow {}^4\text{He}+2n$	7.90 X 10^{-4}	0.16	1000	11.33
$D+{}^3\text{He} \rightarrow {}^4\text{He}+p$	2.2 X 10^{-7}	0.9	250	18.35
$p+{}^6\text{Li} \rightarrow {}^4\text{He}+{}^3\text{He}$	6.0 X 10^{-10}	0.22	1500	4.02
$p+{}^{11}\text{B} \rightarrow 3{}^4\text{He}$	4.60 X 10^{-17}	1.2	550	8.68
$p+p \rightarrow D+e^+ + \nu$	3.60 X 10^{-26}	-	-	1.44 + 0.27(ν)
$p+{}^{12}\text{C} \rightarrow {}^{13}\text{N}+\gamma$	1.90 X 10^{-26}	1.0 X 10^{-4}	400	1.94

Table 1.1: Fusion reactions with cross-sections and other parameters

The variation of the effective cross-section of various fusion reactions as a function of center-of-mass energy is provided for light elements in the figure: 1.2.

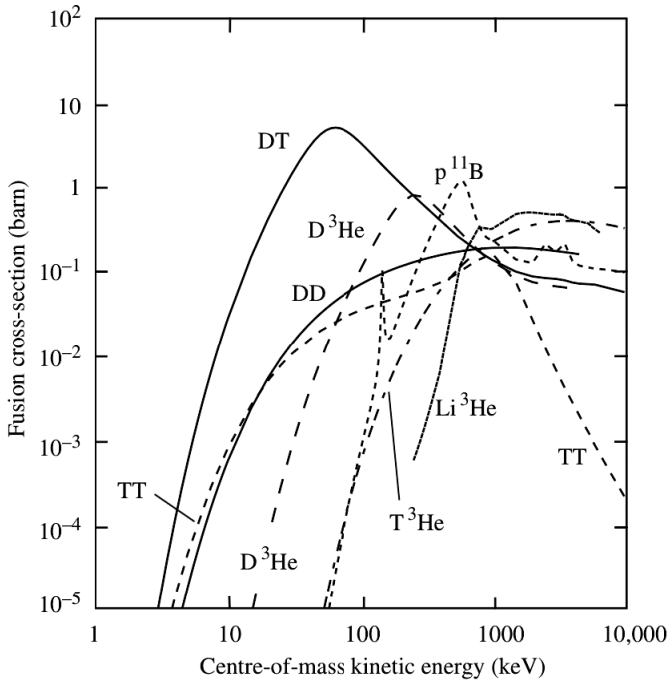

Figure 1.2: Variation of fusion cross-sections for various light elements

The following conclusions can be drawn from the above figure:

1. The fusion reaction cross-sections are of the order of 1 barn (1 barn $= 10^{-28}\ m^2$) which is very less compared with the fission reaction of $^{235}_{92}$U by a thermal neutron(of the order of 600 barns) or in comparison with ionization and Coulomb scattering. This is one of the major difficulties in the production of fusion energy.

2. Fusion reactions have significant cross-sections at temperatures of 100 million degrees(10 keV) or higher. At such temperatures, the matter exists in the plasma state. Plasma is a hot ionized gaseous state consisting of equal numbers of positively charged ions and negatively charged electrons exhibiting collective behavior. Hence to achieve fusion, various mechanisms are utilized to create and heat the plasma to temperatures high enough for the fusion reaction to occur.

3. D-T fusion reaction is the most accessible and hence is the focus of research for the development of controlled fusion reactors. In terms of fuel availability, deuterium is present in abundance in the sea waster whereas tritium exists in only trace amounts.

Therefore, tritium needs to be produced (bred) inside the fusion reactor through neutron-induced reactions in Lithium (Li)[24]. For this reaction, natural stable Li is considered which contains 7.5% ^{6}Li and 92.5% ^{7}Li. The breeding reactions are

$$\begin{aligned} n + {}^6\text{Li} &\rightarrow T + {}^4\text{He} + 4.8MeV \\ n + {}^7\text{Li} &\rightarrow T + {}^4\text{He} + n^* - 2.5MeV \end{aligned} \tag{1.2}$$

In the sun or the stars, the conditions for thermonuclear fusion are obtained by gravity which however is impossible to implement on earth. Hence, to attain fusion on earth various methods like Inertial Confinement [25], magnetic confinement [12], beam-target interaction, beam-beam interaction, etc are utilized. Tokamak and Stellarator are designed to achieve magnetic confinement for plasma and felicitate fusion reaction [26, 27, 28, 29]. In a tokamak, magnetic confinement is achieved by combining the 'poloidal' magnetic field and the 'toroidal' magnetic field to generate helicoidal field lines.

1.1.3 Fusion Reactors

A tokamak is a torus-shaped device that uses a powerful magnetic field to confine a plasma, as given in figure 1.3. Currently, these are the leading candidate for achieving a fusion reaction on a large scale. At present, Tokamaks are in the experimental phase including ITER and will be followed by a demonstration (DEMO) power plants and then commercial fusion power plants. A brief description of the plasma parameter required for ITER and DEMO machines is given below.

ITER

ITER, meaning "the way" in Latin, is a major international experiment with the aim of demonstrating the scientific and technical feasibility of fusion as an energy source. It is jointly built in Cadarache, France by China, the European Union, India, Japan, Korea,

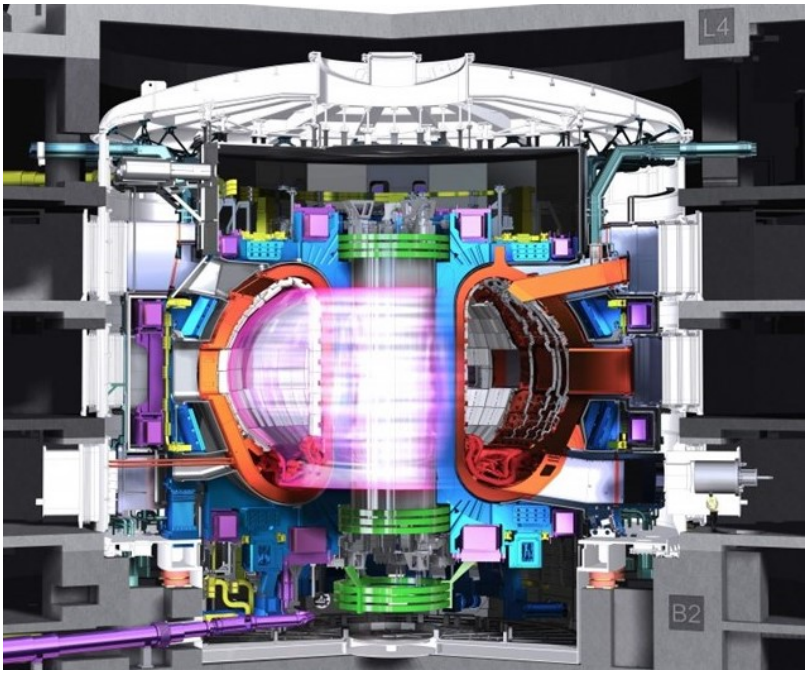

Figure 1.3: Cross-sectional view of ITER tokamak

Russia, and the United States. It is proposed to contain a $50/50$ gaseous mix of deuterium and tritium and will heat this mixture to temperatures of the order of 150 million °C [28]. Intense magnetic fields produced by an array of giant superconducting coils and a strong electrical current will shape and confine the D-T plasma, keeping it away from the vessel walls. ITER is designed to test the following key technologies for future fusion power plants at the reactor scale [30]:

1. Achieve fusion power of 500 MW with $P_{fus}/P_{in}(\equiv Q) \geq 10$ for $300-500$ s (i.e., stationary conditions).
2. To study the possibility of controlled ignition.
3. To demonstrate steady-state operation through the current drive at $Q > 5$.
4. Demonstrate the availability and integration of essential fusion technologies.
5. Test components for a future reactor.
6. Test tritium breeding module concepts, with a 14 MeV average neutron power load on the first wall greater than 0.5 MW/m^2 and an average neutron fluence greater than 0.3 MW/m^2.

DEMO

After ITER, the construction of prototype reactors, currently termed DEMO, is planned to demonstrate the technological and economic feasibility of fusion reactors. Different conceptual DEMO projects are under consideration in many countries. The aims of the DEMO studies are i) to quantify key physics and technology prerequisites for fusion reactors; ii) to identify the most urgent technical issues that need to be solved in physics and technology and iii) to plan and implement supporting physics and technology R&D.

The basic design characteristics of a DEMO reactor are [31]:

1. DEMO will be a prototype reactor with more than $500MW_e$ output and would be coupled with the turbine system to generate electricity. It will be also be integrated with the power grid.
2. It will operate with long pulses, high duty cycle or steady-state plasma for better efficiency in achieving fusion.
3. DEMO will contain a minimum set of diagnostics contrary to ITER. It will have diagnostics only needed for the operations of the plant.
4. Once proper coupling of heating and current drive is achieved in ITER plasma. The DEMO reactors will have a reduced set of Heating and Current Drive systems.
5. For self-sufficiency, the T breeding ratio would be > 1 in DEMO reactors.
6. Due to the high rate of fusion reactions occurring in DEMO, there will be a high neutron fluence and consequentially high radiation damage induced by the neutrons.
7. Due to the high neutron fluence, reduced activation materials would be required for the construction of structural material in the DEMO reactors.

Hence for construction and viability of DEMO reactors following research topics that need to be further developed [32]:

1. achieving plasma stability and confinement for long periods of operation
2. heating systems capable of heating the large plasma

3. tritium breeding modules to achieve tritium self-sufficiency
4. new materials that will be compatible with the high heat and neutron loads [14]
5. a material research facility to study the behavior of various candidate materials under a flux of 14.1 MeV neutrons [33].
6. diagnostic systems that can sustain the heavy neutron loading

It can be seen that two of the major challenges in the realization of commercial fusion reactors are the nuclear analysis of material in the fusion environment (referred to as fusion material in the thesis) and designing of new material with low activation properties [17, 19, 33, 34]. This makes nuclear analysis and development of low activation materials very crucial for the commercial and economic feasibility of the fusion reactors and are the main problems that are addressed through this Ph.D. thesis.

1.1.4 Fusion Neutronics

Fusion neutronics is the study of neutron interaction with matter and subsequent activation, and their impacts on structural and functional materials along with the personnel, the public and the environment in and around any fusion device. It provides various design parameters for the components of fusion devices and their operational life-time. Thus ensuring that the design of fusion devices abide by all necessary safety requirements imposed by governing agencies and provide reliable, sustainable and economic performance.

The neutrons are electrically neutral, thus, the 14.1 MeV neutrons produced by D-T fusion reaction will not be confined by the magnetic fields of the tokamak and would travel throughout the reactor interacting with the structural materials present in and around the reactor. The material upon interacting with neutron may undergo transmutation and could produce radioactive isotopes. The radioisotopes produced via transmutation could emit ionizing radiation. Hence, stringent regulations are implemented on the fusion materials to minimize the damaging effects of neutron irradiation [13, 35, 36, 37]. Thus, the nu-

clear activation study of structural material in a fusion device thus becomes very crucial from an operation, maintenance and safety point of view [15, 16]. Thus commissioning of any nuclear device relies on an intricate nuclear activation calculation and analysis of the entire device and its components [38, 39]. This rigorous nuclear analysis is carried out by efficient computer codes. These codes simulate neutron transport, neutron-induced reaction and radioactive decay occurring in the materials, placed in a neutron environment. Simulation of neutron transport and activation in a single program is very difficult. Hence different codes are written for evaluating energy distribution of neutrons (neutron spectrum) after interacting with materials in a fusion device, and for evaluating change in material composition after undergoing neutron-induced reaction and radioactive decay.

1.2 Neutron transport in the matter

Neutron transport in materials implies the motion of neutron in the material and its interaction with the isotopes present in them using scattering cross-sections from standard nuclear data libraries. Neutron transport simulations are necessary to estimate the energy spectrum of neutrons traversing trough the materials and the energy loss in the materials. These parameters determine the energy distribution of the emerging neutrons which will then be used by activation codes to simulate neutron-induced reactions and radioactive decay. The different mechanism of neutron interaction with materials is given in section 1.2.1, various modes of radioactive decay are given in section 1.2.2 and codes for simulating fusion neutron transport is given in section 1.2.3.

1.2.1 Interaction of neutron with matter

Since neutrons are neutral particles, their flight is unaffected by the electron cloud surrounding the atoms or the electric field caused by a positively charged nucleus. This implies that neutrons can travel in the matter following straight lines until they eventually

collide with a nucleus. The probability of occurrence of such an event is characterized by the nuclear reaction cross-section. Reaction cross-section is broadly expressed in into two ways:

1. **Microscopic** cross-section represents the effective target area of a single target nucleus as seen by an incident neutron beam. It is represented by σ and is measured in units of barn, which is equal to $10^{-28}\ m^2$
2. **Macroscopic** cross-section represents the total "equivalent area" of all target particles per unit volume as seen by an incident neutron beam. The macroscopic cross-section is represented by $\Sigma = n\sigma$, where n is the atomic density of the target and is measured in units of m^{-1}.

The nuclear reaction cross-section for the incident neutron and the target nucleus is a function of incident neutron energy and temperature of the target nuclei. Resonance peaks in the cross-section are observed for incident neutron with energy between 1 eV and 1 MeV and target nuclei of high or medium-mass. Since the neutron cross-sections also depend on the relative velocity between neutron and nucleus, these resonance peaks may broaden with increasing temperature of the reactants. This effect is called Doppler broadening.

Neutrons interact with target nuclei via nuclear forces. Depending upon the type of interaction, nuclear reactions are classified into two broad categories:

Neutron Scattering Reactions

In these kinds of reactions, the incident neutron scatters off a nuclear potential without penetrating the nucleus itself. In such reactions, the difference in energy between the incidents and outgoing neutrons becomes the internal or kinetic energy of the target nucleus. This reaction does not lead to transmutation or change of nuclear species. Depending upon the energy of the outgoing neutrons, neutron scattering reactions are divided into two types:

1. **Elastic Scattering (n,n)** In this kind of reaction both the total kinetic energy and the total momentum of the neutron-nucleus system are conserved in the center-of-mass frame, but its direction of propagation is modified. This implies that no energy is transferred into nuclear excitation.
2. **Inelastic Scattering (n,n')** In this kind of reaction some energy of the incident neutron is absorbed in the target nucleus which leaves the nucleus in an excited state. Thus, the kinetic energy of the system is not conserved.

Neutron Absorption Reactions

In the neutron absorption reaction, the incident neutron is absorbed by the target nucleus, which leads to rearrangement in the nucleus to obtain a more stable configuration and subsequent emission of particles such as a photon, proton, etc. These reactions can occur at very low energies and are strongly dependent on the neutron spectra and the length of irradiation [40]. The absorption reactions are divided into the following categories depending upon the exit channel of the reaction:

1. **Radiative Capture(n,γ)** In this reaction the incident neutron is completely absorbed by the nucleus, leaving the nucleus in an excited state. This excited nucleus then decays to its ground state by emitting one or more gamma rays. This reaction cross-section is denoted by σ_γ and strongly depends on the incident neutron energy and on the target energy (temperature).

2. **Transfer Reaction (n,'X')** In this process, the incident neutron is absorbed by the target nucleus which then decays by emitting charged particles like α ($^4_2$He nuclei), p ($^1_1$H nuclei), etc. The reaction may leave the target nucleus in an excited state, which may then decay to its ground state by emission of gamma.

3. **Neutron-induced Fission Reaction (n,f)** In this reaction the nucleus upon absorbing neutron may decay by disintegrating into two or more fission fragments (nuclei

of intermediate atomic weight) and a few neutrons. For fissionable materials, the absorption cross-section is given by $\sigma_a = \sigma_\gamma + \sigma_f$.

1.2.2 Radioactive Decay

Neutron interaction with matter often leaves the nucleus in an excited state. Radioactive decay is the process by which an unstable atomic nucleus attains stability by the emission of particles or radiation, such as an α particle, β particle, neutrinos or γ rays. This rearranges the nucleus to attain a more stable configuration. For a single atom, radioactive decay is a stochastic process. This makes it impossible to predict when a particular atom will decay, regardless of how long the atom has existed. However, for a collection of atoms, decay constants or half-life can be defined. A collection of radioactive isotopes will reduce on average to half of its initial value during one half-life. The half-life for radioactive atoms spans from nearly instantaneous to more than the age of the universe.

Consider a radioactive isotope A (parent isotope) producing isotope B (daughter isotope) via some decay mode. Therefore, for a given sample of the radioisotope A, the number of decay events dN_A expected to occur in a small interval of time dt is proportional to the number of atoms of isotope A N_A, that is:

$$\frac{-dN_A}{dt} \propto N_A \tag{1.3}$$

Different radionuclides decay at different rates, so decay constant λ can be defined for each pair of a parent and daughter isotope. This implies:

$$\frac{-dN_A}{dt} = \lambda_{AB} N_A \tag{1.4}$$

The solution of this equation can be written as:

$$N_A(t) = N_A(0) e^{-\lambda_{AB} t} \tag{1.5}$$

The half-life($t_{1/2}$) for any radioisotope, is defined as the time in which only half of the initial amount of isotope is left ie. ($N(t_{1/2}) = \frac{N(0)}{2}$). In the case of radioisotope A, it is given by:

$$1/2N_A(0) = N_A(0)e^{-\lambda_{AB}t_{1/2}} \tag{1.6}$$

$$1/2 = e^{-\lambda_{AB}t_{1/2}} \tag{1.7}$$

$$t_{1/2} = -\frac{ln(1/2)}{\lambda_{AB}} \tag{1.8}$$

$$t_{1/2} = \frac{ln(2)}{\lambda_{AB}} \tag{1.9}$$

Various modes for the decay of radioactive atom are listed below:

Beta Decay (β)

A free proton or neutron can decay via the following channels:

$$p \rightarrow n + e^{+} + \nu_e \tag{1.10}$$

$$n \rightarrow p + e^{-} + \bar{\nu}_e \tag{1.11}$$

The symbols ν_e and $\bar{\nu}_e$ stand for the electron neutrino and the electron anti-neutrino, respectively. During the decay process, an electron or a positron is emitted to conserve the charge. At a fundamental level, the neutron decay is caused by the conversion of the negatively charged ($-\frac{1}{3}$ e) down quark to the positively charged ($+\frac{2}{3}$e) up quark by the emission of a $W-$ boson and the $W-$ boson subsequently decays into an electron and an electron anti-neutrino:

$$d \rightarrow u + e^{-} + \bar{\nu}_e \tag{1.12}$$

The proton decay happens because the weak interaction converts a proton into a neutron by converting an up quark into a down quark resulting in the emission of a $W+$ or the absorption of a $W-$. However, free proton decay is not energetically viable as the mass of

the neutron is greater than the mass of the proton. Thus, it can only happen inside nuclei when the daughter nucleus has greater binding energy than the parent nucleus.

Thus, in a nucleus with excess nucleons, stability can be achieved by changing a proton into a neutron or vice-verse. Inside a nucleus, both the decays are energetically possible if the mass of the daughter products plus the mass of the electron or positron is smaller than the mass of the original nucleus. These decays are called β^- and β^+ decays and are written as:

$$ {}^{\mathrm{A}}_{\mathrm{Z}}\mathrm{X} \rightarrow {}_{\mathrm{Z}+1}{}^{\mathrm{A}}\mathrm{X}' + e^- + \bar{\nu}_e \tag{1.13} $$

$$ {}^{\mathrm{A}}_{\mathrm{Z}}\mathrm{X} \rightarrow {}_{\mathrm{Z}-1}{}^{\mathrm{A}}\mathrm{X}' + e^+ + \nu_e \tag{1.14} $$

Where ${}^{\mathrm{A}}_{\mathrm{Z}}\mathrm{X}$ is an isotope of atomic number Z and mass number A. Beta decay leads to the change in nuclear species by increasing or decreasing the atomic number keeping the mass number the same. The difference in mass of the parent nuclei and the daughter products appears as the kinetic energy of the particles and recoil nucleus. The energy corresponding to this mass difference is usually denoted by Q.

Alpha Decay (α)

In this type of radioactive decay, an atomic nucleus emits an alpha particle, thereby transforming the nucleus into a different atomic nucleus with a different mass number and atomic number. An alpha particle is identical to the nucleus of a helium-4 atom, which consists of two protons and two neutrons. This radioactive decay mode usually occurs in the very heavy nucleus due to the quantum tunneling of the alpha particle through the potential barrier of the nucleus. Alpha decay is energetically favorable since for very heavy nuclei the binding energy per nucleon decreases with increasing mass of the nucleus. The

corresponding decay process is given by:

$$^{A}_{Z}X \rightarrow ^{A-4}_{Z-2}X + \alpha \tag{1.15}$$

Gamma(γ) Decay and Isomeric Transition

The nucleons in the nucleus of an atom exist in discrete energy levels according to the nuclear shell model. These energy levels are found by solving the Schrodinger equation for a single nucleon moving in the average potential generated by all other nucleons. The energy difference between the nuclear energy levels is typical of the order of 1 MeV. The daughter product of any radioactive isotope after undergoing a decay process like β^-, β^+ or α decay, might not be in its ground state but in some excited nuclear state. The isotopes then decay to its ground state by emission of gamma(γ) rays.

$$^{A}_{Z}X^{*} \rightarrow ^{A}_{Z}X + \gamma \tag{1.16}$$

Most transitions resulting in the emission of a γ ray are extremely fast. However, for some transitions, the direct decay mechanism is forbidden, and the corresponding decay is much slower. A nucleus that is trapped in one of these metastable states is called an isomer, and this is denoted by a letter m after the mass number, e.g. ^{60m}Co. The decay of an excited nuclear isomer to a lower energy level is called an 'isomeric transition'.

Electron Capture and Internal Conversion

For a very heavy isotope, there is a finite probability that the K- or L- shell electron is present very close to the nucleus. In such cases, the nucleus can capture the orbital electron resulting in a process known as 'electron capture'. The equation for electron capture is given below:

$$p + e^- \rightarrow n + \nu_e \tag{1.17}$$

In most cases, the captured electron is the K-shell electron, but L-shell electron capture also occurs. The electron capture leaves an empty energy level in the electronic structure of the atom. This level is filled by an outer electron jumping to the inner levels and emitting characteristic X-ray. Electron capture sometimes also results in the Auger effect, where electrons are ejected from the atom's electron shell due in the process of seeking a lower energy electron state. Electron capture is a comparatively minor decay mode caused by the weak force and since β^+ decay and electron capture produce essentially the same daughter products, the probability of favored reaction depends on the decay energy. If decay energy is less than 511 keV, the β^+ decay is impossible and only electron capture occurs.

Internal conversion occurs when an excited nucleus interacts electromagnetically with one of the orbital electrons of the atom which results in the emission of electron from the atom. The high-energy electron emitted from the radioactive atom is not from the nucleus and thus, are not called beta particles. An isotope decaying by the internal conversion process exhibits a group of electron energies, the differences in energy being equal to the differences in the binding energies between the electronic orbitals. Internal conversion is a different decay mechanism for transitions that usually emit gamma rays.

1.2.3 Neutron transport codes

The 14.1 MeV neutrons produced during the fusion reaction travel out of the plasma and through various components of the reactor. In its trajectory it may interact with the reactor material via scattering reaction. Neutron losses energy in this process and even may get absorbed. This loss of energy by a neutron is calculated by the transport code. The main output of the transport code is the neutron energy spectrum. These neutrons can also get absorbed by the nuclei and the nuclei may undergo transmutation followed by radioactive decay. This is often calculated by a separate class of codes called the neutron activation codes. Some transport codes can also calculate transmutation but in limited capacity,

details of such codes are given in chapter 4.

The transport codes calculate the neutron spectrum in the desired group structure at each spatial location by using the neutron scattering probabilities and energy loss of neutrons in the material. Neutron transport is simulated using two methods: the Monte Carlo and the deterministic method. Monte Carlo codes simulate the trajectory of individual particles based on interaction probabilities. Using these trajectories, the average behavior of neutrons in any physical system is then inferred. On the other hand, the deterministic codes solve the Boltzmann transport equation to obtain neutron behavior in the system. This is achieved by discretizing the energy, space and time in the transport equation and obtaining an approximate solution with numerical calculation. Deterministic codes give information throughout the phase space of the problem whereas; Monte Carlo codes outputs are obtained for specific tallies requested by the user. The two most popular codes for neutron transport codes from each category are given below.

MCNP

MCNP stands for Monte Carlo N-Particle Transport Code developed by the Los Alamos National Laboratory. It can simulates continuous-energy coupled neutron/ photon/ electron transport [41]. In MCNP, random numbers are used to produce statistical sampling of an individual process which then determines the probability distributions governing each event. The individual probabilistic events that comprise a process are then simulated sequentially. The basic technique for particle transport is to follow each particle from a source throughout its life based on probability distributions to determine the outcome at each step of its life. This process is repeated for a large number of particles to obtain desired statistical accuracy for the calculation. This code does not average or approximate space, energy, and time for the calculations allowing for detailed representation of physical data [41].

ATTILA

ATTILA is a multi-energy group, neutron-gamma discrete ordinates transport code available from Transpire Incorporate. It is designed to solve the linearized Boltzmann transport equation for a wide variety of radiation transport applications. ATTILA solves the following steady-state transport equation using multi-group energy, discrete-ordinate angular discretization and linear discontinuous finite-element spatial differencing (LDFEM).:

$$\hat{\Omega} \circ \nabla \psi(\vec{r}, E, \hat{\Omega}) + \sigma_t(\vec{r}, E)\psi(\vec{r}, E, \hat{\Omega}) = Q_S(\vec{r}, E, \hat{\Omega}) + Q_f(\vec{r}, E, \hat{\Omega}) + q(\vec{r}, E, \hat{\Omega}) \quad (1.18)$$

Based on user-supplied input, these equations are solved to produce a particle distribution function in space, angle, and energy. From this particle distribution function, outputs for various quantities can be produced. ATTILA uses 3D, unstructured, tetrahedral mesh grids for discretizing space, more details are available in articles [42, 43, 44].

The neutron spectrum generated by the transport code is then used by activation codes to evaluate neutron-induced reactions like transfer reaction, radiative capture, and fission reaction. The activation code further calculates radiological quantities like activity, biological dose rate, etc from the ionizing radiations emitted from radioactive isotopes, details of activation code will be discussed in the section below.

1.3 Neutron-induced activation

To evaluate activation, transmutation and the subsequent radioactive decay, neutron spectrum from transport codes along with initial material composition and irradiation scenario(neutron source strength as a function of time), are used as input. The mathematical description of activation is given in section: 1.3.1, various parameters used to quantify activation is given in section 1.3.2 and some example of famous activation codes are given in section: 1.3.3.

1.3.1 Mathematical description

Nuclear activation is defined as the generation of radioactive isotopes via the process of nuclear reactions (transmutations) or radioactive decay. It is governed by the first-order linear differential equation, known as the Bateman equation [45]. In a homogeneous, infinite and infinitely dilute material, the time evolution rate of nuclides 'i' can be written as: [46]

$$\frac{dN_i}{dt} = -(\lambda_{ii} + \bar{\sigma}_{ii}\Phi)N_i + \sum_{j \neq i}(\lambda_{ij} + \sigma_{ij}\Phi)N_j \tag{1.19}$$

The first term on the R.H.S is the loss term for nuclide N_i. λ_{ii} is the total decay coefficient and $\bar{\sigma}_{ii}$ is the total loss due to transmutation. The second term on the R.H.S is the gain term, the production of nuclide N_i from various other nuclides N_j. λ_{ij} is the decay of isotope N_j to isotope N_i and σ_{ij} is the average transmutation probability of isotope N_j to isotope N_i. The time evolution rate for all the 'n' isotopes in the material is a set of 'n' coupled first-order linear differential equations. Since λ_{ij} and $\bar{\sigma}_{ij}$ are independent of N_j, these can be written in a matrix form [47]:

$$\frac{d\mathbf{N}}{dt} = -\Lambda\mathbf{N(t)} \tag{1.20}$$

where $\mathbf{N}$ is the matrix containing the concentration of all isotopes at time t and Λ is thee matrix of coefficients given as $\Lambda_{ij} = \lambda_{ij} + \sigma_{ij}\Phi$. The solution of the above equation is:

$$\mathbf{N(t)} = e^{-\Lambda t}\mathbf{N(0)} \tag{1.21}$$

For all practical/calculation purposes, reaction cross-section data is condensed into groups using the formula:

$$\bar{\sigma}_g = \frac{\int_{E_{gi}}^{E_{gf}} \sigma(E)\Phi(E)dE}{\int_{E_{gi}}^{E_{gf}} \Phi(E)dE} \tag{1.22}$$

where $\bar{\sigma}_g$ is the average condensed cross-section for group g, $\sigma(E)$ is the reaction cross-section at energy E, $\Phi(E)$ is the value of fusion spectrum at energy E, E_{gf} is the upper bound of group stricture and E_{gi} is the lower bound for the group g. Further details of condensation and reaction cross-section can be obtained from Ref [48]. The neutron spectrum is also segregated into groups. The most common group structure for fusion devices is the 175 Vitamin-J group [49]. The multigroup cross-section and neutron spectrum are then used to construct the coefficient matrix using the formula:

$$\Lambda_{ij} = \lambda_{ij} + \sum_{g} (\bar{\sigma}_{ij}^{g} * \Phi^{g}) \tag{1.23}$$

where λ_{ij} is the radioactive decay constant of the isotope j to i, σ_{ij}^{g} is the groupwise reaction cross-section of the isotope j to i and Φ^{g} is the groupwise neutron spectrum.

The typical coefficient matrix generated using eq: 1.23 is usually very stiff and sparse [50]. The stiffness of the matrix is because of the large variation in decay constants of the radioactive isotopes. For single target nuclide with one step nuclear interaction, kinematically possible reaction can produce nuclides with atomic numbers $<= Z$ of the target, while sequential reaction like (p,n), (d,n) and (α,n) produce additional nuclides with higher Z value [51]. This implies that the probability of the nuclear reaction cross-section ($\sigma_i j$) from any nuclei j to nuclei i is always zero except in few cases. Same is also true for radioactive decay process. As each isotope can produce only a handful of different isotopes, the resultant coefficient matrix has huge sparsity i.e. most of the matrix elements $\Lambda_{ij} = \lambda_{ij} + \sum_g (\bar{\sigma}_{ij}^{g} * \Phi^{g}) = 0$. This sparsity makes it difficult to use conventional methods to calculate the exponential of the matrix given by eq: 1.21 [52]. Most commonly 3 main mathematical methods are used by the activation codes to model such a complicated physical system, they are:

- Ordinary Differential Equation (ODE) Solver: Activation codes that use this method solves the set of modified Bateman equation given by 1.19 for each isotope present in the material or the isotopes that could be created in the material. Various meth-

ods like Sidell method, Euler method etc are used to solve equation 1.19 for small increments of time.

- Matrix Exponential Solver: Activation codes that use this method solves the equation 1.21 for all the isotopes present in the data library. Most commonly the exponent of the matrix is solved by expanding it in the power series. Various other methods used to calculate the exponential of a matrix is given in article [52].

- Linear Chain Solver: Activation codes that use this method analytically solves the Bateman equation for a chain of production of isotopes, details of the method are given in Appendix A.

Various codes that use these solvers are given in the section 1.3.3 and can be found in the reference [46, 53, 54, 48].

1.3.2 Typical parameters of activation

The radioactive nuclides generated in a material after neutron irradiation would emit ionizing radiations like α, β and γ rays. These radiations affect materials and living beings differently and to different extents. Hence to quantify the radio-toxicity in an activated material typical parameters are defined. These parameters can be used for radioactivity level assessments, accident analyses, radiation dose assessments, decommission studies, etc. Typical activation parameters used in the fusion systems are given below:

1. **Activity** is defined as the number of decays per unit time of radioactive isotope. The activity of any material is equal to the sum of the activity of all its radioactive isotopes. The unit of activity is the Becquerel (Bq). $1Bq = 1disintegration/s$. The Specific activity is usually used to characterize the radioactivity of the material and is defined as the ratio of the total activity of the material to its mass, in units of Bq/kg. Activity can be further classified into alpha, beta and gamma activity

depending upon the various decay modes of the isotope.

2. **Decay Heat** is defined as the heat produced through the deposition of energetic particles or radiations emitted from the decay of radioactive isotopes in an activated material. It is the main heat source in nuclear materials during periods of reactors shutdown. Thus, is one of the main safety concern in the fusion devices.

3. **Radwaste Index** Any material is called radioactive waste or radwaste if it has a prolonged activity even after the shutdown of the reactor. These materials contain long-lived radionuclides that do not decay to background levels after the decommissioning of the reactor. Proper classification and disposal of these waste are mandatory to prevent radiation leakage and other harmful effects. There are two major rad-waste classification scheme used by the fusion community. The Clearance Index, classification scheme defined under IAEA guidelines and the ANDRA Classification, rad-waste classification scheme defined under French guidelines.

4. **Dose Rate** The radiation fields emitted from activated material in the fusion systems can be absorbed by living and non-living matter near the source. To quantify the effects of radiation after being absorbed, various dose rates are defined.

   Absorbed dose is the measure of the energy deposited in the matter by ionizing radiation per unit mass. The SI unit of measure is the gray (Gy), which is defined as one Joule of energy absorbed per kilogram of matter. To incorporate the biological effects of the radiation "Equivalent" and "Effective" dose are defined.

   Equivalent dose gives the stochastic health effects of low levels of ionizing radiation on the human body. The SI unit of measure for equivalent dose is the sievert, $1Sv = 1Joule/kg$. Gamma Dose rate defined for fusion systems is the measure of biological(equivalent dose rate) received by the exposure to gamma radiation and is also measured in Sv/hr.

   Effective dose is the tissue-weighted sum of equivalent dose for all tissue and organs of the human body defined by the International Commission on Radiological

Protection (ICRP) system of radiological protection. It represents the stochastic health risk to the whole body, which gives the probability of cancer induction and genetic effects of low levels of radiation. It takes into account the type of radiation and the nature of each organ or tissue being irradiated and enables a summation of organ doses due to varying levels and types of radiation, both internal and external, to produce an overall calculated effective dose.

5. **Biological Hazard Potential** The biological hazard potential represents the impact on the human body caused by the leakage of radionuclides. The biological hazard potential is described by the inhalation dose and ingestion dose.

A detailed description of the quantities and the procedure used to calculate them are given in Chapter 2.

1.3.3 Neutron activation codes

Various nuclear activation codes are developed over the years to simulate neutron-induced reactions and radioactive decay using various different strategies to solve modified Bateman Equation [55, 56, 53]. Few codes that are widely used for activation calculations were the focus of the literature survey and are given below:

ALARA

ALARA stands for Analytic and Laplacian Adaptive Radioactivity Analysis. It is an activation code developed at Fusion Technology Institute, University of Wisconsin [54]. ALARA models the neutron activation using linear chains with an appropriate truncation method. For each chain, it then adaptively chooses between analytical method and expansion technique to evaluate isotopic inventory. Given a group-wise neutron flux, ALARA uses data from a variety of libraries to determine the altered material composition which

is then used to calculate the activity, and β-, γ-, and α-heating. In addition, a group-wise γ-ray source flux can be computed by ALARA to be used for the calculation of doses. Finally, if provided with an adjoint importance field based on flux-to-dose conversion factors and the gamma source distributions, ALARA can directly calculate the biological dose. ALARA can also perform 3-dimensional activation calculations on volume interval defined by the user or calculated by code [57].

FISPACT-2007

FISPACT is an inventory code, developed by Culham Centre for Fusion Energy(CCFE), UK, that can calculate neutron-, deuteron- and proton-induced activation calculations for materials in the fusion devices [46]. FISPACT is a part of the European Activation System (EASY). The current version of FISPACT is FISPACT-II [58]. FISPACT-2007 code can evaluate amount (number of atoms and grams), the activity(Bq), α, β and γ energies(kW), *gamma* dose-rate (Sv/h), the potential ingestion and inhalation doses (Sv), the legal transport limit (A2 value) and the clearance index for each nuclide, in a material after being irradiated with neutron or charged particle. It can also give the pathways by which these nuclides are formed. FISPACT uses external libraries of reaction cross-sections and decay data for all relevant nuclides. At the end of each time interval, the dominant nuclides for each radiological quantity and the pathway data for the production of these nuclides can be shown. FISPACT solves the following set of differential equations that describe the amounts of atoms of various nuclides present following the irradiation of a given material in a neutron field.

$$\frac{dN_i}{dt} = -N_i(\lambda_i + \sigma_i\phi) + \sum_{j\neq i} N_j(\lambda_{ij} + \sigma_{ij}\phi) + S_i \tag{1.24}$$

$$S_i = \sum_k N_k \sigma_k^f \phi Y_{ik} \tag{1.25}$$

where N_i is the amount of nuclide i at time t, λ_i is the decay constant of nuclide i, λ_{ij} is the decay constant of nuclide j producing i, σ_i is the total cross-section for reactions on i, σ_{ij} is the reaction cross-section for reactions on j producing i, σ_k^f is the fission cross-section for reactions on actinide k, ϕ is the neutron flux, S_i is the source of nuclide i from fission, and Y_{ik} is the yield of nuclide i from the fission of nuclide k. FISPACT uses Sidell Solution with exponential function for step length to solve the coupled ODE. FISPACT is the widely accepted activation code for fusion devices. Hence, in this thesis, it is used as a standard code for most of the benchmarking exercises and validation studies.

The key disadvantage of FISPACT-2007 is that it is not scalable to perform multipoint activation calculations. FISPACT takes one neutron spectrum as an input, hence to perform calculations at different locations of the same material, it needs to be run in a sequential manner. Also, due to the unavailability of the source code for the authors, it becomes difficult to add new data libraries, to couple it with other codes for photon transport and to evaluate any additional radiological quantities.

FORNAX

FORNAX is an activation module built-in the ATTILA transport code. FORNAX tracks the population of isotopes created through nuclear transmutation and decay processes. The nuclear activation problem is defined as:

$$\frac{d\mathbf{N}}{dt} = \mathbf{A}.\mathbf{N}(t) \quad \Longrightarrow \mathbf{N}(t) = \mathbf{N}(0)exp(\mathbf{A}t) \tag{1.26}$$

where $exp(\mathbf{A}t)$ is the matrix exponential of coefficient matrix $\mathbf{A}$ and $\mathbf{N}(0)$ is the array of nuclides concentration at $t = 0$. FORNAX uses a McLaurin series expansion to compute the matrix exponential:

$$exp(\mathbf{A}t) = I + (\mathbf{A}t) + \frac{1}{2}(\mathbf{A}t)^2 + \frac{1}{6}(\mathbf{A}t)^3 + ... \tag{1.27}$$

Atom density calculated by FORNAX can be used directly by the activation source generator (ASG) to produce an activation source file. For more details refer [42]. FORNAX uses the Vitamin-J multi-group (175 neutron + 42 photon) version of the FENDL 2.1 fusion-specific nuclear data library in DTF format.

The major disadvantage of FORNAX is that it has a very limited library of only 1300 isotopes. Also, not all decay mechanisms and decay energy are considered in the data libraries. This makes it unsuitable for complete activation calculation.

ACTYS

The initial framework of ACTYS as a single point activation code was developed prior to the thesis at ITER-India. ACTYS calculates the time evolution of the nuclide inventory and radioactivity of isotopes in a material when irradiated with the constant neutron spectrum using the analytical linear chain method. Details of the linear chain method can be found in appendix A and details on the truncation of the linear chains can be found in the article [48].

ACTYS calculates the isotopic concentration of each isotope produced from decay and transmutation of initial isotopes in the material and activity of radioactive isotopes. It, however, lacks many key features of a complete activation code like calculation of Gamma Dose rate, radwaste, etc and is not validated for fusion systems. In order to make the ACTYS code mature, in the scope of the thesis, various methods were developed to evaluate radiological quantities like contact dose rate, gamma spectrum, decay heat, and radwaste index and were added. An extensive validation was also performed using standard benchmarking problems. Details are given in Chapter 2.

1.4 Motivation for the present work

The basic design parameters of the fusion systems which make nuclear activation study of structural material in the fusion devices very crucial are given below:

- High neutron energy with a complex energy spectrum.

  Fusion reactor will produce 2.45 MeV and 14.06 MeV neutrons via D-D and D-T fusion reactions, respectively.

$$D + T \rightarrow 4He(3.52MeV) + n(14.06MeV) \tag{1.28}$$

  The fusion energy per process $E_{fus} = E_{\alpha} + E_n = 17.58$ MeV. The α-particle produced will contribute towards heating the plasma and to maintain the conditions for fusion. The fusion neutrons will interact with lithium in the tritium breeding blankets and would produce tritium via breeding reaction given in equation: 1.2. Tritium itself is radioactive and the system must be designed to ensure that tritium is confined within the reactor. Also, the neutron is the dominant energy carrier and activates the structural material as it passes through generating radio-toxicity. Therefore, accurate assessment of the concentration of radioisotopes and the radiations emitted from these isotopes is mandatory to assess the damage caused to the structural and functional materials.

  This damage is evaluated in 2 stages, first, the neutron energy spectrum is evaluated by transport codes and then neutron-induced activation is calculated by the activation codes. As the activation codes require the neutron spectrum as input, the proper coupling is required between transport and activation codes. For this purpose, an accurate and flexible activation code needs to be developed that can generate a highly resolved radiation map of the device in very little time and can be easily coupled to transport codes.

- The large size and heterogeneous distribution of materials.

The fusion reactors are huge devices with a diameter of the order of tens of meters that contains thousands of intricate components and hundreds of different materials. Moreover, a large number of gaps and open channels are reserved for placement of fusion diagnostics. The complex structure and material distribution lead to varying neutron flux and neutron spectrum throughout the device. Hence, the activation calculation needs to be performed at various locations of a reactor. A trivial way to perform activation calculation for large devices is to call an activation code sequentially for each location [59, 54]. This kind of sequential run is computationally very expensive.

To overcome this and to produce an accurate radiation map through the fusion device, the multi-point activation strategy needs to be developed. Moreover, such calculations generate an enormous amount of data. For nuclear analysis and damage study, representation of this data in an easily understandable format is also required.

- The large volume of low-level radioactive wastes (LLW).

  Structural materials irradiated with fusion neutrons during the operation period would become activated and would emit radiations even after the shutdown. Material with prolonged radioactivity even after shutdown is called as radioactive waste or radwaste. In reference, [60] authors report that after 30 years of operation 38,000 tons of radwaste will be generated in ITER. This would mean that, in a fusion power reactor where neutron flux would be significantly higher than ITER, the radwaste produced maybe 20 to 50 times higher than that in ITER. Moreover, the authors in paper[61] reports that the tritium inventory in a 1 GWe fusion power reactor may reach the level of 10 kg and the tritium would migrate through the structural material in the forms of HT, HTO, and tritium dust.

  This generates a requirement to develop low activation materials to reduce the overall quantity of radwaste generated in any device. Low activation materials not only

increase the lifetime of the components used in the reactors, but it also reduces the overall cost of the reactor and hence the cost of electricity. This implies that tools need to be developed to evaluate optimized material composition in order to minimize the radiological response of fusion materials.

Many activation codes available today may fulfill some of the above criteria, but no code to the knowledge of the author contains inbuilt material optimization scheme or faster multipoint calculation strategy. The aim of the thesis is to overcome such drawbacks by developing an activation code that is fast, accurate, versatile, flexible and can perform multi-point activation calculations. The development of such indigenous codes would help the community towards self-reliance in nuclear calculations.

1.5 Thesis structure

A brief outline of the chapters of the thesis is given below:

- In **Chapter 2**, introduction to types of nuclear data libraries and their importance for activation calculations are given. The chapter presents a method developed to read standard nuclear data libraries and processing the data in a usable format. The chapter also presents the methods developed to evaluate radiological quantities like activity, biological dose rate, decay heat, and radwaste classification, using the information extracted from the data libraries. These methods are implemented in the code ACTYS and successfully benchmarked against standard benchmarking exercises given by IAEA (International Atomic Energy Agency) and with realistic ITER calculations.

- In **Chapter 3**, the importance of multipoint activation calculation in complex geometries is given. This chapter introduces the method for fast multipoint activation calculation. This method approximates a material placed at multiple locations and

experiencing different neutron spectrum using a small set of isotopes called the superlist. This concept of superlist is implemented in the code ACTYS-1-GO. Validation of the radiological quantities calculated by ACTYS-1-Go is performed using the benchmark exercise given by IAEA. Time comparison between ACTYS-1-GO and standard codes like FISPACT and FORNAX is also evaluated.

- In **Chapter 4**, the requirement for coupling activation codes with neutron transport codes is given. This chapter presents the tool developed for coupling ACTYS-1-GO with external neutron transport code, ATTILA. The biological dose rate produced by the decay gammas that are emitted from the activated materials is evaluated using this scheme. This chapter also establishes the importance of a highly resolved radiation map of the fusion reactor and thus the need for a fast multipoint activation code like ACTYS-1-GO.

- In **Chapter 5**, the requirement of low activation materials for future fusion reactor development is given. This chapter presents a method to optimize the composition of the fusion materials, based on spatial and temporal variation of various radiological responses produced by the material. The optimization is carried out within the upper and lower limits for each element provided by the user. This method is implemented in the code ACTYS-1-GO. This chapter also gives a demonstration of the capabilities of the optimization scheme based on some upper and lower limits.

- In **Chapter 6**, the construction and details of various radiation response diagrams are given. These diagrams are developed as an aide to the composition optimization scheme. The importance and utility of these diagrams are also discussed in the chapter.

- Finally, in **Chapter 7** the conclusion of the present work is given along with all the future works arising from the thesis.

Chapter 2

Nuclear Data Libraries and Methods to Evaluate Nuclear Responses

As discussed in Chapter 1, the initial framework of ACTYS uses the linear chain method to evaluate isotopic inventory and activity for a given material irradiated with a given neutron spectrum and irradiation scenario. ACTYS is primarily written in FORTRAN-95. The chain solver of ACTYS is benchmarked against various analytical and experimental results, the details can be found in the paper [48]. ACTYS, however, is incomplete to perform nuclear analysis for fusion systems due to the unavailability of modules to evaluate radiological quantities. As mentioned in section 1.3.2, various radiological quantities are required to quantify the activation in neutron irradiated material. Hence, under the scope of the thesis, various methods were developed and added to the ACTYS code to obtain radiological quantities necessary for activation analysis. These quantities are given in section 1.3.2. To evaluate these quantities, the decay data of various isotopes are required. This information is read from decay data libraries. In this chapter a brief introduction to nuclear data libraries is given in section 2.1, extraction of particle and radiation spectrum from ENDF-6 format data libraries is given in section 2.2.1, various methods to evaluate various radiological quantities is discussed in section 2.2.2 and addition of these methods

to ACTYS and benchmarking it against standard benchmarking exercises is given in the section 2.3.

2.1 Role of nuclear data for fusion nuclear technology

Accurate data needs to be provided to activation codes for accurate assessment of radiation dose, radiation-induced damage to materials/components, shielding efficiency, tritium breeding capability, and estimate the nuclear power generated in the system [62]. Thus, the availability of high-quality nuclear data is a prerequisite for reliable nuclear calculations. Nuclear data is available for all 85 naturally occurring elements with 290 stable isotopes and more than 2500 radionuclides. It is a compilation of decay properties of the atomic nuclei and the fundamental physical relationship governing their interactions with incident neutrons. The following information is stored in the data libraries:

- interactions of neutrons with atomic nuclei as a function incident neutron energy.
- probability of formation of (stable or radioactive) product nuclei through neutron-induced reactions.
- the information regarding the kind and the energy of secondary particles emitted from the nuclei as a result of nuclear reaction or by radioactive decay.

The nuclear data are commonly categorized into two main groups [63]:

1. Nuclear Reaction data

   It describes the interactions of various projectiles such as neutron, proton or photons with target nuclei. It includes reaction cross-section, angular and energy distribution of secondary particles, resonance parameters, and related quantities.
2. Nuclear structure and decay data

   It describes nuclear levels, half-lives, and radioactive decay schemes, atomic masses, etc.

For both groups, the type of information given can be experimental data or evaluated data or bibliographic.

1. Experimental data: Results of individual measurements as reported by the authors. The most important example is EXFOR/CSISRS, the library for experimental nuclear data
2. Evaluated data: These libraries contain recommended data based on all the data available from experimental and/or theory, arrived at after critical analysis of experimental data and their uncertainties, interpolation, and extrapolation, and/or nuclear model calculations. These are stored in strictly defined formats such as ENDF-6 (Evaluated Nuclear Structure Data File).
3. Bibliographic data: References with some description of the contents, but no numerical data. Examples are CINDA (Computer Index of Nuclear DAta) and NSR (Nuclear Science References).

2.1.1 ENDF-6 Format for Radioactive Decay Data

The ENDF system was developed for the storage and retrieval of evaluated nuclear data to be used for applications of nuclear technology. The ENDF system is divided into formats and procedures. Formats describe how the data are arranged in the libraries and give the formulas needed to reconstruct physical quantities such as cross-sections and angular distributions from the parameters in the library. Procedures are the more restrictive rules that specify what data types must be included, which format can be used in particular circumstances, and so on, more details on ENDF format can be found in ENDF-6 Manual [64]. The ENDF/B library maintained at the National Nuclear Data Center (NNDC) contains the recommended evaluation for each material. The spontaneous radioactive decay data are given in section 457 of ENDF-VII data libraries. Reaction types (MT) are identified by an integer number from 1 through 999. The main purpose of MT=457 is to describe the energy spectra resulting from radioactive decay and give average parameters

useful for applications such as decay heat, waste disposal, depletion and buildup studies, shielding, and fuel integrity. The information in this section can be divided into three parts: general information about the material, decay mode information for each mode of decay, and resulting radiation spectra. The format and other details regarding the ENDF format can be found in the ENDF manual given in reference: [64], the basic structure of the ENDF format is given in the figure below:

```
[MAT, 8,457/  ZA,    AWR, LIS, LISO,    NST, NSP]HEAD     (NST=0)
[MAT, 8,457/ T1/2, ΔT1/2,    0,    0,   2*NC,    0/(Ex,ΔEx) / LIST
[MAT, 8,457/ SPI,    PAR,    0,    0, 6*NDK, NDK/
         RTYP1, RFS1, Q1, ΔQ1, BR1, ΔBR1,
         --------------------------------
         RTYPNDK, RFSNDK, QNDK, ΔQNDK, BRNDK,ΔBRNDK] LIST
         <Subsection for Spectrum1>
         <Subsection for Spectrum2>
         --------------------------------
         <Subsection for SpectrumNSP>
[MAT, 8,  0/ 0.0, 0.0, 0, 0, 0, 0] SEND
```

The basic structure of nuclear data in ENDF format

```
[MAT, 8,457/ 0.0, STYP, LCON, 0, 6, NER/
         FD, ΔFD, ERAV, ΔERAV, FC, ΔFC] LIST
[MAT, 8,457/ ER1, ΔER1, 0, 0, NT, 0/
         RTYP1, TYPE1, RI1, ΔRI1, RIS1, ΔRIS1,
         RICC1,ΔRICC1, RICK1,ΔRICK1, RICL1,ΔRICL1] LIST
         ------------------------------------
         ERNER, ΔERNER, 0, 0, NT, 0/
         RTYPNER,TYPENER, RINER, RINER, ------------] LIST
         (omit these LIST records if LCON=1)
[MAT, 8,457/ RTYP, 0.0, 0, LCOV, NR, NP/ Eint / RP(E) ] TAB1
         (omit if LCON=0)
[MAT, 8,457/ 0.0, 0.0, 0, LB, 2*NPP, NPP/ (Ek,Fk) ] LIST
         (omit if LCOV=0 or LCON=0)
```

The structure of the subsection for spectrum in ENDF format

Explanation of a few keywords used to define the structure of ENDF format is given in the table: 2.1, the rest of the keywords can be found in ENDF-6 Manual [64].

ZA	designation od the nuclide ZA=1000Z+A
NST	Nucleus stability flag (NST=0, radiaoactive; NST=1, stable)
Ex	Average decay energy (eV) of radiation x
NDK	Total number of decay modes given
RTP	Mode of decay of the nuclide in its LIS state
STPY	Decay radiation type
ER	discrete energy (eV) of radiation produced (E_γ,E_β ,$E_{e.c.}$, etc.)
RI	intensity of discrete radiation produced (relative units).
LCON	Continuum spectrum flag
	LCON=0, no continuous spectrum is given
	LCON=1, only continuous spectrum is given
	LCON=2, both discrete and continuum spectra
FD	Discrete spectrum normalization factor
NER	Total number of tabulated discrete energies for a given spectral type (STYP)
ER_{AV}	Average decay energy of radiation produced.

Table 2.1: Explanation of keywords to read ENDF data library

2.2 Evaluation of radiological quantities

Various methods are developed to evaluate radiological quantities like biological dose rate, gamma spectrum, decay heat, multi-channel pathways, and ANDRA radwaste classification. These methods consist of reading the raw data from nuclear data libraries and processing the data in a readable format and developing efficient algorithms for the evaluation of these quantities. These methods are then implemented in the activation code ACTYS. Extensive validation of ACTYS is also performed using standard benchmarking problems given by the International Atomic Energy Agency (IAEA).

2.2.1 Extracting radiation decay data for data libraries

In the scope of the thesis a tool named 'spectrum generator' is developed. It reads the radioactive decay data directly from ENDF-6 format JEFF-3.1.1 and JEFF-2.2 radioactive decay data libraries and extracts relevant data for the evaluation of nuclear responses. JEFF (Joint Evaluated Fission and Fusion) project, is a collaborative effort among NEA data bank member countries to develop a reference nuclear data library for use in different

energy applications. More details regarding NEA Data Bank and JEFF libraries can be found in references [65, 66]. Spectrum generator reads the MF=8, MT=457 section of the JEFF decay library. The following information is extracted from the data libraries and stored in a file named SPECTRUM:

1. Decay energy: The average decay energies for light particles, electromagnetic radiation, and heavy particles are read and stored for use respectively in the calculation of beta, gamma and alpha decay heat produced by radioactive inventory. A list of all the decay modes read from JEFF libraries is given in table 2.2.

STYP		Radiation Type	Code
0	γ	gamma rays	gamma
1	$\beta-$	beta rays	beta
2	ec,($\beta+$)	electron capture	ec
		and/or positron emission	beta+
4	α	alpha particles	alpha
5	n	neutrons	n
6	SF	spontaneous fission fragments	SF
7	p	protons	p
8	e−	discrete electrons	e−
9	x	X-rays and annihilation radiation	x

Table 2.2: Decay modes in ENDF-6 files

2. Gamma spectrum: Discrete gamma and X-ray spectral lines (STYP= 0 or 9) are read from JEFF libraries and are used to create groupwise spectra by the nearest grid point binning method. Common energy bins structures used in activation calculations are given in table 2.3. Each spectral line is characterized by an energy E_r in eV, a relative intensity R_I and a normalization factor F_D. For any gamma group 'i', let $E(i)$ and $E(i+1)$ be the lower and upper limit of the group, then the contribution of the spectral line to the gamma group i for any nuclide is defined as:

$$If \quad E(i) \leq E_r < E(i+1) \qquad then \quad G_i = F_D \times E_r \times R_I \tag{2.1}$$

Where G_i is the line intensity of gamma in the gamma energy group 'i'. Likewise,

to evaluate the gamma spectrum for each nuclide, G_i arising from each decay mode of that nuclide is summed together.

Algorithm to read Radioactive decay data libraries

Algorithm developed to read and extract radioactive decay data from JEFF libraries and store the information in file named SPECTRUM, is given below:

```
Read isotope Z(atomic number) and A(mass number);
Read NST and NOS;
if NST = 1 or NST = 2 then
    STABLE Isotope;
end
else
    Read Ex and DEx ;
    Calculate Bremsstralung Radiation ;
    Read NDK ;
    for i = 1, NDK do
        Read RTPY(i) ;
    end
    for i = 1, NOS do
        Read STPY(i),LCON(i),NER(i) ;
        Read FD(i), ER(i)_avg ;
        if LCON(i) = 2 or LCON(i) = 3 then
            for j = 1, NER do
                Read ER(j), RI(j) ;
                if STPY = 0 or STPY = 9 then
                    Group ER(i) ;
                    if ER(i) > E(g) then
                        G(i) = G(i) + ER(j) * RI(j) * FD ;
                    end
                end
            end
        end
    end
end
Result: Print Group averaged Gamma Spectrum in file "SPECTRUM"
```

Algorithm 1: Spectrum generator for ACTYS

Table 2.3: Common gamma group structures (All the energies are given in MeV units)

VITAMIN-J (42)			(24)		
grp	Lower Bound	Upper Bound	grp	Lower Bound	Upper Bound
1	1.00E-03	1.00E-02	1	0.00E+00	1.00E-02
2	1.00E-02	2.00E-02	2	1.00E-02	2.00E-02
3	2.00E-02	3.00E-02	3	2.00E-02	5.00E-02
4	3.00E-02	4.50E-02	4	5.00E-02	1.00E-01
5	4.50E-02	6.00E-02	5	1.00E-01	2.00E-01
6	6.00E-02	7.00E-02	6	2.00E-01	3.00E-01
7	7.00E-02	7.50E-02	7	3.00E-01	4.00E-01
8	7.50E-02	1.00E-01	8	4.00E-01	6.00E-01
9	1.00E-01	1.50E-01	9	6.00E-01	8.00E-01
10	1.50E-01	2.00E-01	10	8.00E-01	1.00E+00
11	2.00E-01	3.00E-01	11	1.00E+00	1.22E+00
12	3.00E-01	4.00E-01	12	1.22E+00	1.44E+00
13	4.00E-01	4.50E-01	13	1.44E+00	1.66E+00
14	4.50E-01	5.10E-01	14	1.66E+00	2.00E+00
15	5.10E-01	5.12E-01	15	2.00E+00	2.50E+00
16	5.12E-01	6.00E-01	16	2.50E+00	3.00E+00
17	6.00E-01	7.00E-01	17	3.00E+00	4.00E+00
18	7.00E-01	8.00E-01	18	4.00E+00	5.00E+00
19	8.00E-01	1.00E+00	19	5.00E+00	6.50E+00
20	1.00E+00	1.33E+00	20	6.50E+00	8.00E+00
21	1.33E+00	1.34E+00	21	8.00E+00	1.00E+01
22	1.34E+00	1.50E+00	22	1.00E+01	1.20E+01
23	1.50E+00	1.66E+00	23	1.20E+01	1.40E+01
24	1.66E+00	2.00E+00	24	1.40E+01	
25	2.00E+00	2.50E+00			
26	2.50E+00	3.00E+00			
27	3.00E+00	3.50E+00			
28	3.50E+00	4.00E+00			
29	4.00E+00	4.50E+00			
30	4.50E+00	5.00E+00			
31	5.00E+00	5.50E+00			
32	5.50E+00	6.00E+00			
33	6.00E+00	6.50E+00			
34	6.50E+00	7.00E+00			
35	7.00E+00	7.50E+00			
36	7.50E+00	8.00E+00			
37	8.00E+00	1.00E+01			
38	1.00E+01	1.20E+01			
39	1.20E+01	1.40E+01			
40	1.40E+01	2.00E+01			
41	2.00E+01	3.00E+01			
42	3.00E+01	5.00E+01			

2.2.2 Evaluation radiological quantities and their validation

Methods to evaluate radiological quantities are implemented in ACTYS using FORTRAN subroutines. To validate the accuracy of these methods and the calculation of nuclear responses, a component of ITER diagnostics system namely the X-Ray Crystal Spectrometer(XRCS) is selected to be used as a benchmark problem, the details can be found in article [38]. XRCS system uses a small streaming gap, called as the sight tube, for measuring the x-rays emitted from the plasma. Along with the x-rays, neutron would also enter this sight tube. The neutron spectrum at the sight tube is used as the sample spectrum for the validation exercise. The validation is carried out against the widely accepted and ITER approved activation code FISPACT-2007. The sight tube neutron spectrum is obtained from the reference [38], and activation calculations are performed using the ITER specified SA2 irradiation scenario. Different materials are used for the validation of different radiological quantities for completeness. The neutron spectrum(n/cm^2s) in 175 energy group structure is shown in figure: 2.2 and irradiation scenario is used for ITER neutronics calculations given in table: 2.4.

Source Strength (n/s)	Duration	Repetition
2.68E16	2 years	1
2.06E17	10 years	1
0	0.667 years	1
4.15E17	1.33 years	1
0 5.0E18	3920 secs 400 secs	17
0 7.0E18	3920 secs 400 secs	4

Table 2.4: SA2 Neutron irradiation scenario

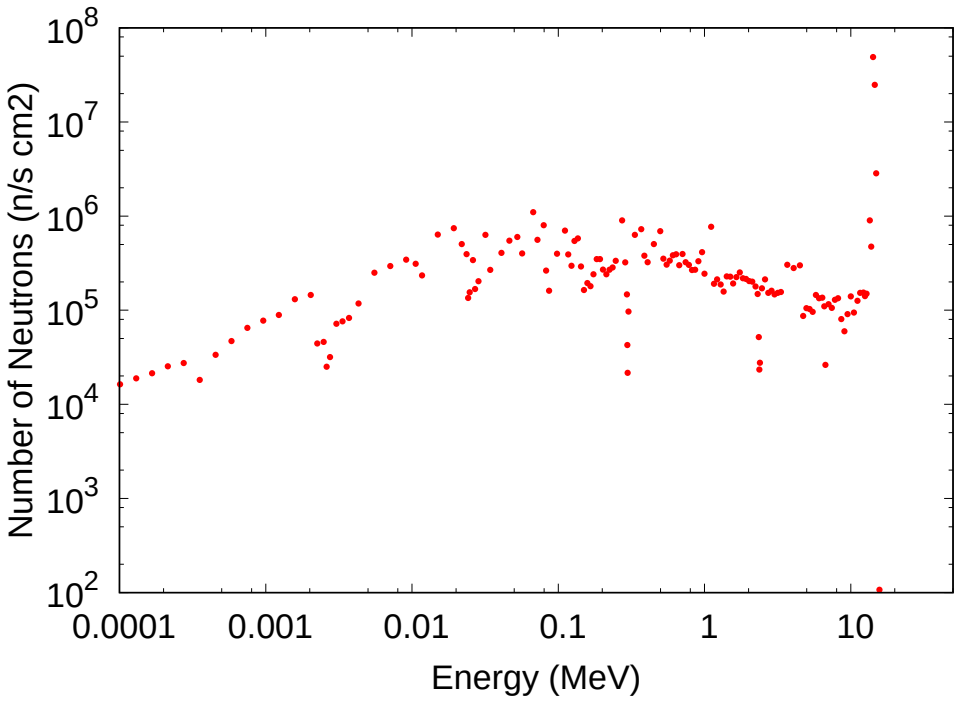

Figure 2.2: Neutron spectrum at the sight tube location in ITER XRCS diagnostic system

Gamma Spectrum

Discrete gamma, x-rays and bremsstrahlung radiation (all EM radiation will be referred under the common name gamma) are emitted from the decay process. The gamma spectrum of any activated material is the sum of energy-wise discrete gamma lines emitted from each individual isotope. After solving the Batman equation 1.19 and obtaining N(t) which is the isotopic concentration of each daughter nuclide at the time 't'. The list N(t) is sorted to identify radioactive isotopes. Out of these radioactive isotopes, isotopes emitting gamma radiation along with their gamma spectra are obtained from file 'SPECTRUM'. Total gamma emission from an activated material is calculated using the formula:

$$\gamma_i = \sum_j P_i E_i A_j \tag{2.2}$$

Where γ_i is the intensity of gamma-ray emitted in the energy group 'i', P_i is the probability of emission of gamma in energy group 'i', E_i is the energy of emitted discrete gamma line in energy group 'i', A_j is Activity of isotope 'j'.

To validate the gamma spectrum generated from ACTYS and FISPACT, activation calculation of CuCrZr alloy irradiated with sight tube neutron spectrum for SA2 irradiation scenario is carried out. The 24-energy group gamma spectrum generated by both the codes are compared. The results are given in percentage difference [1] in figure 2.3. It can be clearly seen that the gamma spectrum generated is in good agreement with the FISPACT code.

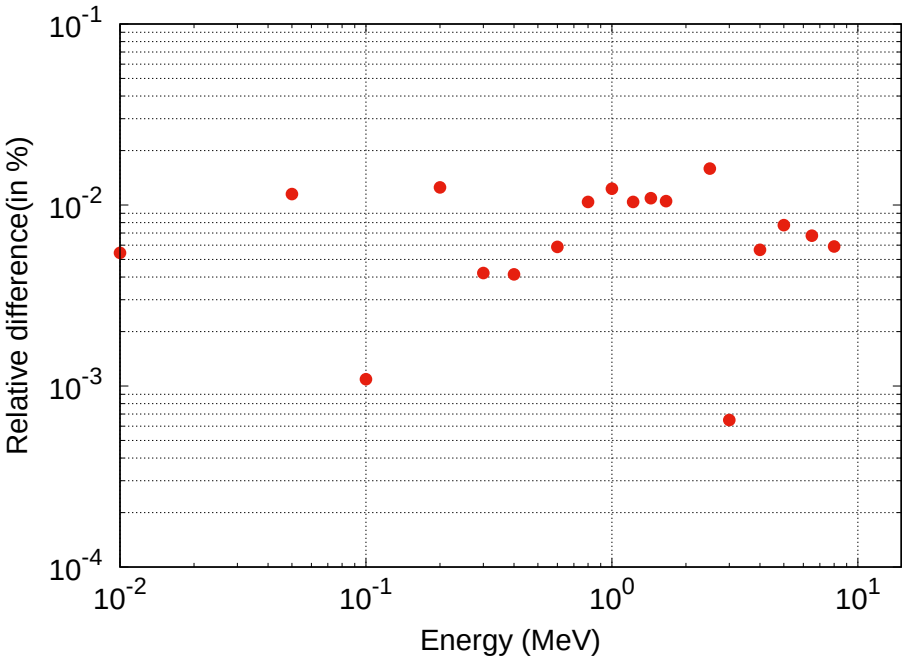

Figure 2.3: Relative difference (in %) for 24- energy group gamma spectrum generated by ACTYS and FISPACT-2007

Decay Heat

Average alpha, beta and gamma energy emitted from the radioactive isotope is deposited in the material locally, in the form of heat. This decay heat(H_i) is generated in an activated material by various radioactive isotopes. Using the data given in the file 'SPECTRUM',

[1]
$$\mathrm{RD}(\%) = \frac{abs(A-F)}{F} * 100 \tag{2.3}$$

where *RD* is the relative difference in percentage, A is the value obtained from ACTYS and F is the value obtained from FISPACT-2007.

isotopes are identified with finite alpha, beta and gamma emission energy. The decay heat generated by these isotopes is calculated by using the formula:

$$H_i = A_i * E_i * C \tag{2.4}$$

where A_i is the activity of the isotope 'i', E_i is the energy of the emitted radiation (α, β or γ) and C is the conversion factor from MeV/s to KW/hr.

To validate the decay heat production, stainless steel is irradiated with the sight tube neutron spectrum for the SA2 irradiation scenario. The results are compared with Fispact-2007 and are shown in figure 2.4. The relative difference between beta and gamma decay heat results calculated by this method and FISPACT-2007 is $<< 0.1\%$.

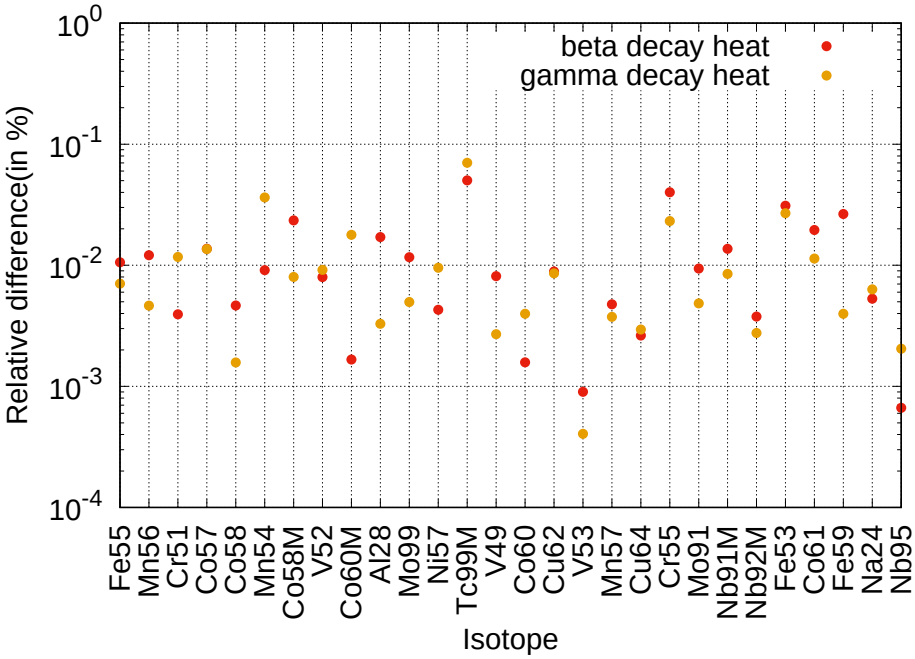

Figure 2.4: Relative difference of beta decay heat and gamma heat produced by various isotopes after activation calculation by FISPACT and ACTYS

Contact Dose Rate

The equivalent dose rate is the most relevant radiological quantity in relation to the health of the workers in reactors and locals in the nearby area. The contact dose rate is the

measure of the equivalent dose rate received at the surface of the irradiated material by gamma radiation. The formula for the contact dose rate is derived from the reference [67]. It assumes that the material is homogeneous and the isotope under consideration is the only active radiation source in the material emitting mono-energetic photons. Contact dose rate is the dose rate at the surface of a semi-infinite uniform volume source and is given by the formula:

$$D_i = C\frac{B}{2}\sum_g \frac{\mu_a}{\mu_m} E_g \frac{A_i}{M} \qquad \text{where} \qquad \mu_m = \sum \frac{m_i}{M}\mu_i \tag{2.5}$$

Where D_i is the contact dose rate for each nuclide 'i', C is the conversion factor from Mev/s to Sv/hr, B is the buildup factor, μ_a is the attenuation coefficient in air, $\mu_m$is the attenuation coefficient in material, E_g is the energy of the emitted gamma radiation in the group 'g', A_i is the activity of the isotope and M is the mass of the material. To

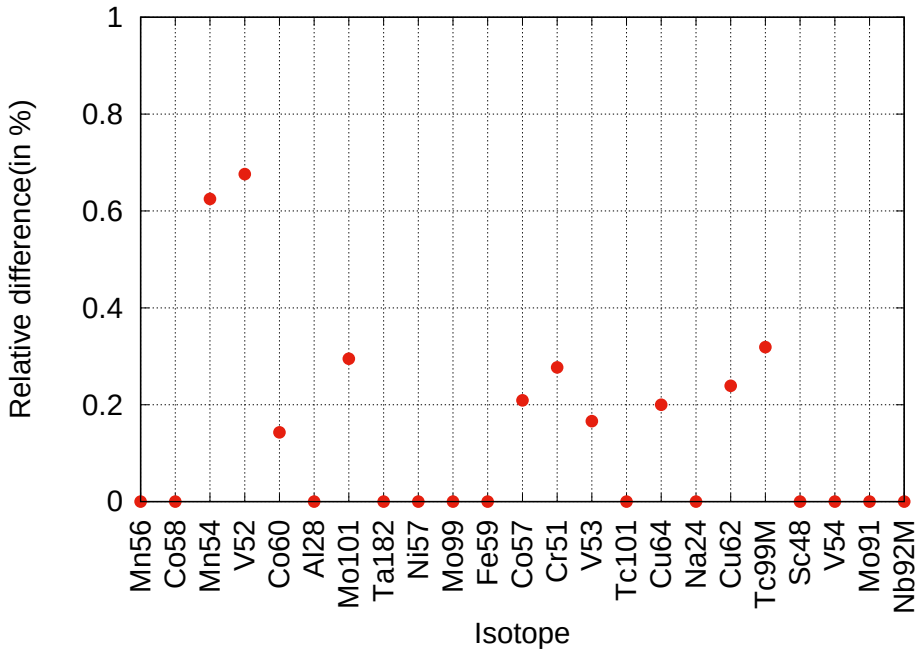

Figure 2.5: Relative difference of contact dose rate produced by various isotopes calculated by FISPACT and ACTYS

validate the contact dose rate calculated by this method, stainless steel is irradiated with neutron spectrum at sight tube for SA2 irradiation scenario. The results are compared

with Fispact-2007 and are shown in figure 2.5. From the figure, it can be seen that the relative difference in dose values $<< 1\%$.

Radwaste Index

Radioactive waste (Radwaste) includes any material that is either intrinsically radioactive, or has been contaminated by radioactivity, and have no further use. Radwaste is created inside nuclear reactors. These are activated materials that have prolonged radioactivity even after the shutdown of the reactor. Radioactive waste is typically classified as either low-level (LLW), intermediate-level (ILW), or high-level (HLW), depending primarily on its level of radioactivity. As a part of the thesis, methods are developed for evaluating radwaste classification under ANDRA rad-waste classification scheme defined under French guidelines.

ANDRA classification scheme is being used for classifying the radwaste that would be produced in ITER. According to ANDRA, nuclides are classified into 3 main types:

- Intermediate-level and long-lived radwaste (Type B) mainly from in-vessel component replacement.
- Purely tritiated waste (not irradiated by a neutron, but contaminated by tritium) from tritium plant and fuelling system operation and maintenance
- Low-level solid and liquid radwaste (Type A)
- Very low-level radwaste (TFA)

Under this scheme, a quantity called the IRAS index is also defined.

$$IRAS = \sum \frac{A_i}{10^{C_i}} \tag{2.6}$$

where A_i is the activity of radioisotope, C_i is the class of radioisotope.

Isotopes listed under the ANDRA classification stored in a file along with their class and

LMA values [68]. The final inventory calculated by equation 1.19 is then scanned for isotopes under the ANDRA scheme. If an isotope listed under ANDRA is present, its specific activity is calculated. If the specific activity of an isotope is more than its LMA value, the material is classified as TYPE B Rad-Waste. If all the isotopes have specific activity less than LMA value, then the IRAS index is calculated on the basis of class of the nuclides. If the IRAS index is found to be less than 1, then the material is classified as TFA waste, else the material is TYPE A category waste. Radwaste calculation of the XRCS system has been carried out as a part of the thesis and is reported in reference [38].

Pathways

Pathway analysis plays a crucial role in nuclear analysis for determining parents and reactions that contribute towards the production of radioactive isotopes, gas and gamma spectrum in the material. Calculation of pathways according to different reactions and decay channels and their contributions are developed under the scope of the thesis. The generation of multi-channel pathways is explained below.

During the activation process, isotopes present in the material are converted into other isotopes via nuclear reaction. These second-generation isotopes can further be converted into different isotopes via transmutation or radioactive decay, which can further decay or transmute into other isotopes forming a tree-like structure as given in figure: 2.6. Each branch signifies a radioactive decay or transmutation of parent isotope into a daughter isotope. Isotope 'A' is the initial parent present in the material. It can decay or transmute into two daughters 'B' and 'C' forming branches. Isotope 'D' and 'F' can decay or transmute to the same isotope 'E', such a pro-

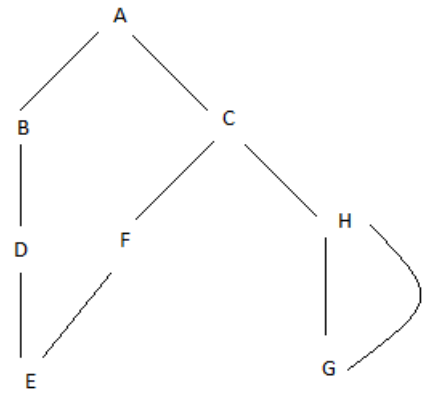

Figure 2.6: Activation tree for isotope A. (containing branching, cross-linking and loops)

cess is called cross-linking. Isotopes 'G' and 'H' have a finite probability of transmuting into one another forming a loop. This forms a complex activation tree with the same isotopes created at different generations (rank) or even forming a loop [54]. Such complex activation trees are difficult to solve, as each isotope is linked to the creation and destruction of other isotopes. The chain solver in ACTYS breaks these large activation trees into long linear chains of isotopes, starting from the initial parent in the material. These chains can be infinite in length. So for practical calculation, these chains are truncated depending upon the transmutation probability to the next isotope. Details of chain truncation can be found in Ref [48]. This implies that the inventory of the isotopes as well as its quantity depends on the value of transmutation coefficient $(\sum_g(\bar{\sigma}_{ij}^g * \Phi^g)/\lambda_{ij})$ of the parent and daughter isotopes.

As the inventory of the isotopes is calculated using the chain method, simultaneously the transmutation term from one isotope to another is stored in a matrix. These terms give the amount of isotope production from each chain. Also, during the formation of the coefficient matrix $\bar{\sigma}_{ij}^g$ and λ_{ij} contribution from each relevant reaction channel or decay channel is stored in a separate matrix. These values are used to give the amount of isotope produced from each channel. For example, ^{63}Cu produces ^{62}Ni via two reaction channel, (n,np) and (n,d), as given below:

$$^{63}\text{Cu} \rightarrow [(n,np) : 9.83E-01][(n,d) : 1.66E-02]^{62}\text{Ni} \tag{2.7}$$

The above example shows a pathway for two competing reactions that would produce the same daughter product but one reaction channel is more likely than the other. Pathways can also illustrate the probability of a nuclear reaction or radioactive decay from the parent to the daughter isotope. This information provides key insights into the nuclear process happening in the material. As an example, a sample pathway generated by ACTYS is given in figure 2.7.

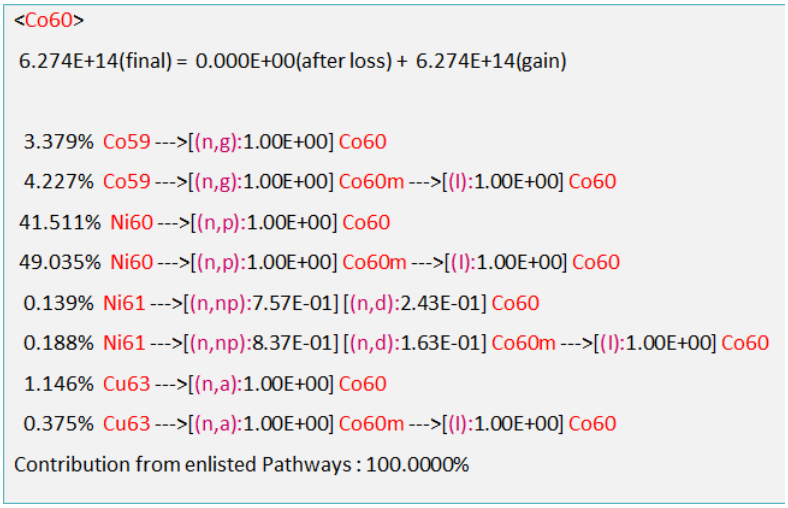

Figure 2.7: Multi-channel pathway generated by ACTYS for ^{60}Co isotope

Three ways to generate pathways are developed in ACTYS:

- The pathways of dominant nuclides responsible for various radiological quantities like Activity, Dose Rate, Decay Heat, and Radwaste Index.
- The pathways of all the significant parents of any desired daughter nuclide.
- The pathways of all the significant daughters of a parent nuclide.

2.3 Benchmarking ACTYS for fusion activation study

ACTYS needs to be benchmarked for fusion activation studies. The benchmark exercise selected for this task is the second international Activation calculation benchmark comparison study, carried out by IAEA in 1994 [21]. Following conditions were listed for the code to qualify as a candidate for fusion activation study:

- Ability of the code to read standard libraries
- Accurate (within 5%) prediction of the amounts of nuclides in the multi-step pathway
- Ability to calculate light nuclides
- Ability to treat isomeric states present in the libraries

To study the ability of the codes, $1kg$ of natural iron and 10^{25} atoms of $Cr-50$ atoms were irradiated for 1 year using the GAM-II 100 group neutron spectrum, as given in figure: 2.8. This spectrum is the typical spectrum evaluated at the first wall fusion with neutron wall loading of $5MW/m2$, and was provided by the benchmark study.

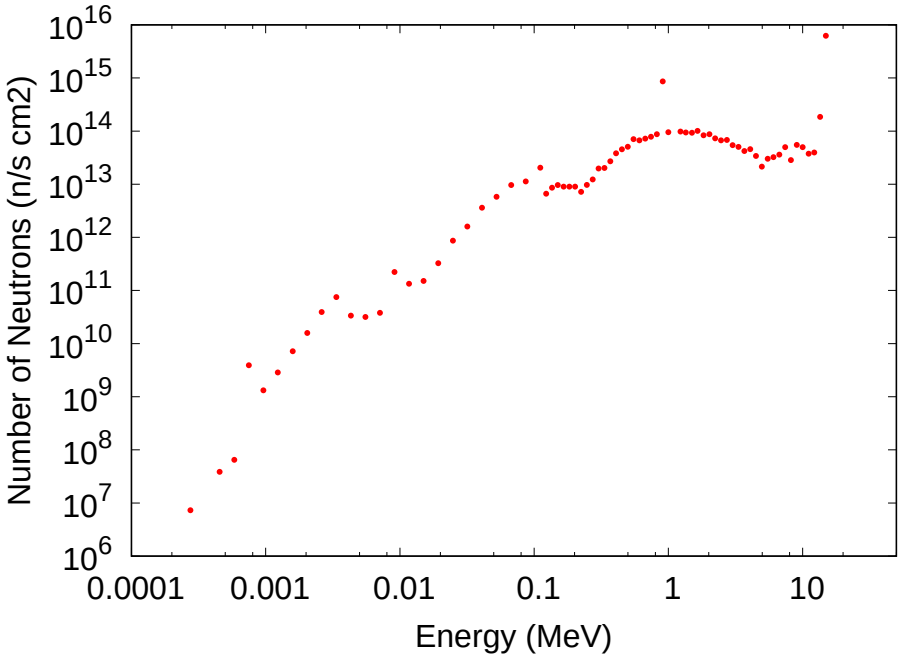

Figure 2.8: Neutron spectrum in 100 group structure (Normalized to 5 MW/m^2 Wall loading

In this study, 11 codes from 7 countries were tested for the suitability of an inventory code for fusion reactor studies. Based on the above criteria and analytical solution, ACAB and FISPACT were found suitable and satisfactory for fusion activation calculation. In order to further validate ACTYS, the same tests were carried out for ACTYS and compared with FISPACT. Results of the above study carried out by ACTYS, along with the relative difference in the values as compared to FISPACT are mentioned below in tables 2.5 and 2.6.

Table 2.5: Results of FENDL activation benchmark study for Activation of 1 Kg of Natural Fe

Isotope	Fispact	Actys	% Diff
H1	2.96694E+22	2.96693E+22	3.37E-04
H2	9.10313E+20	9.10310E+20	3.30E-04
H3	4.08236E+18	4.08235E+18	2.45E-04
He3	1.22354E+17	1.22354E+17	0.00E+00
He4	6.40120E+21	6.40117E+21	4.69E-04
Ti48	1.19553E+17	1.18609E+17	7.90E-01
Ti49	6.09094E+16	6.09080E+16	2.30E-03
V49	1.58625E+16	1.58618E+16	4.41E-03
V50	3.38904E+18	3.38903E+18	2.95E-04
V51	6.41086E+20	6.41085E+20	1.56E-04
Cr50	5.47542E+18	5.47541E+18	1.83E-04
Cr51	7.85402E+19	7.85401E+19	1.27E-04
Cr52	2.52390E+20	2.52389E+20	3.96E-04
Cr53	5.33019E+21	5.33018E+21	1.88E-04
Cr54	1.42708E+21	1.42708E+21	0.00E+00
Mn53	2.14680E+21	2.14680E+21	0.00E+00
Mn54	2.82310E+21	2.82309E+21	3.54E-04
Mn55	1.51918E+22	1.51917E+22	6.58E-04
Mn56	6.50459E+18	6.50456E+18	4.61E-04
Mn57	7.11596E+14	7.11595E+14	1.41E-04
Fe54	6.22810E+23	6.22809E+23	1.61E-04
Fe55	4.88698E+22	4.88697E+22	2.05E-04
Fe56	9.82065E+24	9.82061E+24	4.07E-04
Fe57	2.33155E+23	2.33155E+23	0.00E+00
Fe58	3.02564E+22	3.02564E+22	0.00E+00
Fe59	4.19192E+18	4.19191E+18	2.39E-04
Co59	1.96777E+19	1.96776E+19	5.08E-04
Co60	1.16798E+16	1.16788E+16	8.56E-03
Co60M	4.59589E+11	4.59571E+11	3.92E-03

Table 2.6: Results of FENDL activation benchmark study for Activation of 10^{25} atoms of Cr-50

Isotope	Fispact	Actys	% Diff
H1	8.71976E+22	8.71976E+22	0.00E+00
H2	1.45138E+21	1.45139E+21	6.89E-04
H3	5.29759E+17	5.29761E+17	3.78E-04
He3	1.27515E+17	1.27515E+17	0.00E+00
He4	9.39013E+21	9.39013E+21	0.00E+00
Ti48	1.64709E+20	1.64688E+20	1.27E-02
Ti49	9.65421E+21	9.65412E+21	9.32E-04
V49	2.16046E+22	2.16045E+22	4.63E-04
V50	5.81864E+22	5.81865E+22	1.72E-04
V51	1.06652E+22	1.06652E+22	0.00E+00
Cr50	9.88899E+24	9.88899E+24	0.00E+00
Cr51	1.30259E+21	1.30259E+21	0.00E+00
Cr52	7.56736E+18	7.56723E+18	1.72E-03
Cr53	1.59478E+15	1.59497E+15	1.19E-02
Cr54	5.52446E+11	5.52312E+11	2.43E-02

From the table, it can be concluded that the results of ACTYS are in good agreement (percentage differences are $<< 1\%$) with FISPACT-2007. The above results are also analyzed to see if ACTYS follows the above-given criteria.

- Ability to read standard libraries

  ACTYS has an inbuilt ENDF reader, which can read nuclear reaction cross-sections in 100, 175 and any other user-defined group format.

- Accurate prediction of amounts of the nuclide in multi-step pathways

  All the isotopes produced from multi-step pathways are calculated to very good accuracy as can be seen from the table. As an example of multi-step pathways, V49 pathways are given below:

  $94.234\% \quad Cr50 \rightarrow [(n,np) : 9.51E-01][(n,d) : 4.91E-02] \quad V49$

  $0.944\% \quad Cr50 \rightarrow [(n,p) : 1.00E+00]V50 \rightarrow [(n,2n) : 1.00E+00] \quad V49$

  $4.821\% \quad Cr50 \rightarrow [(n,2n) : 1.00E+00]Cr49 \rightarrow [(b+) : 1.00E+00] \quad V49$

- Production of Light elements

  The light nuclides H1, H2, H3, He3, and He4 are produced by ACTYS via (n,p),

(n,d), (n,t), (n,He3) and (n,α) reactions. The number of atoms of each species produced by ACTYS is in very good agreement with FISPACT-2007.

- Ability to treat isomeric states present in the libraries

  ACTYS is able to read cross-section and decay data from standard libraries for the generation and decay of Co60M, which is an isomeric state of Co60.

As can be seen from the above points, ACTYS fulfills all the criteria required for a code suitable for fusion activation calculations. This validates the code as well as the methods developed for the code like the calculation of inventory (chain method), reading and processing of nuclear data and evaluation of radiological quantities.

2.4 Chapter Summary

In the scope of the thesis, a method was developed to read and extract radioactive decay data from standard nuclear data libraries. The information extracted from these libraries is stored in a file named SPECTRUM. This file contains discrete energies of the decay particles and radiations, condensed into energy groups. ACTYS uses this data during the activation calculation to evaluate radiological quantities like activity, biological dose rate, gamma spectrum, decay heat, and radwaste index. Method to evaluate multi-channel pathways for any isotope undergoing nuclear reaction or radioactive decay is also developed. These pathways depict various chains and reaction/decay channels from which an isotope can be produced along with their respective contributions.

Methods to evaluate radiological quantities are benchmarked against widely accepted activation code FISPACT, using a sample neutron spectrum taken from the reference [38], ITER diagnostics system X-Ray Crystal Spectrometer. All the radiological quantities evaluated, using the models developed in the thesis, are found to be in agreement with the values calculated by FISPACT. The relative difference between the calculation by ACTYS

and FISPACT was found to be less than 0.1% in all cases. ACTYS is also benchmarked against the activation study developed by IAEA. It lists four criteria to check the suitability of any code for fusion activation calculation. The study also designed two activation problems to check the ability of code on the above-mentioned criteria. ACTYS satisfies all the criteria given by IAEA and the results of the activation problem were also found to be in close agreement with that of FISPACT. Thus making ACTYS suitable for fusion activation calculations. In the next chapters using ACTYS linear chain solver as a base code, ACTYS is extended to include multipoint activation algorithm and material optimization scheme. The contents of this chapter along with the chain solver methods developed for ACTYS is published in article ***Ann Nucl Energy*** **2017;107:71-81**.

Chapter 3

Method for Multi-point Activation Calculation

In fusion devices like ITER and DEMO, because of the huge volume and large variation in the composition of structural materials, there will be a high spatial variation of neutron spectrum and hence of the radiological quantities [69, 70, 28, 71]. Plasma diagnostics and other major components are intricately placed inside the tokamak increasing the complexity of the calculations [38]. Therefore detailed and highly spatially resolved activation calculation is required. A trivial way to perform multi-point activation calculation and generate gamma source is to call an activation code sequentially for each mesh [59, 54]. This kind of sequential run is computationally very expensive as it solves the Bateman equation at each mesh independently. For example activation of a mixture of stainless steel(SS) and water(H_2O) for an irradiation period of 3 years with total neutron flux $1.3E11\ cm^{-2}s^{-1}$ takes $\sim 2secs$ for FISPACT or ACTYS. Therefore for 1 million meshes, it is expected to take $\sim 23days$. Hence, to save computation time activation calculation performed by taking the average neutron spectrum for large regions of the device [72]. This, however, may not yield desirable results for radiological quantities if the material is experiencing a large gradient of neutron spectrum as shown in section 4.3. Also,

such calculations may lead to overestimation or underestimation of some important radiological parameters and can cause problems in the selection of shielding material and other preventive measures. A comparison of fine mesh calculation with coarse mesh calculation is given in section: 4.3. Hence to achieve a highly resolved, fast and accurate radiation map, a methodical way of multi-point calculation needs to be developed.

This chapter reports the development of such a tool for fast and accurate activation calculations at all meshes within the geometry in one step. The method is then developed into a computer algorithm and implemented in the code ACTYS-1-GO (Activation analysis in 1 go). The mathematical details for multi-point modified Batemen equation is given in section 3.1, concept developed to perform multipoint activation and its implementation to obtain fast activation calculation is given in section 3.1.1, addition of the method in activation code ACTYS-1-Go is given in section 3.1.2 and, validation exercises and study of the computational performance is given in section 3.2.

3.1 Mathematical model for multi-point activation

As given in chapter 1, the nuclear activation problem is governed by first-order linear differential equation, known as the modified Bateman equation. The coefficient matrix for the equation can be written in a matrix form [47]:

$$\Lambda_{ij} = \lambda_{ij} + \sum_{g} (\sigma_{ij}^{g} * \Phi^{g}) \tag{3.1}$$

where λ_{ij} is the radioactive decay constant of the isotope j to i, σ_{ij}^{g} is the groupwise reaction cross-section of the isotope j to i and Φ^{g} is the groupwise neutron spectrum. The coefficient matrix is usually very stiff[1] and sparse[2] [50]. For example, a matrix constructed for activation calculation of a mixture of stainless steel and water, which is

[1] A matrix is called stiff if the ratio of the largest to smallest eigenvalue is much greater than one.
[2] Sparse matrix is a matrix which contains very few non-zero elements.

irradiated for 3 years with the flux of $1.30E+11\ cm^{-2}s^{-1}$, has a sparsity of 99.99%, as shown in figure 3.1a. In this figure, 2043 is the number of isotopes considered for the activation calculation in the code and hence the size of the coefficient matrix is 2043 $\times$ 2043, the dark region in the matrix corresponds to the non-zero values of the sum of decay constant λ_{ij} and transmutation probability $\sum_g(\sigma_{ij}^g * \Phi^g)$.

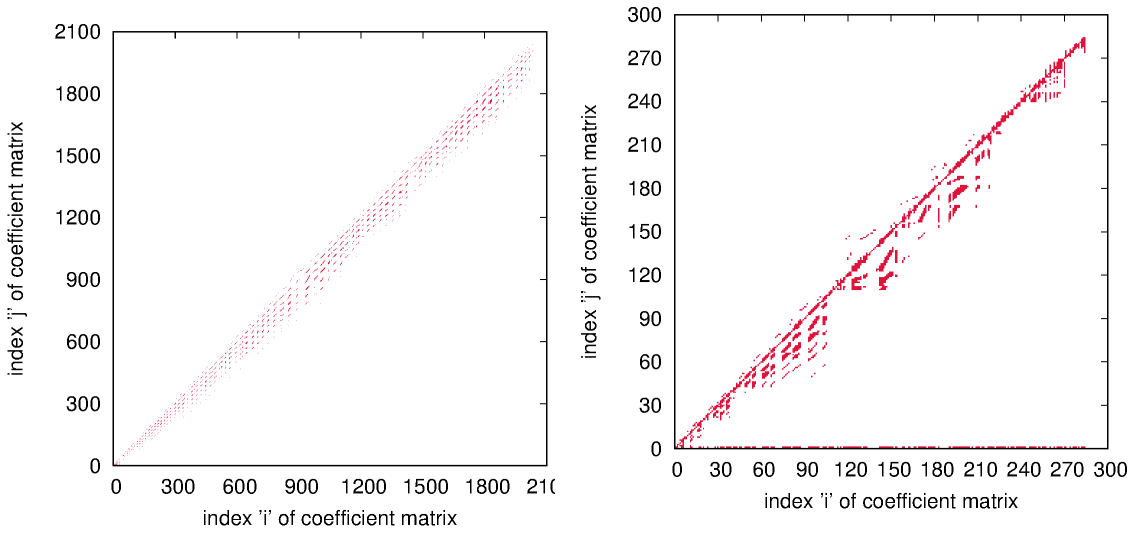

(a) Common Coefficient matrix $\sum_g(\sigma_{ij}^g * \Phi^g)$

(b) Reduced coefficient matrix consisting only the elements in superlist $\sum_g(S_{ij,g} * \Phi^g)$

Figure 3.1: Coefficient matrix generated for activation calculation of mixture of SS and H_2O

3.1.1 Multi-point calculation strategy and Superlist

In multi-point calculations, the entire computational domain of the nuclear device is divided into small sections called meshes. Each mesh contains a different set of material and neutron spectrum, with a general possibility of the same material spanning over various meshes. Imagine a section of a fusion reactor divided into 24 mesh and comprising of 3 different materials. Each color in figure 3.2 corresponds to a different material. So, there are 3 ma-

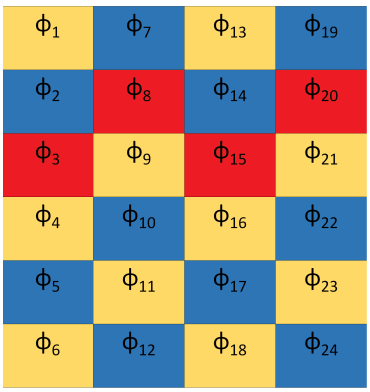

Figure 3.2: An example of different materials located at various meshes in a fusion device. Each color corresponds to different material

terials experiencing 24 different neutron spectrum with ϕ_k as the total neutron flux at that location. The material 'red' is located at 4 different locations with 4 different neutron spectrum (ϕ_3, ϕ_8, ϕ_{15} and ϕ_{20}). From figure 3.2, it can be seen that each mesh will be a unique combination of one neutron spectra and one material. For such a system, the Bateman equation can be rewritten as:

$$\frac{dN_{ik}}{dt} = -(\lambda_{ii} + \sum_g (\sigma_{ii}^g \Phi_k^g))N_{ik} + \sum_{j \neq i} (\lambda_{ij} + \sum_g (\sigma_{ij}^g \Phi_k^g))N_{jk} \tag{3.2}$$

Where ϕ_k^g is the groupwise neutron spectrum at k^{th} mesh and N_{ik} and N_{jk} are isotopic concentrations of parent nuclides at k^{th} mesh. For all the meshes containing the same material, regardless of their location, properties like the material composition, radioactive decay constants, neutron reaction cross-sections, and irradiation scenario will be the same, and only the neutron spectra will be different. A different spectrum would lead to a different coefficient matrix (see eq 3.1) and hence different radiological responses. Dependence of the coefficient matrix on neutron flux and the spectrum makes the multi-point calculation time consuming, as for every mesh a new coefficient matrix needs to be created.

A trivial way to overcome this difficulty is to split the exponential of the coefficient matrix into 2 parts:

$$e^{\Lambda} = e^{-\lambda t} e^{\sigma \phi t} \tag{3.3}$$

And only evaluate the $e^{\sigma \phi t}$ for each mesh run and evaluate $e^{-\lambda t}$ only once for the entire calculation. This, however, is not possible as the matrices $(-\lambda t)$ and $(\sigma \phi t)$ do not commute and so equation 3.3 is not true in case of the coefficient matrix generated for nuclear activation [3].

Hence a new innovative method needs to be developed to efficiently utilize the constants

[3] For two matrices X and Y, if $XY = YX$ then $e^X e^Y = e^{X+Y}$

and the variables at each mesh for activation calculation, according to the equation: 3.2. We know that during the activation process isotopes present in the material form a tree-like structure, as given in figure: 2.6. Also, the production of the next isotope in the tree depends on the value of transmutation coefficient ($\sum_g(\sigma_{ij}^g * \Phi^g)$ and/or decay constant λ_{ij}) of the parent and daughter isotopes, which in turn depends on the incident spectrum (Φ^g). This fact is used to develop the present formulation for multipoint activation calculation. The improvement in multipoint activation is achieved by three steps:

1. creation of a common coefficient matrix
2. creation of a superlist
3. removing sparsity of the coefficient matrix

Creation of common coefficient matrix

In the linear chain method, a cutoff is defined. If the transmutation probability ($\lambda_{ij} + \sum \sigma_{ij}^g \Phi^g$) is greater than the cutoff, the linear chain continues else it is truncated. As the transmutation probability depends on the incident neutron spectrum, so does the termination of a linear chain. This implies that the higher the values in the neutron spectrum, the longer will be the decay-transmutation chain. In the figure: 3.3, assume that there is a material that only contains atoms of isotope 'A'. The corresponding linear chains generated if this material is irradiated with three single group neutron spectrum Φ_1, Φ_2 and Φ_3, with $\Phi_1 < \Phi_2 < \Phi_3$, are given in figure 3.3. Now since $\Phi_2 > \Phi_1$, all the isotopes in the chain created by Φ_1 are contained in the chain produced by Φ_2. Now imagine a set of single group neutron spectrum, Φ_k where $k = 1, 2, ...n$. Another single group neutron spectrum Φ_m can be defined such that $\Phi_m > \Phi_k \; \forall \; k \neq m$. Then the linear chain produced by Φ_m would contain all the isotopes that could be produced from any Φ_k. Thus, for a set of neutron spectrum Φ_k, the isotopes produced by Φ_m is the superset of all the isotopes produced by any individual Φ_k. This would also be true in the case of the groupwise neutron spectrum if Φ_m^g is defined as the spectrum containing groupwise highest value for

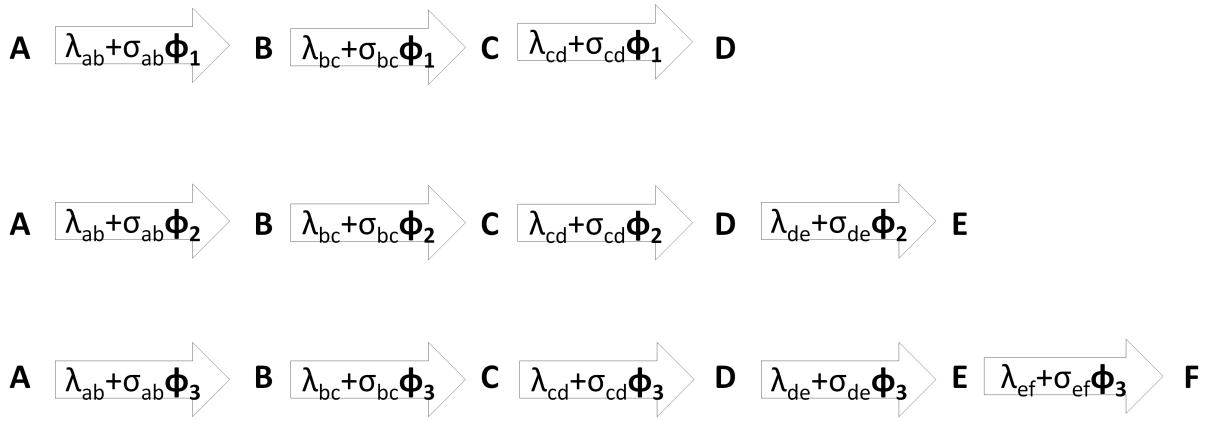

Figure 3.3: Typical chains generated during activation for 3 different single group neutron spectrum

all the Φ_k^g in the set.

During activation calculation, a set of all the neutron spectrum where the material is located is taken as the initial set Φ_k^g and a groupwise highest fictitious spectrum (Φ_m^g) is evaluated from them. The coefficient matrix generated for this fictitious spectrum will be the common coefficient matrix for the material. It would contain all transmutation and decay coefficients required to perform activation calculation at each mesh. This matrix will almost be of the size of any matrix created for the neutron spectrum Φ_k and would still be very sparse. For example in the case of a mixture of stainless steel and water which is irradiated for 3 years with the flux of $1.30E+11\ cm^{-2}s^{-1}$, the size of the common coefficient matrix is 2043×2043 with a sparsity of 99.99%. This step avoids the concurrent and repeated reading of the data library for the meshes with the same material composition but does not significantly reduce the time required for activation calculation. Further reduction in matrix size is achieved by creating the "Superlist".

Generation of Superlist

In the above section, it was demonstrated that the isotopes produced from the groupwise highest spectrum would be the superset of all the isotopes produced by any individual

spectra. The same is true for the list of dominant isotopes [4] of each radiological quantity. For a set of neutron spectrum $\Phi_k^g \; \forall \; k = 1,2,3...n$ and its groupwise highest neutron spectrum Φ_m^g generated from all these Φ_k^g, the list of dominant isotopes of each radiological quantity along with their parents produced from Φ_m^g is a superset of all the dominant isotopes of each radiological quantity along with their parents produced by each individual Φ_k^g. Let the set of dominant isotopes and all intermediate parents generated by Φ_m be $\mathbb{P}$ and that from each Φ_k be $\mathbb{P}_k$. This implies that all elements of each $\mathbb{P}_k$ are contained in $\mathbb{P}$. Hence if activation calculation is only carried out for the isotopes in the set $\mathbb{P}$ at any mesh location k, then it would yield the same radiological quantities as produced by $isotopes \in \mathbb{P}_k$ at that location. This reduces the problem size drastically. The entire set of meshes where the material is located can now be approximated by just the chains and isotopes produced at the groupwise highest spectrum. *All the dominant isotopes of each radiological quantity produced at the groupwise highest spectrum along with their parents are called as the superlist*. This superlist captures the essence of the multipoint point calculation into a small set of isotopes. The activation calculation using only these isotopes at each mesh location would yield accurate radiological quantities for that location. The superlist has the following properties:

- The superlist constructed is unique for every material, irradiation scenario and the set of the mesh where it is located.
- It contains all the dominant isotopes, for every desired radiological response, at each time step in the activation and decay scenario.
- The size of the superlist depends on the radioactive nuclides formed in the material and the number of chains contributing to each dominant isotope. For example, the size of the superlist for low z nuclides like Beryllium is ~ 10, whereas in the case of a complex material like Stainless Steel the size of the superlist can be ~ 300.
- Strictly speaking, the superlist is not a complete set of isotopes for activation calculation. Isotopes and chains that are not contributing towards radiological quantities

[4] Isotopes contributing the most towards any radiological quantity

are missing from the superlist. This may lead to incorrect inventory calculation nevertheless, this inaccuracy is only for less significant or stable isotopes. As these omitted isotopes do not contribute towards any radiological quantities like activity, dose rate, and decay heat, any error in the amount of these isotopes does not affect the nuclear analysis of the device/reactor.

- The list can be modified to include any other parameters as well. The addition of the radiological parameter would not significantly increase the size of the superlist.
- The addition of time steps in the irradiation scenario only slightly increases the time taken for the creation of a superlist.

In the case of activation calculation, the isotopic inventory generated at the groupwise highest neutron spectrum is scanned to identify isotopes contributing towards the desired radiological quantity. All the isotopes contributing up to 99.99999% of the total radiological quantity are considered (for all practical purposes, this is expected to provide the required level of accuracy for all the different neutron spectrum). Now all the chains corresponding to these dominant isotopes are scanned and all the isotopes in this chain, including all the intermediate parents, are stored in the "Superlist". It should be noted that the dominant isotopes are sorted and stored for each time step in the irradiation scenario.

The generation of superlist effectively reduces the size of the coefficient matrix. For example, in the case of a mixture of stainless steel and water which is irradiated for 3 years with the flux of $1.30E+11\ cm^{-2}s^{-1}$, the size of the superlist is 285. All dominant isotopes contributing to activity, dose rate, decay heat, and gamma spectrum are considered for the creation of this superlist. The corresponding coefficient matrix size for only the elements in the superlist will be 285×285, which is much smaller than a common coefficient matrix of size 2043×2043. In this particular example, the matrix size is reduced by 51 times. For N meshes, this translates to a reduction of $N \times 51$. This reduction in matrix size enables 6 times faster calculation of inventory and radiological quantities as compared to the sequential and independent solution at each mesh location. As can be seen from the

figure: 3.1b, the reduced matrix constructed for the isotopes in the superlist still has a sparsity of 96.69%. Further reduction in problem size and hence the computation time is obtained by reducing the sparsity in the coefficient matrix.

Removing sparsity from sigma matrix

The coefficient matrix can be decomposed into two terms L and S defined as $L_{ij} = \lambda_{ij}$ and $S_{ij} = \sum_g (\sigma_{ij}^g * \Phi^g)$. Since at each mesh only the value of neutron spectrum (Φ_k^g) is changing, matrix **L** is constructed only once during the entire activation calculation. Instead of creating matrix S every time for each mesh, it can be further divided into two parts $S^g = \sigma_{ij}^g$ and $F^g = \Phi_k^g$. This breaking of the matrix **S** into S^g and **F** is expected to reduce the sparsity of the coefficient matrix. Any isotope can only produce a few isotopes via neutron-induced reactions. This means that only a small fraction of isotopes in the superlist have finite reaction cross-section σ_{ij}^g values. This implies that only saving groupwise reaction cross-section for possible reactions is equivalent to saving the entire matrix S

$$S_{ij}^g = \sigma_{ij}^g \quad \text{for } i, j \in \text{superlist} \tag{3.4}$$

In the example of stainless steel and water which is irradiated for 3 years with the flux of $1.30E+11\ cm^{-2}s^{-1}$, only 2028 non-zero reaction cross-sections are present for 285 isotopes in the superlist. This constitutes only 2.496% space of the matrix. As only these reactions are responsible for producing dominant isotopes at each mesh where the material is located, only these cross-sections are required for accurate activation calculation. This rewriting of the **S** matrix serves two purposes. Instead of constructing a matrix of size 285×285 for every mesh for a particular material, a two-dimensional array of size $2028 \times N_g$ is stored once, N_g is the number of energy groups for the neutron spectrum. This not only reduces the size of matrix **S** but also creates a matrix S^g that can be used at each and every mesh, without reading the entire cross-section library again and again. This matrix S^g can be multiplied with respective neutron spectrum at each mesh to create the required

coefficient matrix, as given in eq:

$$\Lambda_{ij} = L_{ij} + \sum_{g} (S^g \times F^g) \tag{3.5}$$

This reduces the sparsity of the matrix from $\sim$ 97% to almost zero.

Removing the sparsity of this matrix also reduces memory allocation required for storing large matrix and further reduce the time for a number of read-write operations. This splitting of the matrix without constructing the superlist would not be possible. First, because identifying a S^g that would work for any material is difficult without constructing the superlist first. Second, if the splitting is done after the construction of the common coefficient matrix, the resulting matrix S^g_{ij} would still be very large and computation time for multi-point activation calculation would not be reduced significantly.

In summary, a problem of material at a set of mesh locations can be solved in three steps. Firstly, a common coefficient matrix is created for the material for one irradiation scenario by performing activation calculation at the groupwise highest neutron spectrum. This fictitious spectrum is calculated from all the neutron spectra experienced by the material, by taking the highest value from each group for all the neutron spectra. Secondly, a superlist is created such that it only includes the dominant isotopes contributing to the radiological responses of interest, from the isotopes listed in the common coefficient matrix. Finally, the sparsity of the coefficient matrix is reduced by separating it into two terms so that the common matrix is separated as:

$$L_{ij} = \lambda_{ij} \quad \text{and} \quad S^g = \sigma^g_{ij} \quad \text{for } i, j \in \text{superlist} \tag{3.6}$$

Further, only L_{ij} and S^g for isotopes in the superlist are stored to perform activation calculation for the material and mesh locations where it is located. This formulation is included in the code ACTYS-1-GO for a faster and accurate activation calculation.

3.1.2 Algorithm and implementation in ACTYS-1-GO

The complete formulation for the multipoint activation calculation discussed above is written in this algorithm 2 and implemented in the code ACTYS-1-GO:

Data: λ,σ,Φ_k,material composition, irradiation scenario, and geometry details
sort materials in the device ;
store flux for each location;
construct list of location where material is available;
while *j<# materials* **do**
    For **material(j)**;
    evaluate maximum flux from the set of meshes where material(j) is located;
    run activation calculation at with maximum flux;
    scan for dominant isotopes of each radiological quantity and their parents using multi-channel pathways;
    store the list in superlist array;
    For all the isotopes in superlist, preserve λ_{ij} matrix;
    save parent daughter pair of all the possible reactions in superlist;
    read cross-section data for the pair from the reaction cross-section file;
    save groupwise cross-section data only for relevant reactions $\bar{\sigma}_{ij}^{g}$;
    Data: λ_{ij} matrix, $\bar{\sigma_{ij}}^{g}$ array, flux at each mesh, Material composition, irradiation scenario
    Data: N is the number of mesh
    Result: Gamma Spectrum at each mesh
    initialization;
    while *i<n* **do**
        create matrix $L_{ij} + \sum_g (S_{ij,g} * \Phi^g)$;
        call chain solver using smaller matrix;
        save the final inventory of the isotopes created from activation;
        calculate activity, dose, decay heat the mesh;
        calculate groupwise gamma spectrum for the mesh;
    end
end

Algorithm 2: Multi-Point Activation code

The above algorithm is explained here. For multipoint activation calculation, first, all the material and their corresponding fluxes are sorted and stored in an array. Then for a particular material and set of the mesh where it is located, groupwise highest neutron spectrum is calculated. The material composition and irradiation scenarios are obtained from the input file. Thereafter, a complete activation calculation is performed using this fictitious spectrum. After the final inventory is generated, all the radiological quantities

are evaluated and the dominant isotopes are sorted out. Then pathways for these isotopes are constructed. All the dominant isotopes along with their parents are stored as superlist. For the creation of superlist all the chains contributing towards 99.99999% of the dominant isotope's concentration, are considered. After obtaining the Superlist, decay constants and reaction cross-sections of each isotope in the Superlist is stored in the matrices **L** and **S**. This process takes about ~ 3 to ~ 10 secs depending upon the number isotopes present in the material. Now for activation calculation at each mesh, the groupwise neutron spectrum is multiplied by the groupwise reaction cross-section σ_{ij}^{g} to obtain group averaged reaction cross-section for all the relevant reactions. It is then added to the Λ matrix to obtain the final coefficient matrix at that mesh. After the matrix is obtained, activation calculation is performed at the mesh by linear chain method using the above coefficients only. This same procedure is repeated for the set of meshes where the said material is located. Various radiological quantities like activity, dose, decay heat and gamma spectrum are printed in the output file. Activation calculation carried out only for isotopes listed in superlist, yield radiological quantities with more than 99% accuracy. The inaccuracy of $<< 1\%$ is negligible in comparison with the uncertainty in reaction cross-section values.

3.2 Benchmarking and computational performance

The validation of ACTYS-1-GO is discussed in the sections below.

3.2.1 Comparison and benchmarking with FISPACT

To benchmark ACTYS-1-GO's ability for fast and accurate activation calculation, it is benchmarked against widely accepted activation code FISPACT. Like most of the activation codes used for fusion systems, FISPACT can not perform activation calculations at multiple locations simultaneously. Hence, this benchmarking exercise will also establish

the advantage of ACTYS-1-GO over conventional methods.

FENDL activation benchmark model

To validate the ACTYS-1-GO, the FENDL Activation Benchmark study reported in the article [73] is chosen. The IAEA FENDL Activation Benchmark is based on the reference steel/water shielding blanket design in ITER outline design, including materials from inboard magnet to the outboard vacuum vessel as given in figure 3.4 [73].

The design includes:

- 14 mm thick first wall consisting of 8 mm thick Beryllium coating and 5 mm Copper attached to 1 mm thick Stainless steel.
- Shielding blanket is of 526 mm thickness with alternating layers of 316 SS and water.
- A double-wall Inconel 625 vacuum vessel is used with single size water-cooled 316 SS balls. The vacuum vessel walls are 50 mm thick. A 50 mm thick back shield zone made of lead and boron carbide is used at the back of it. The total vacuum vessel thickness is 455 mm in the inboard region and 619 mm in the outboard region.

The design is a 1-D toroidal cylindrical model with inboard and outboard regions modeled simultaneously. The model includes 51 zones, as given in figure 3.4, which is further divided into 468 intervals. In the study out of these 468 intervals, only 317 are occupied by 9 different materials, rest are void. A uniform 14.1 MeV isotropic neutron source is used in the plasma zone. The neutron spectrum is obtained from reference [74] in the VITAMIN-J 175 group structure for each of the 468 intervals (fine meshes) included in the 51 zones (coarse meshes). These fluxes were calculated in the study using ONEDANT deterministic neutron transport code with a $14.1 MeV$ isotropic neutron source normalized to inboard and outboard neutron wall loading of 1 and 1.5 MW/m^2, respectively.

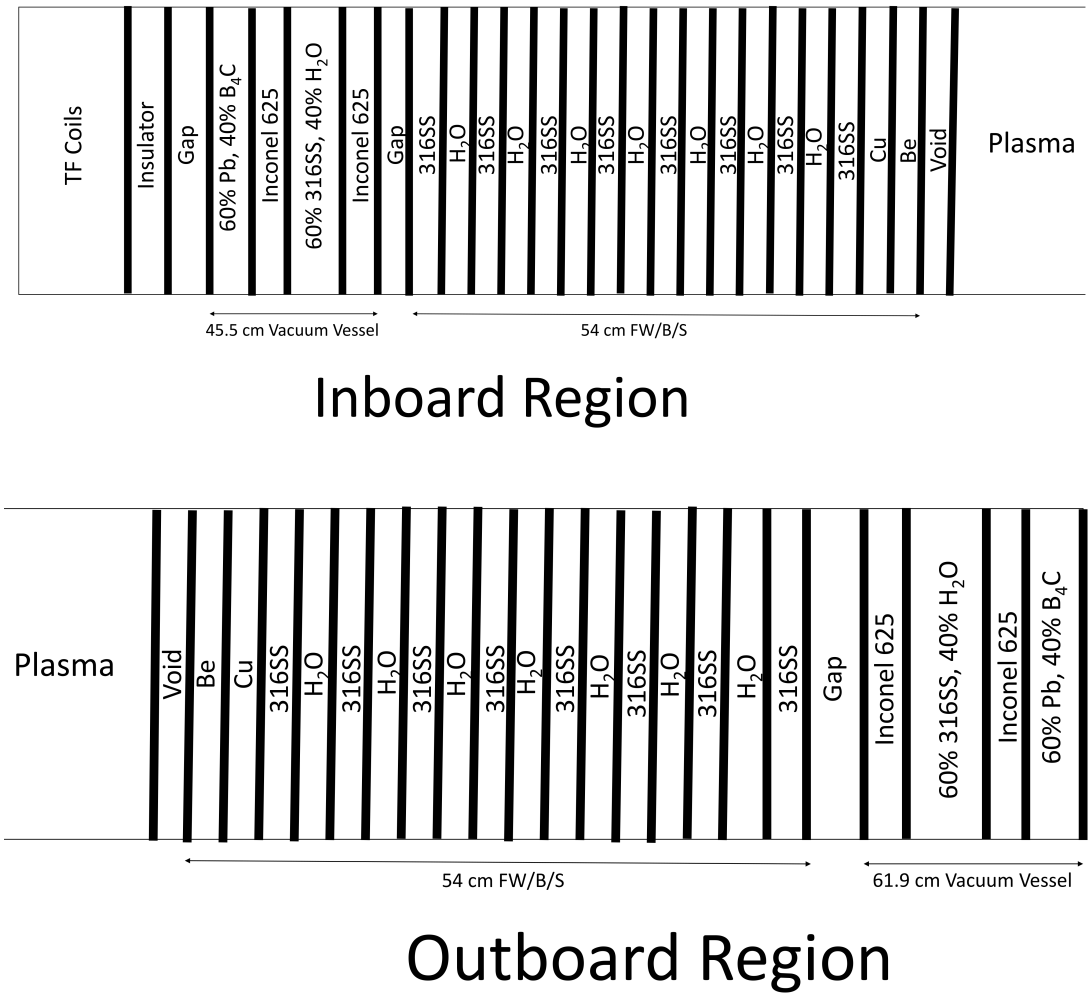

Figure 3.4: Geometrical model of FENDL Activation Benchmark Study based on the reference steel/water shielding blanket design of ITER.

Validation of radiological quantities

To validate the results produced by using the superlist formalism in ACTYS-1-GO, the gamma spectrum generated by ACTYS-1-GO and FISPACT/EASY-2007 is compared. The same data libraries are used for both the codes to avoid any difference that would arise due to data libraries. The activation calculation is performed for 3 years of steady-state irradiation. The 24 group gamma spectrum generated at the end of irradiation for all the 9 materials in the problem (see figure 3.4) is calculated using both FISPACT and ACTYS-1-GO. The results of the validation are given below. The figure: 3.5 shows the relative

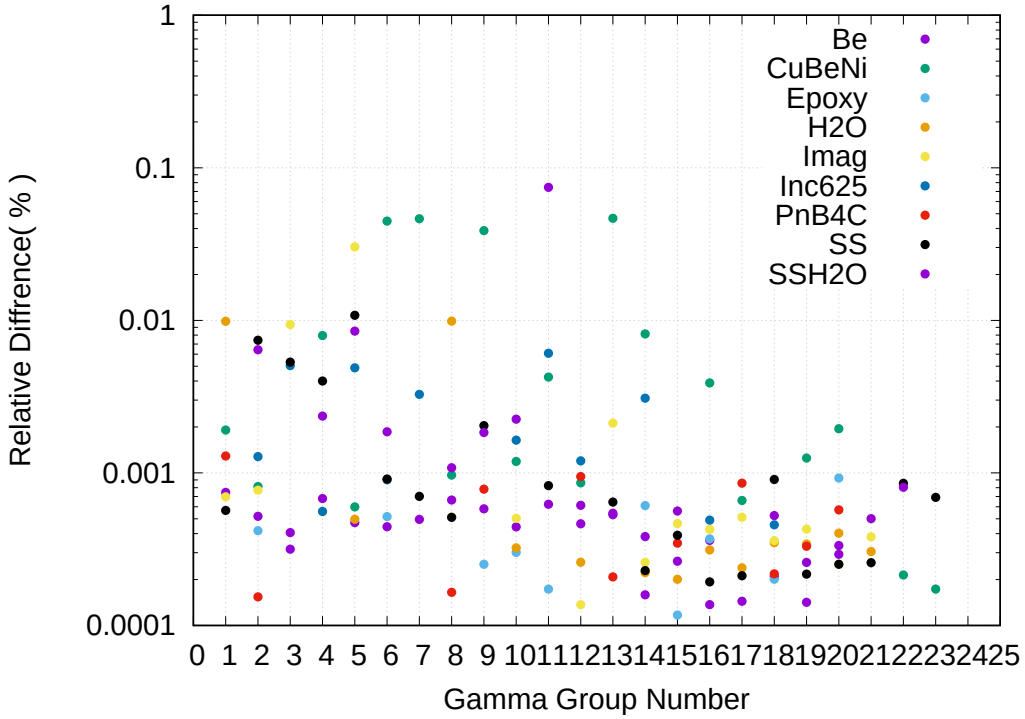

Figure 3.5: Relative difference in 24 group-Gamma Spectrum for all 9 materials considered in the FENDL Activation Benchmark Comparison Study

difference between the 24 gamma spectrum calculated by both the codes at one mesh for every 9 materials. It can be seen that ACTYS-1-GO results are in good agreement with that of FISPACT and the relative differences are less than 0.1%. Further comparison is made for other important radiological quantities like activity, gamma dose rates and decay heat using coarse meshes(51 zones). Activation calculation at each zone, excluding the zone with the void region, is performed using ACTYS-1-GO and FISPACT. The relative differences for each radiological quantity calculated by FISPACT and ACTYS-1-GO are summarized in tables 3.1 and 3.2. The maximum difference is found to be less than 0.25%.

Table 3.1: Relative difference in percentage between ACTYS and FISPACT for radiological responses of all the materials in the coarse mesh

Material	Zone	Relative difference in percentage		
		Activity	Dose rate	Decay heat
Imag	2	4.82E-04	2.03E-01	<1.00E-06
Epoxy	3	<1.00E-06	1.52E-01	<1.00E-06
PbB4C	5	<1.00E-06	1.19E-01	<1.00E-06
PbB4C	51	2.87E-04	1.19E-01	5.73E-04
SSH2O	7	2.41E-03	1.46E-01	1.32E-03
SSH2O	49	2.79E-03	1.47E-01	2.28E-03
SS	10	7.10E-04	2.18E-01	<1.00E-06
SS	12	3.02E-04	2.17E-01	1.49E-04
SS	14	<1.00E-06	2.17E-01	<1.00E-06
SS	16	<1.00E-06	2.17E-01	4.54E-04
SS	18	<1.00E-06	2.17E-01	8.98E-04
SS	20	6.02E-04	2.17E-01	6.68E-04
SS	22	3.12E-04	2.17E-01	6.49E-04
SS	24	7.85E-04	2.17E-01	9.70E-04
SS	32	9.31E-04	2.17E-01	1.76E-03
SS	34	9.39E-04	2.17E-01	9.99E-04
SS	36	8.45E-04	2.17E-01	9.57E-04
SS	38	<1.00E-06	2.18E-01	<1.00E-06
SS	40	2.83E-04	2.18E-01	<1.00E-06
SS	42	<1.00E-06	2.17E-01	<1.00E-06
SS	44	4.18E-04	2.18E-01	2.07E-04
SS	46	<1.00E-06	2.18E-01	<1.00E-06
CuBeNi	25	8.82E-04	1.32E-01	<1.00E-06
CuBeNi	31	7.83E-04	1.32E-01	<1.00E-06
Inc625	6	6.90E-04	2.42E-01	4.59E-03
Inc625	8	1.82E-04	2.42E-01	4.04E-03
Inc625	48	5.31E-04	2.42E-01	4.90E-03
Inc625	50	9.58E-04	2.42E-01	4.86E-03
Be	26	2.51E-02	5.08E-01	8.23E-04
Be	30	2.43E-02	4.96E-01	2.53E-04

Computational Performance

As the main objective of ACTYS-1-GO is to solve complex activation problems quickly, thus, the computational performance between ACTYS-1-GO and sequential FISPACT calculations are performed for the above problem. Here, sequential FISPACT calculation refers to generating input files for each location in the geometry and calling FISPACT executable for that location. The sequential run using FISPACT is also automated, using

Table 3.2: Relative difference in percentage between ACTYS and FISPACT for radiological responses of all the materials in the coarse mesh [Cont.]

Material	Zone	Relative difference in percentage		
		Activity	Dose rate	Decay heat
H2O	11	6.50E-04	2.90E-02	<1.00E-06
H2O	13	2.54E-04	2.87E-02	2.17E-04
H2O	15	<1.00E-06	2.92E-02	<1.00E-06
H2O	17	<1.00E-06	2.89E-02	<1.00E-06
H2O	19	<1.00E-06	2.89E-02	<1.00E-06
H2O	21	<1.00E-06	2.91E-02	2.18E-04
H2O	23	3.81E-04	2.87E-02	3.26E-04
H2O	33	<1.00E-06	2.94E-02	7.33E-04
H2O	35	<1.00E-06	2.89E-02	1.38E-04
H2O	37	<1.00E-06	2.90E-02	2.92E-04
H2O	39	2.36E-04	2.90E-02	2.02E-04
H2O	41	4.08E-04	2.88E-02	3.49E-04
H2O	43	1.71E-04	2.88E-02	<1.00E-06
H2O	45	<1.00E-06	2.91E-02	<1.00E-06

FORTRAN subroutine created in the scope of the thesis. The calculations with both the activation codes are carried out on a Dell desktop with Intel Core i5 CPU 650 with a clock speed of 3.20GHz and 4Gb RAM.

Activation calculation is performed at every 317 intervals of the FENDL Activation Benchmark study, which contains one of the 9 materials, using ACTYS-1-Go and FISPACT. It is found that ACTYS-1-GO is 16 times faster than the sequential calculations of FISPACT. The total computation time of 31.73 seconds was taken by ACTYS-1-GO, out of which 50% was used for creating superlist for all the 9 materials. As the superlist is created only once for a given material, further improvement in the performance of ACTYS-1-GO is expected if the number of meshes increases. To understand this effect we have repeated calculations at each interval, thus fictitiously increasing the number of meshes. Four more activation calculations are performed by repeating the neutron spectrum available for 317 intervals 10, 100, 1000 and 3000 times. The ratio of speeds between FISPACT sequential calculations and ACTYS-1-GO is given in figure 3.6. From figure 3.6, it can be seen that initially, the performance of ACTYS-1-GO increases rapidly with the number of meshes and then start saturating around one million meshes. This happens because a fixed amount

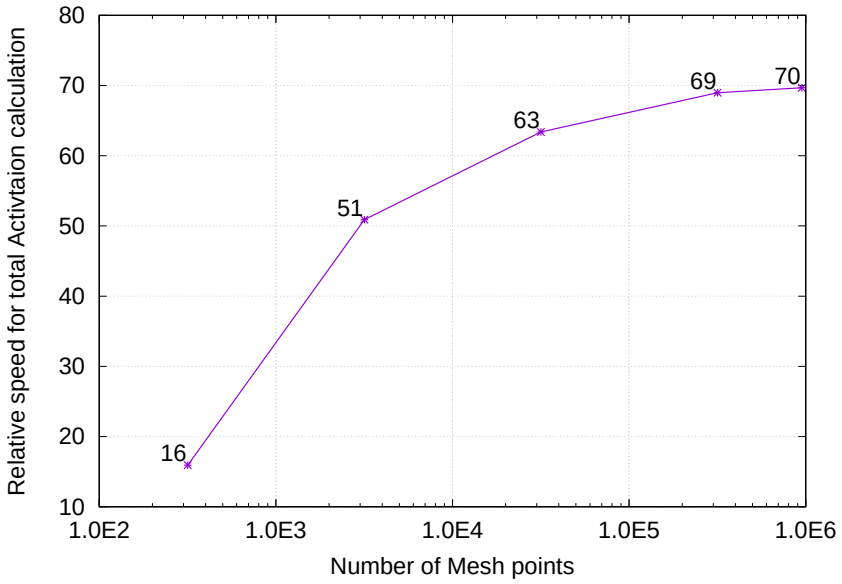

Figure 3.6: Ratio of computational time between ACTYS-1-Go and FISPACT for activation calculation

of time is spent on the creation of the superlist for each material at the beginning of the activation run. Once the superlist is created for the material, the computational time is only the time taken by activation calculation for each mesh. So, as the number of meshes increases the computational time will be almost equal to the time taken for activation calculation at each mesh and the speed would saturate. At around 1 million meshes the ACTYS performs 70 times faster than the FISPACT sequential calculations. For $\sim$ 1 million meshes ACTYS-1-GO takes around 6 hours while sequential FISPACT calculations take around 17 days. More precisely, ACTYS-1-GO solves $\sim$44.23 meshes/second while FISPACT solves 0.63 mesh in a second. Thus it can be concluded that ACTYS-1-GO takes at the most 1.4% of the computation time as compared to sequential activation codes for evaluating activation calculations at 1 million meshes, with more than 99% accuracy.

3.2.2 Comparison and benchmarking with ATTILA-FORNAX solver

Results of activation calculation obtained from ACTYS-1-Go can not be compared with FORNAX as both the codes uses different data libraries for nuclear recation cross-section

and radioactive decay. Moreover, FORNAX has data for only 1300 isotopes whereas ACTYS-1-GO library contains close to 3500 isotopes. However a comparison of the speed of ACTYS-1-GO is done with ATTILA-FORNAX solver. 'ITER Shutdown Dose Rate Benchmarking problem' is used as the reference model to compare the computational performance of ACTYS-1-GO and Fornax. This model roughly mimics the upper port plug of ITER with a gap for the streaming of radiation and particle for diagnostic equipment. A detailed description of the problem is given in Ref [75], a brief description of immediate reference is given below in figure 3.7.

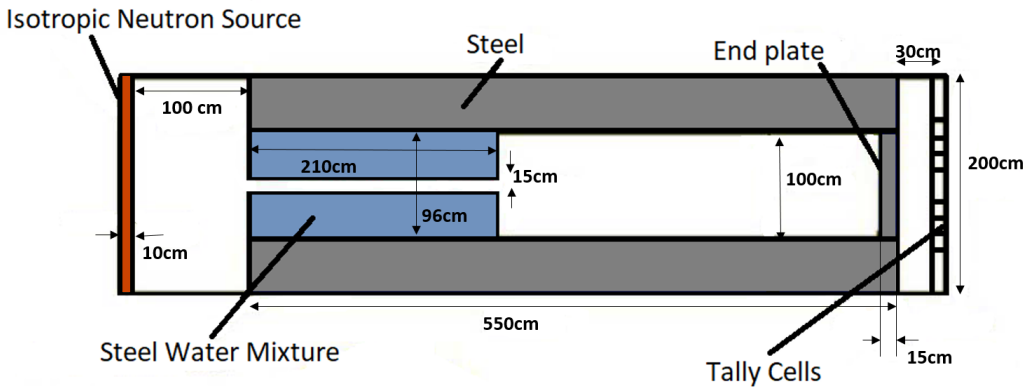

Figure 3.7: Cross-sectional view of the Cylindrical model, for ITER Shutdown Dose Rate Benchmark Study with geometrical specifications and material description.

The model consists of a 7 m long cylinder of radius 1 m made of 100% stainless steel. It has a central straight streaming path of radius 0.075 m. A 0.48 m radius stainless steel water $(80\% - 20\%)$ shielding zone is included which surrounds the central streaming path and has a length of 2.1 m. The outer cylinder has a rear stainless steel plate of thickness 0.15 m, here referred to as the *endplate*. There is a 0.02 m straight gap between the outer and inner shielding zones which extends all the way from one end to another. There is a large cavity of length 3.25 m between the back of the stainless steel-water shield and the rear plate. A 14.1 MeV isotropic neutron source is represented by a disk region placed at a distance of 0.1 m from the front edge which has a thickness of 0.01 m. Four tally discs (DT1, DT2, DT3, and DT4) of thickness 0.1 m each are are placed in the air at a distance of 0.3 m from the endplate. The inner-outer radii of each disc are: 0.45 m-0.6 m, 0.3

m-0.45 m, 0.15 m-0.3 m and 0.0 m-0.15 m respectively.

Table 3.3: Irradiation scenario for comparison study between ACTYS-1-GO and ATTILA-Fornax

Source Strength (n/s)	Irradiation scenario
1.00E+20	3 years
0.00E+00	6 months
1.00E+20	2 Years
0.00E+00	1 month

The model is divided into tetrahedral meshes and the endplate consists of 2085 meshes. The neutron spectrum for this model is calculated in 175 energy group structure using the ATTILA transport code. The detailed activation calculation is performed for 2085 meshes in the endplate at a workstation with intel Xenon CPU E5 2650 V3 @ 2.3 GHz with a RAM of 128 GigaByte. A comparison between the computation speed of ACTYS-1-GO and FORNAX is carried. Attila output file reports the speed of activation calculation by FORNAX to be 185 meshes/seconds. This excludes the time taken by Attila for read-write operations and calling FORNAX multiple times. The speed of ACTYS-1-GO is obtained to be 347 meshes/second. This implies that ACTYS-1-GO is significantly faster than FORNAX, moreover, ACTYS-1-GO performs activation calculations using the latest nuclear data libraries making ACTYS-1-GO fast and more suitable for multipoint activation calculation.

It should be noted that nuclear activation calculations are sometimes performed in conjunction with transport codes [76, 41, 59, 42]. Although transport code makes up for a large portion of computation time, in many cases the computation time for activation calculation is also significant. In the Ref [77], the nuclear analysis of the Neutral Beam Injection(NBI) system for ITER is carried out for approximately 30,000 cells. It can be noted from Ref [77], MCNP run takes about 5 days on 128 cores to complete. Thereafter it takes 24 hours on 64 cores for MCR2S code to perform activation calculation. The time taken by photon simulation is another 5 days on 64 cores. This implies that the time taken for the activation calculation is $\approx$ 10% of the total time taken for nuclear analysis

of the system. Any reduction in computational time would reduce the calculation period significantly. For such cases, ACTYS-1-GO is expected to reduce the computational time for activation calculations. Furthermore, the results of activation calculations are useful for shielding calculations and radwaste classification. Thus, any reduction in time would allow for better analysis time.

3.3 Chapter Summary

In the present work, the modified Bateman equations are rewritten for activation calculation at multiple locations and are simplified by developing the concept of 'superlist'. It is shown that there exists a set of isotopes ($\mathbb{P}$) uniquely defined for each material and each set of incident neutron spectrum, such that nuclear responses produced from $N_{pk}(t)$ (p $\in$ $\mathbb{P}$) would be equivalent to nuclear responses produced from $N_{ik}(t)$ (i $\in$ set of all possible isotopes that can be created at each mesh). For a given material, this set is identified as the set of all the dominant isotopes for each radiological quantity evaluated at the group-wise highest neutron spectrum for the set of all the neutron spectrum experienced by the material. The matrices $L_{ij} = \lambda_{ij}$ and $S^g_{ij} = \sigma^g_{ij}$ are constructed for all the non-zero values of the coefficients of isotopes in the superlist and are used to solve multi-point activation at each location independently. This reduction in problem size enables the linear chain solver to evaluate the final isotopic concentration and radiological quantities in just 1.5% of the time it would take to solve the activation equation individually for each isotope at each location. Proper validation of the mathematical formulation with realistic problems like ITER radial buildup model is performed and the concept of superlist is found to be satisfactory for approximating the fusion activation equations with more than 99% accuracy in radiological quantities. This improvement in computational times allows for better analysis time, accurate design parameters and fine mesh calculation. All of these would yield a better radiological map for the fusion reactor/device. The details of fine mesh calculation using ACTYS-1-GO are elaborated in section 4.3. The contents of this

chapter are published in the article ***Fusion Eng Des.*** **2017;122**.

Chapter 4

ACTYS-ASG, a tool for faster ShutDown Dose Rate calculations

Gamma rays are emitted through neutron interactions during the operation phase and emitted by radioactive decay of activated material during operation and shutdown phase. Since gamma rays are ionizing radiation that can travel large distances without losing much energy, these radiations contribute towards the biological dose received by living tissue in and around the nuclear device [38, 39]. The biological dose rate produced from gamma emitted from activated material during the shutdown phase is referred to as the ShutDown Dose Rate (SDDR) and is one of the major concerns for reactor design. Accurate assessment of SDDR is needed to demonstrate that the operation, maintenance, and waste disposal planning will meet worker safety requirements [15, 16, 69, 78]. A detailed assessment of SDDR evaluation is especially critical for the personnel to safely access nuclear facilities during maintenance and repairs. The complex geometry of fusion reactors makes it difficult to accurately map the radiation field generated in the device. Thus a fast and reliable tool is required for estimating SDDR and to achieve better design parameters for fusion devices.

In order to calculate SDDR, two methods are used, Direct One-Step method (D1S) and

Rigorous Two-Step method (R2S) [79, 80, 81]. The D1S method estimates the decay gamma spectrum and thus evaluates SDDR in one coupled neutron-photon transport calculation. The method assumes that only the isotopes produced during the interaction of neutrons with a stable isotope, in the initial material composition, would emit gammas. Thus D1S method only considers a one-step reaction for a limited number of isotopes that would produce long-lived isotopes. The major disadvantage of the D1S method is that it does not consider multi-step reactions. If any long-lived isotope is produced through a multi-step reaction, SSDR calculation using the D1S method would yield incorrect results. Moreover, since only long-lived isotopes are considered, the dose rate produced by short-lived isotopes are neglected. Thus D1S method, would not yield correct results for dose rates just after the neutron source is cutoff. Such estimates are required for maintenance and accident scenarios. To overcome this, the Rigorous-2-Step method is used. R2S method performs two transport calculations, one for neutron and one for photon, and an intermediate activation calculation. In the first transport calculation, neutrons emitted from the core are tracked throughout the device using transport codes like MCNP or ATTILA. These codes generate the neutron spectrum at various locations in the device as output. Now using these neutron spectra as input, activation calculation simulates all the possible reactions and chains formed by isotopes during irradiation and decay periods. This is achieved by dedicated activation codes like FISPACT, ALARA, ACTYS, ACTYS-1-GO, giving gamma spectrum and other radiological quantities as the output. Since gamma photons do not deposit their energy locally in the material, a second transport calculation is done to evaluate the energy deposited by the decay gamma and hence evaluate SDDR. Thus for performing R2S, one to one coupling of a transport code (like MCNP, ATTILA) and activation code (like ACTYS-1-GO, FISPACT, ALARA)is warranted[41, 42, 48, 82, 46, 54, 53, 76, 59, 83].

As we know, huge volume and large variation in the composition of structural materials in fusion devices leads to a high spatial variation of activation and corresponding radiation fields generated by the activated materials. The conventional method to perform activation

calculation and gamma source generation under the R2S scheme for many large devices is to call an activation code sequentially for each mesh [59, 83]. As shown in the previous chapter, such sequential calculations are computationally expensive and thus, a dedicated algorithm is required to effectively couple radiation transport codes like MCNP or ATTILA, with fast multipoint activation code ACTYS-1-GO. To achieve this, ACTYS-ASG (ACTYS- Activation Source Generator) is developed. It couples ACTYS-1-GO with the transport code ATTILA, under the R2S scheme. The coupling strategy and validation of ACTYS-ASG are discussed in this chapter. Section 4.1 describes the ACTYS-ASG code system by systematically defining gamma source generation in ACTYS-1-GO and then discussing the coupling strategy with ATTILA. Validation exercise is carried out using the ITER Shutdown Benchmark problem and is elaborated in section 4.2. Using the same benchmark model as an example, the importance of fine mesh calculation and the ability of ACTYS-1-GO to achieve it is discussed in section 4.6a.

4.1 ACTYS-ASG code system

The activated fusion materials emit ionizing radiation like gamma radiation. Activation source or gamma source for these materials is defined as the groupwise gamma spectrum produced by them and is given by:

$$S_g = \sum_i (\sum_j I_j * E_j) A_i \quad \forall \quad E_j \in group \quad g \tag{4.1}$$

Where I_j and E_j is the intensity and the energy of emitted gamma rays from isotope 'i' with radioactivity A_i. All the gamma lines emitted in the energy group 'g' contribute towards the gamma source 'S_g'. ACTYS-1-GO can generate gamma source in any user desired group structure. The only constraint is that to achieve coupling for a given problem both ATTILA and ACTYS-1-GO should use the same group structure for the sake of compatibility and consistency. Activation source is generated by the ACTYS-1-GO

with the help of the latest ENDF libraries for Radiation Decay Data (RDD) and nuclear reaction cross-sections [65]. The SDDR is given using the formula:

$$SDDR = \sum_{g} S_g * \sigma_d \tag{4.2}$$

where σ_d is the flux-to-dose-rate conversion factors [84].

As discussed in the section: 1.3.3, ATTILA has a built-in activation capability based on the R2S formalism called the FORNAX transmutation module. Atom density calculated by FORNAX can be used directly by the ATTILA's activation source generator (ASG) to produce an activation source file. However, FORNAX has a limited data library consisting of only 1312 isotopes and considers a limited number of nuclear reactions for transmutation. This creates a discrepancy of about 15% for some results between FORNAX and other detailed activation codes [85].

ACTYS-ASG is a set of FORTRAN subroutines that couples the outputs and inputs of deterministic transport code ATTILA with the multipoint activation code ACTYS-1-GO. The coupling is achieved using the mesh-based R2S methodology substituting FORNAX with ACTYS-1-GO. The detailed working of the code is given below in figure: 4.1.

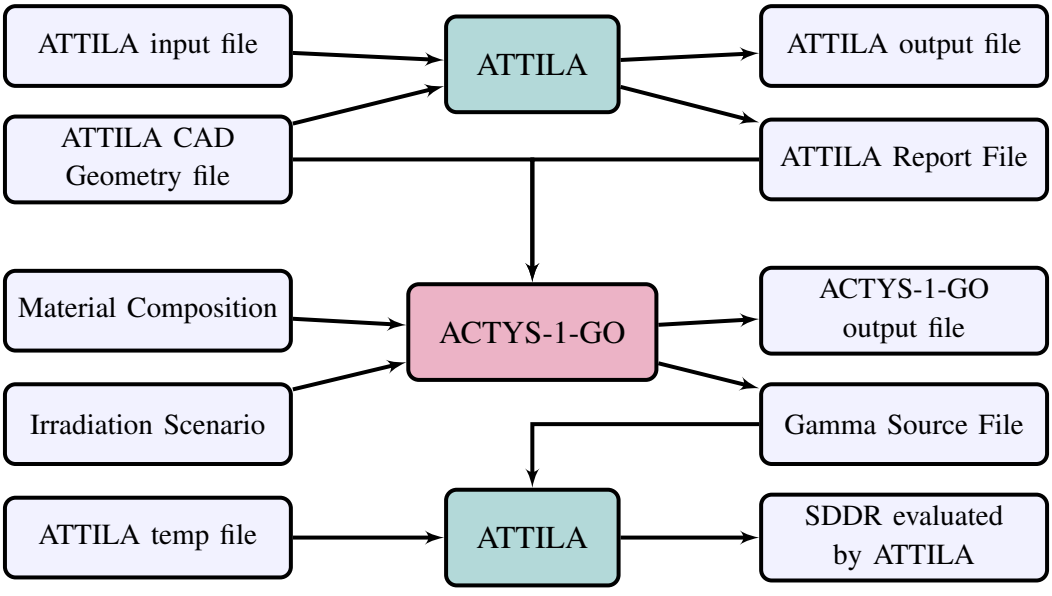

Figure 4.1: Systematic steps in the execution of ACTYS-ASG code systems

In the first transport step, the neutron flux is determined in the regions where activation calculations have to be performed. This step generates a spatial neutron field, discretized in required energy bins, and is provided as input data to ACTYS-1-GO for activation calculation. The coupling between the transport and activation code is achieved by a built-in FORTRAN subroutine inside ACTYS-1-GO. The subroutine reads the material description from the ATTILA input file, mesh specifications from the CAD geometry file (which contains mesh location and co-ordinates of each tetrahedral mesh), and the neutron spectrum from the Attila output file. The geometric details enable the subroutine to store the position of each mesh and calculate its volume. Based on the volume and density provided in the input file, the mass of the material at each mesh point is calculated for the subsequent activation calculation and gamma source generation. It also recasts the neutron flux and material description in the required formats for the use of ACTYS-1-GO. The activation calculation is then performed using a specified irradiation scenario and material composition at each mesh point. Once the activation calculations are complete, a mesh-based decay gamma source is evaluated. The gamma source is calculated and discretized in the required energy bins using the equation: 4.1. Since each mesh point in the given problem is activated with its corresponding neutron spectrum, the resulting gamma source has the same spatial resolution as the neutron spectrum. The mesh-based gamma source thus generated from activation calculation is saved in a file, which is in the format of ATTILA source file definition. The file is then read by ATTILA and is used for a subsequent gamma transport calculation and SDDR evaluation.

Along with the gamma source file, a plot file is also created by ACTYS-1-GO. This file contains the mesh location and various radiological quantities calculated at each mesh point at every time step in the irradiation scenario. This file can be plotted using the PYTHON script which is inbuilt in ACTYS-1-GO. The script also generates a video of the time evolution of the radiological quantities at each mesh in the activated region. These plot files when view together gives a pretty clear picture of the spatial and temporal variation of any radiological quantity.

4.2 Results and Validation

'ITER Shutdown Dose Rate Benchmark Problem' is used as the reference model to evaluate and demonstrate the performance of ACTYS-ASG [75]. The details of the model are given in section 3.2.2. The quarter geometry of the model is given in the figure below for immediate reference.

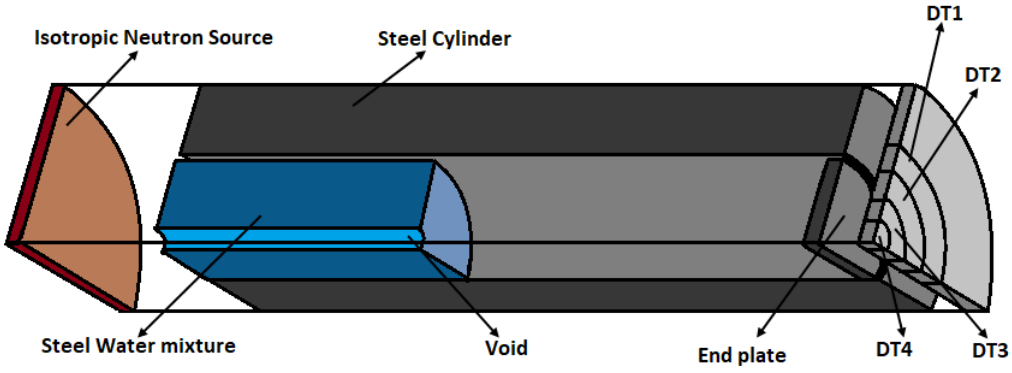

Figure 4.2: Quarter geometry of the model that is used for neutron transport and subsequent SDDR calculation.

The model has cylindrical symmetry, therefore, transport calculation is performed on the quarter cylinder as shown in figure 4.2. The model is divided into more than 50 thousand fine meshes and a biased quadrature with an S_N order of 32 is used in the Attila transport calculations. The endplate consists of 2085 mesh points out of 51858 mesh points generated in the entire quarter geometry. The transport calculation yields 175 group neutron spectrum at each mesh in the geometry. After the neutron spectrum is generated, activation calculations using ACTYS-1-GO and ATTILA-FORNAX at the endplate are performed. The activation of the endplate considering 2085 meshes, stainless steel composition, and SA2 irradiation scenario, is performed and is given in table 2.4. A comparison of total gamma source strength at the endplate, calculated by ACTYS-ASG using the JEFF radiation decay data library and FORNAX is shown in figure 4.3.

After the Gamma source is generated from the activation calculation, a second transport run is performed to obtain the ShutDown Dose Rate(SDDR) at various tally cells in the

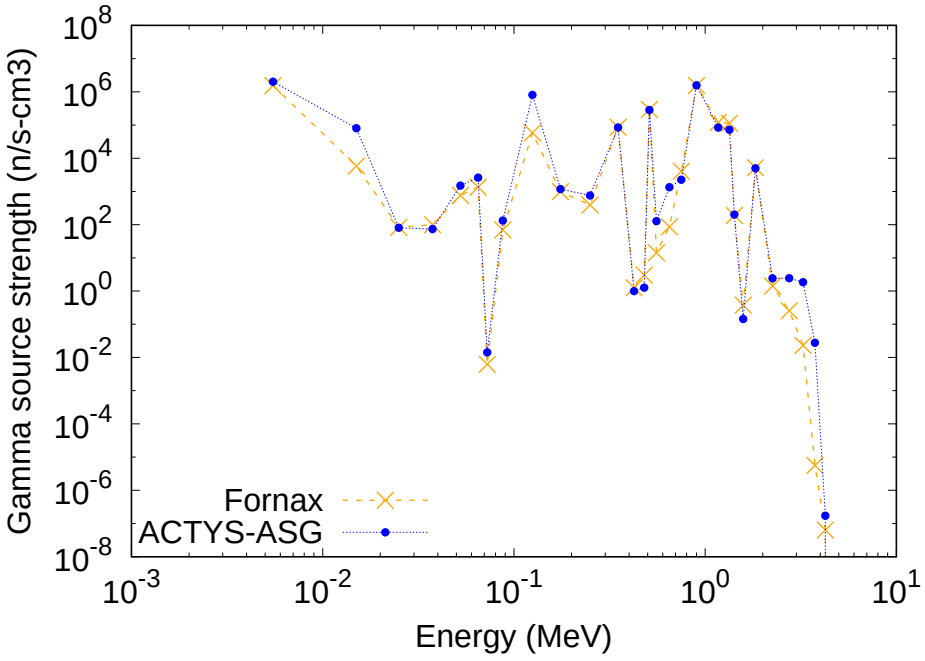

Figure 4.3: A comparison of total Group-wise gamma source strength generated by ACTYS-ASG and FORNAX at the endplate of the ITER shutdown dose rate benchmark model

model labeled as DT1, DT2, DT3, and DT4 in figure 4.2. The SDDR is evaluated at tally cells using ACTYS-ASG and FORNAX modules are tabulated in the table: 4.1.

Table 4.1: Comparison of SDDR values in the units $\mu Sv/hr$ calculated at Tally cells by ATTILA-FORNAX and by ACTYS-ASG code system

	ATTILA-FORNAX-ATTILA	ATTILA-ACTYS-ASG-ATTILA	Relative Difference
DT1	4.86778E+03	4.53349E+03	6.87%
DT2	7.80865E+03	7.27329E+03	6.86%
DT3	1.16690E+04	1.09295E+04	6.34%
DT4	1.46944E+04	1.38210E+04	5.94%

It can be seen clearly that the results of ACTYS-ASG and FORNAX produce similar results for gamma source and SDDR. The difference in the values is because of the difference in the nuclear reaction cross-section libraries used by ACTYS-1-GO and FORNAX. A similar difference has been observed between ATTILA-FORNAX and FISPACT and is reported in the article: [85]. FISPACT also attributes the discrepancy in dose rate due to the difference in data libraries [85]. Due to the unavailability of data libraries used by

ATTILA, authors could not make a proper comparison between dose rates obtained by ACTYS-1-GO and FORNAX.

It is important to note that the total time taken by the FORNAX module is 1805 seconds whereas ACTYS-ASG took only 255.31 seconds. Which makes ACTYS-ASG 7 times faster than FORNAX. In totality, ACTYS-ASG can be used as a substitution for FORNAX, because of its more advanced libraries, better computation performance, and flexibility. Such a tool is very useful at a domestic scale as some commercial activation codes do not provide (or provide limited) nuclear data libraries for activation calculation.

Another advantage of ACTYS-1-GO is the generation of plot files. These graphs represent the enormous data produced during the activation calculation in an easily understandable format. An example of the plots generated by ACTYS-1-GO is given in figure 4.4. These plots are for the contact dose rate calculated at each mesh location for stainless steel after being irradiated with the SA2 scenario as given in problem 4.2. The color bar indicates the values of contact dose rate with the highest value (dark red) in the bar being the highest dose value produced at any mesh during the activation process and the lowest value (dark blue) being the background dose rate. These plots show, how the dose rate slowly goes to background level after the shutdown of the device.

Figure 4.4: Contact dose rate(Sv/hr) calculated at each 2085 mesh location at various time steps after shutdown shutdown

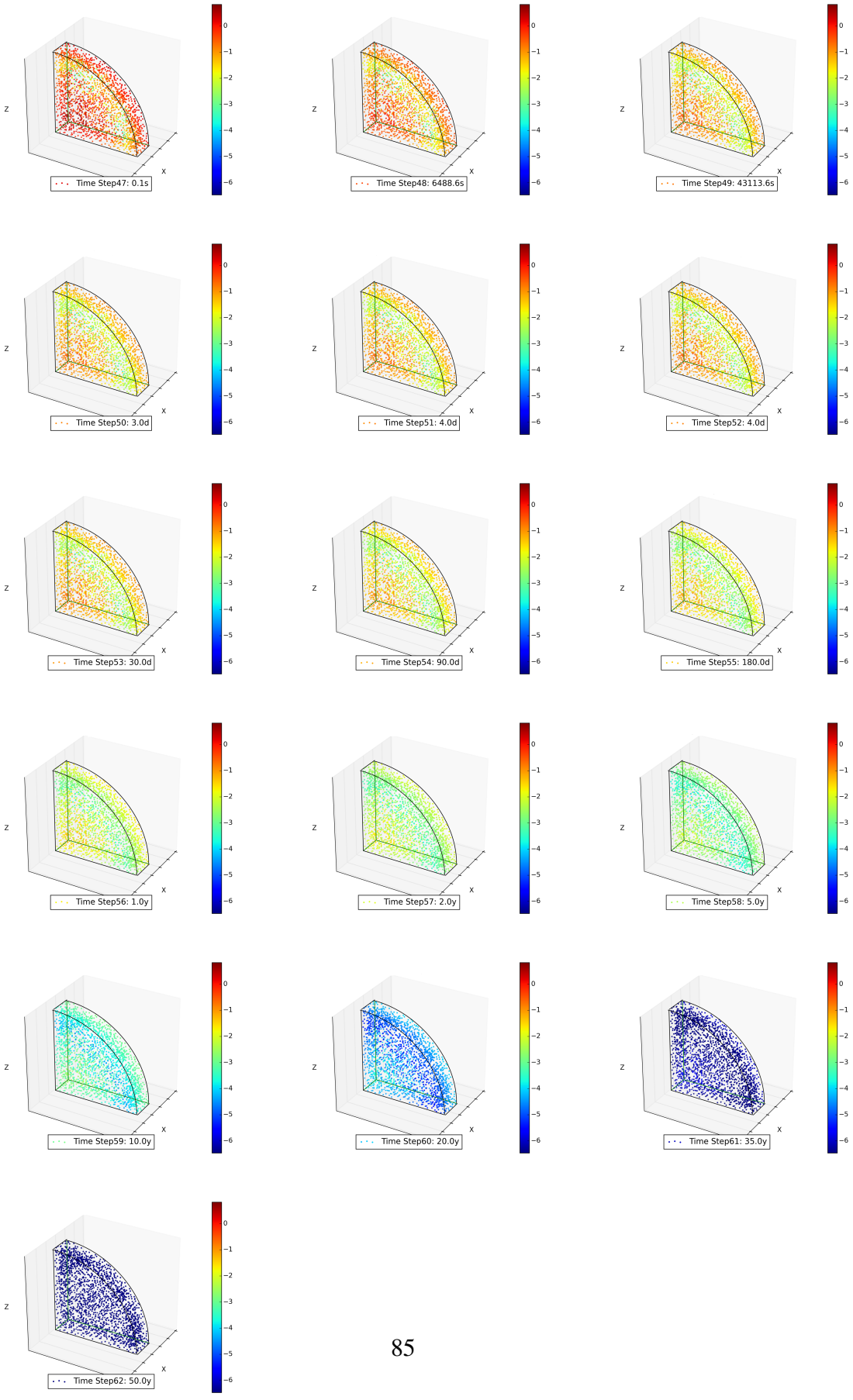

4.3 Importance of fine mesh calculations in fusion relevant systems

It has been demonstrated that ACTYS-1-GO can perform fast nuclear activation calculations for complex and larger nuclear machines like ITER, DEMO and future fusion reactors. Conventionally coarse meshing is used to perform activation calculations for large systems. Coarse mesh activation calculation means performing a calculation over a larger region of geometry which would otherwise contain variations in the neutron spectrum. This happens due to large computation time that is spent on transport and activation calculation. The article [72], reports rad-waste calculation for ITER using MCNP (for neutron transport) and FISPACT (for activation calculations). A total of 3500 cells (meshes) were used for the analysis. Considering the larger size and number of different components in the reactor, increasing the number of meshes for calculation would only enhance the design freedom for the reactor. This fine mesh calculation could be easily obtained by ACTYS-1-GO. A detailed analysis and discussion of the difference in results between the coarse mesh and fine mesh calculations for typical fusion relevant problems are discussed here.

4.3.1 Model-1: FENDL Activation Benchmark Study

In this section, the difference in results of various radiological quantities with coarse and fine meshes is examined for the FENDL activation benchmarking problem, discussed in section 3.2.1. In this problem, we have selected an inboard magnet placed at zone-2 to understand the difference between activation calculation performed at the coarse mesh and fine meshes. In the model, this zone is divided into 90 intervals and a separate neutron spectrum is available for each interval and the zone. The neutron spectrum at the zone is the average of the neutron spectrum at each interval. Activation calculation is carried out using the neutron spectrum given for the zone and for its constituent intervals. Various

radiological quantities like activity, dose, nuclear heat and gamma spectrum (in 24 groups) are calculated using ACTYS-1-GO for both the cases. The results are summarized in figures 4.5a to 4.5d.

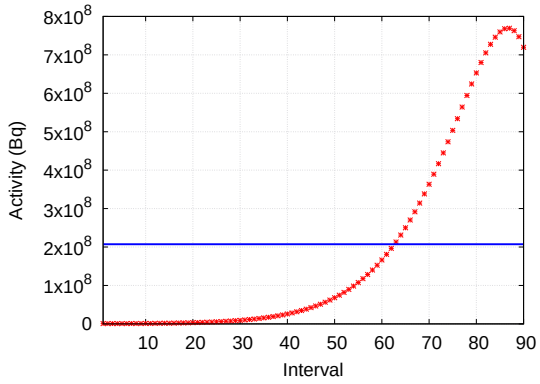

(a) Activity profile inside Zone 2

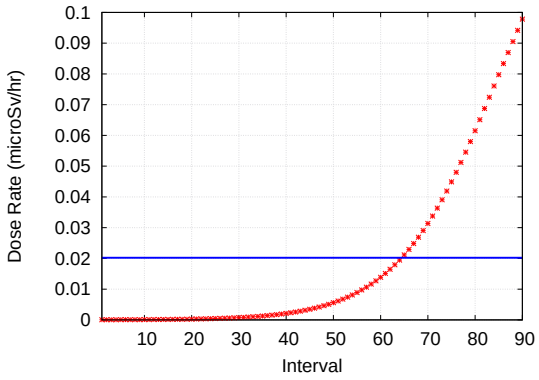

(b) Dose profile inside Zone 2

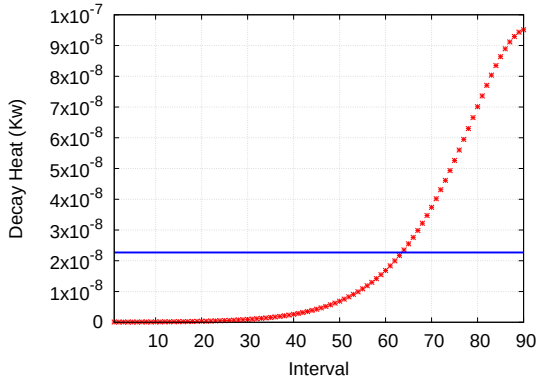

(c) Nuclear heat profile inside Zone 2

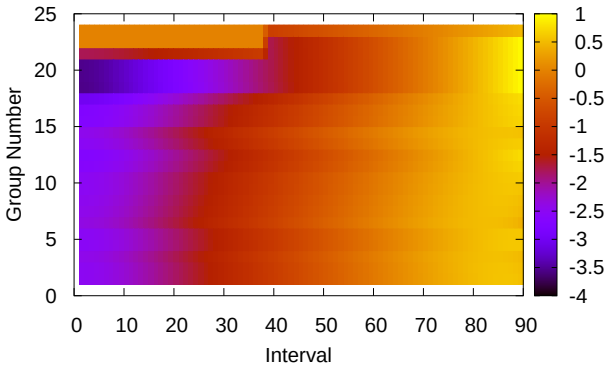

(d) Groupwise normalized gamma spectrum inside Zone 2

Figure 4.5: Radiological quantities at every 90 intervals in zone 2

In figure 4.5a, the variation of activity within the zone is shown. The blue line is the activity of the inboard magnet, considering the neutron spectrum provided at the zone. The red points show the value of activity at each interval within the zone, calculated considering the neutron spectrum provided for each interval. A large variation of activity within the zone can be seen from figure 4.5a with maximum value 4 times higher than the average zone activity value and the minimum value 3 orders lower than that. Similar trends can be seen in figures 4.5b and figure 4.5c, which shows the variation in dose rate and decay heat at each interval within the zone. The figure 4.5d is constructed by

taking the 24-energy group gamma spectrum produced at each of the 90 intervals and normalizing it with the spectrum produced at the zone. The normalized spectrum at each interval for 24 groups is then shown in figure 4.5d in the log-10 scale. From the figure, it can be concluded that the gamma spectrum calculated using coarse mesh and the fine mesh has a maximum difference of the order of 10^4. Thus implying the inaccuracy in results because of the use of coarse mesh. For structures with large size that has a variation of the neutron spectrum within its body would show even larger variations in radiological quantities.

4.3.2 Model-2: ITER Shutdown Benchmark Study

ITER Shutdown benchmark problem is already discussed in section 4.2. In this section, the difference in contact dose rate with respect to coarse and fine meshes is examined.

For this purpose, the meshing of the endplate is averaged using a small program. Each tetrahedral mesh sharing a common node is clustered to form a zone. Then at each zone, the neutron spectrum is calculated by taking the average of all the neutron spectrum of each mesh in that zone. There would be 4 tetrahedral mesh that would share a common node. The neutron spectrum at these meshes is then equated to the average neutron spectrum evaluated for these set of four meshes. Now, using the average neutron spectrum evaluated for each mesh, activation calculation by ACTYS-1-GO is performed with the SA2 irradiation scenario. The resulting contact dose rate is plotted for all 2085 mesh point 12 days after shutdown (after SA2 irradiation is over) and is given in figure: 4.6b. Another activation calculation is performed by ACTYS-1-GO, using the actual neutron spectrum at every 2085 meshes. The contact dose rate obtained at each mesh 12 days after the shutdown, using their own neutron spectrum is given in figure:4.6a

The figure: 4.6a shows a clear band of low activation area formed due to shielding from steel and water mixture as shown in the figure 4.2. In figure 4.6b, contact dose rate

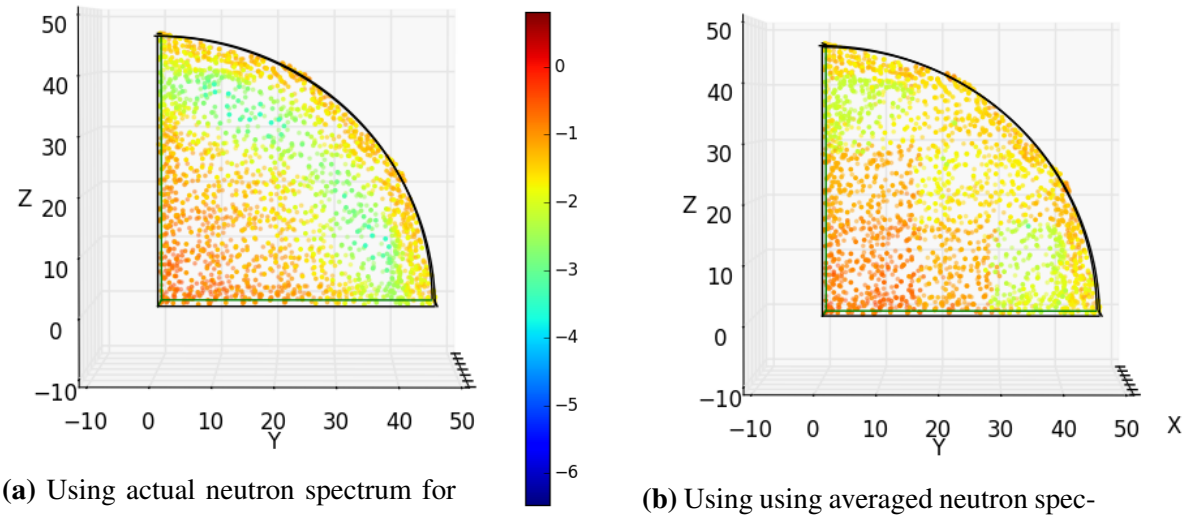

(a) Using actual neutron spectrum for 2085 meshes

(b) Using using averaged neutron spectrum for 2085 meshes

Figure 4.6: Contact dose rate (Sv/hr) evaluated at 2085 mesh points in the endplate (quarter geometry) the using actual neutron spectrum and using averaged neutron spectrum. Values are in Log_{10} scale, with the background dose rate of $3.42E-07$ Sv/hr as the minimum value on the scale

evaluated at each 2085 mesh points using the average flux according to the scheme stated above, shows no such clear band of low activation area. This would imply that the effect of neutron shielding is not reflected properly when meshes with averaged neutron spectrum are used for activation calculations. Such averaged calculation might even neglect small hot spots created in the geometry and would have great implications in shield design parameters.

As seen from the figure: 4.6, contact dose rate profile from a simple geometry like that of the ITER Shutdown Dose rate Benchmark model cannot be mapped properly using average flux or coarse mesh. For bigger devices with complex geometry, these problems would escalate. Further, the radiological quantities resulting from the activation of larger areas with a large gradient in the neutron spectrum can lead to overestimation or underestimation of crucial design parameters. Hence to obtain better design parameters for fusion reactors, detailed radiation maps are required, which can be easily achieved by ACTYS-1-GO.

4.4 Chapter Summary

The gamma photons travel a large distance from the site of production before getting absorbed. Hence to evaluate the SDDR (ShutDown Dose Rate produced by decay gamma emitted from activated materials), photon transport is carried out after generating gamma source from activated materials. This is achieved by Rigorous-2-Step (R2S) method in which activation calculation is performed in between a neutron and a photon transport. Hence, in the scope of the thesis, ACTYS-ASG is developed for evaluation of highly resolved gamma source that can be coupled with deterministic transport code ATTILA for SDDR calculations. It performs intermediate activation calculation for the neutron and photon transport. ACTYS-ASG can read geometry files, ATTILA input files, and ATTILA output files, and can produce gamma source in a format compatible with ATTILA. The coupling subroutine and ACTYS-1-GO are compatible with both Linux and Windows platforms. Such a coupler is very useful at a domestic scale as some commercial activation codes do not provide (or provide limited) nuclear data libraries for activation calculation.

Another important point demonstrated in this chapter is the importance of fine mesh calculation in fusion devices and ACTYS-1-GO ability in achieving it. Two models, the FENDL Activation Benchmark Study and the ITER Shutdown Benchmark Study are taken as an example. Activation calculations for both the models are performed using fine and coarse meshing. The results of the activation calculation conclude that to accurately map regions of high and low activation in complicated structures like fusion devices, fine meshing is required. As it was demonstrated in the earlier chapter that ACTYS-1-GO can perform activation calculation much faster than existing activation codes, ACTYS-1-GO is suitable for performing highly resolved activation calculation to generate a very accurate radiation map of the device. The contents of this chapter are published in the article ***Fusion Eng Des.* 2018;129**.

Chapter 5

Multi-Parameter Composition Optimization Scheme for Fusion Materials

As discussed in earlier chapters, one of the major challenges for the design and construction of fusion reactors is the development and qualification of materials to withstand complex loading conditions which include high thermal and mechanical strains along with nuclear responses produced in the material by the incident fusion neutrons[86, 87, 88, 89, 33]. These high-energy (up to 14.1 MeV) and high flux (up to $1.0E16\ n/cm^2$) neutrons produced in fusion reaction would irradiate the materials that make up the reactor vessel and its sub-systems. Thus the selection of material for the nuclear application becomes a complex process with many factors to consider. Not only must a material withstand extreme mechanical and thermal conditions, but it must do this while being bombarded by neutrons. The incident neutrons interact with the material producing solid and gaseous transmutants that accumulate in the material and change its composition leading to a measurable change in the thermo-mechanical properties.

Displacement per atom or dpa is defined as the average number of lattice atom displaced

from their initial position due to the energy imparted by the incoming energetic particles like neutron and ions [18]. Dpa gives an estimate of the radiation damage incurred by the material and used to the compare effect of various different radiation on the material. In the articles, [90, 91], the author reports that pure Tungsten (W) will become Tungsten-Rhenium-Osmium alloy (W-18Re-3Os) after 50 dpa of irradiation, and addition of 5% of Re to pure W decreases the thermal conductivity and diffusivity to half, respectively. This implies that transmutation resistance is highly desired in fusion systems. It is also predicted that more than 25-30 dpa will be achieved in DEMO blankets within one year of operation [92]. Hence for DEMO design and licensing, all necessary materials need to be qualified to 70-80 dpa [92]. The gaseous transmutants produced, particularly Helium(He), diffuse through the bulk material and form clusters in existing cracks or in grain boundaries, leading to increased brittleness and swelling in the material [93, 94, 95]. He atoms are essentially insoluble in metals and strongly interacts and binds with numerous micro-structure features [96]. Since many of these gas-producing nuclear reactions have threshold energies, gas production and subsequent swelling are more of a concern in a fusion reactor compared to fission reactors [13].

In addition, to the changes in elemental composition and accumulation of residual products, the transmutants could also be radioactive. These radioactive isotopes could emit ionizing radiation that would be harmful to the surrounding equipment and the personnel working in and around the reactor [94]. Hence, radiological responses of materials should be considered before the selection of the material for the following areas of operation: 1) reactor maintenance, 2) accident scenarios, 3) reclamation of end-of-service material, 4) waste disposal and 5) associated potential public exposure. Safety requirements in each of these areas have different implications for materials selection and can depend both on the activation and physical properties of the material. In principle, it is possible to choose the structural materials of a reactor to minimize the consequences of the induced radioactivity, though in practice there are several possible sets of requirements, not all of which can be satisfied simultaneously. Materials selection is further complicated by the fact that

activation properties are described by a number of different radiological quantities:

- The specific radioactivity (Bq/kg), which defines the rate at which nuclei disintegrate.
- The surface γ dose rate (Sv/h) or the Contact dose rate, is the measure of the biological effect of gamma radiation when living tissue is in contact with the irradiated material.
- The Decay heat is the amount of heat deposited by the ionizing radiation in the material.
- Radwaste classification gives the type and amount of harmful radioisotopes present in the material after the reactor is shutdown. This indicates the duration and the type of cooling/storage facility required for the irradiated material.

Accurate measurements of all radiological quantities and their co-relation with the incident neutron spectrum and initial material composition is warranted to assess and qualify materials for application in a fusion environment. These nuclear responses add another dimension or degree of freedom, namely, interaction with radiation, to the characterization of the material. This implies that the challenge of materials-selection is to find a material that has the required combination of physical, chemical, and nuclear properties [97].

Hence, a careful strategy is required, which would incorporate all the different radiological responses to develop Low Activation Materials (LAM) to be used in a fusion environment. To achieve this, a method for quantifying isotopic nuclear response to the overall material response is reported in reference [98]. This method quantifies the gamma dose rate and predicts the best material composition for material irradiated with a single neutron spectrum. Since the material in a fusion environment faces a large variation in the neutron spectrum, optimization of material composition for a single spectrum or mesh

location is not ideal. Moreover, one radiological quantity cannot give a detailed picture of the damage endured by the material. Hence, a method needs to be developed which would include the variation in the neutron spectrum and various radiological quantities to generate an optimized material composition. In the scope of the thesis, a novel method for multi-parameter optimization of material composition based on the spatial and temporal variation of various radiological quantities is developed. This would help the material developer to choose radiation-resistant elements to construct an ideal LAM.

Section 5.1 gives the details of the composition optimization scheme for a single neutron spectrum and single radiological quantity. This section gives an introduction to various factors defined to quantify the nuclear response of the material in terms of initial material composition. Section: 5.2 reports the inadequacy of the optimization method discussed in section 5.1 and the requirement for multi-parameter composition. The methodology and algorithm for composition optimization based on the spatial and temporal variation of radiological quantities are also given in section 5.1. Section 5.3 presents the results of a multi-parameter optimization scheme using the ITER shutdown benchmark study as an example. The effectiveness of the scheme and domain within which optimization is carried out are also discussed in the section 5.3.

5.1 Material optimization formalization based on single neutron flux and single radiological response

The method to quantify radiological responses of the material in terms of initial material composition and to optimize the material according to a single neutron spectrum is given in the article [98], our own work parallel to the thesis. A brief description of the techniques, in the context of the present work, and detailed derivation of the optimization factors are given below.

The solution of the Bateman equation can be written in a matrix form [47]:

$$\frac{d\bar{N}}{dt} = -\Lambda\bar{N} \tag{5.1}$$

where $\bar{N}$ is the vector containing the concentration of all isotopes at time t and Λ is the matrix of coefficients given as $\Lambda_{ij} = \lambda_{ij} + \sum_g \sigma_{ij}^g \Phi^g$. The solution of above the equation is:

$$N\bar{(}t) = e^{-\Lambda t}\vec{N}(0) \quad \Rightarrow \quad \vec{N}(t) = \mathbf{T}\vec{N}(0) \tag{5.2}$$

Where $e^{\Lambda t}$ is written as matrix $\mathbf{T}$, transfer matrix. In order to evaluate various radiological responses of the irradiated material, the isotopic concentration of the nuclides calculated at time t for the incident neutron spectrum Φ^g, is used. For example activity for any isotope 'i' at any 't' is defined as:

$$A_i = \lambda_i N_i(t) \tag{5.3}$$

Activity for all the isotopes in the material can be written in matrix form as

$$\vec{A} = \lambda\vec{N}(t) \quad \Rightarrow \quad \vec{A} = \lambda\mathbf{T}\vec{N}(0) \tag{5.4}$$

where λ can be written as some matrix $\mathbf{G}_A$, which implies that

$$\vec{A} = \mathbf{G}_A\mathbf{T}\vec{N}(0) \quad \Rightarrow \quad \vec{A} = \mathbf{F}_A\vec{N}(0) \quad \textit{where} \quad \mathbf{F}_A = \mathbf{G}_A\mathbf{T} \tag{5.5}$$

Similarly, contact dose rate at the surface of a semi-infinite uniform volume source calculated by the formula given in equation 2.5, can be written as:

$$\dot{D} = \mathbf{G}_D\vec{N} \Rightarrow \dot{D} = \mathbf{G}_D\mathbf{T}\vec{N}(0) \Rightarrow \dot{D} = \mathbf{F}_D\vec{N}(0) \tag{5.6}$$

where $\mathbf{F}_D = \mathbf{G}_D\mathbf{T}$. This would be true for any radiological quantity, and the quantity

calculated at the time 't' can be rewritten as:

$$R = \mathbf{G}_R\vec{N}(t) \Rightarrow R = \mathbf{G}_R\mathbf{T}\vec{N}(0) \Rightarrow R = \mathbf{F}_R\vec{N}(0) \tag{5.7}$$

Thus, any radiological quantity can be related to the initial concentration of isotopes or elements in the materials, here referred to as parents. The parent elements/isotopes of any material are responsible for the production of radionuclides, which in turn produce the radiological quantities. Thus for any parent isotope 'j', contribution IC_j, towards a radiological quantity 'R' and the contribution factor ICF_j can be expressed as:

$$IC_j^R = \frac{F_j * N_j(0)}{R} \quad \Rightarrow IC_j^R = \frac{R_j}{R} \quad and \quad ICF_j = \frac{IC_j}{af_j} \tag{5.8}$$

where $R_j = F_j * N_j(0)$ is the radiological response produced by the isotope j, R is the total radiological response produced by the isotopes and af_j is the atomic fraction of isotope 'j'. Similarly, the elemental contribution of any element 'e' EC_e, is defined as the sum of all the isotopic contribution IC_i for all isotopes 'i' of element 'e', $i \subset e$.

$$EC_e^R = \sum_i (\frac{R_i}{R}) \quad \Longrightarrow \quad \sum_i IC_i \tag{5.9}$$

Likewise, ECF or Elemental Contribution Factor for any radiological quantity can be defined as:

$$ECF_e^R = \frac{[\sum_i (\frac{R_i}{R})]}{wf} \quad \Longrightarrow \quad \frac{[\sum_i ICF_i]}{wf} \quad \Longrightarrow \quad ECF_e^R = \frac{EC_e^R}{wf} \tag{5.10}$$

Where R_j is the contribution of isotope j to the total radiological quantity R and wf is the weight fraction of the element. ECF gives a direct correlation between the radiological quantities and the elements present in the initial material composition. Thus minimizing the parents with the highest ECF values would lead to the minimization of radiological responses. Similarly, ICF determines the impact of the reduction of the isotope on the

total response of the material and minimizing the isotopes with the highest ICF values would lead to the minimization of responses. The new radiological response based on minimizing elements with highest ECF can be written, as given in [98]:

$$R^{'} = R(1 + \sum_{e}(ECF_e \delta_e)) \tag{5.11}$$

Where $R^{'}$ is the new response, ECF_e is the ECF of each element in the initial material composition and δ_e is the change in the composition of the material calculated by recursively minimizing the elements with highest ECF values and adding to the elements with least ECF. δ_e is the allowable change in the composition of the material and it is calculated within a closed range defined prior to calculation.

$$\delta_e \in [wf_{lw}, wf_{up}] \tag{5.12}$$

Where wf_{lw} is the 'lower limit' of the weight fraction and wf_{up} is the 'upper limit', provided as inputs. If the predicted minimization in material composition turns out to be less than the 'lower limit' of δ_e provided, the predicted value is substituted with the 'lower limit'. Similarly, if the predicted addition in the composition of any elements exceeds the 'upper limit', the calculated δ_e is substituted with the 'upper limit'. The final composition is then generated based on the δ_e calculated for each element and the new response is calculated according to equation 5.11

ECF/ICF are functions of the incident neutron energy spectrum, which means the calculation of ECF/ICF and minimizing the highest ECF/ICF contributors for a single spectrum would result in the minimization of radiological quantities for that spectrum only. As we know, nuclear reactions are a strong function of incident neutron energy, the change in energy spectrum would change the coefficient matrix Λ and transfer matrix '**T**', as given in equation 1.21 and equation 5.2. This would, in turn, change the ECF/ICF values of each parent for every radiological quantity with the change in neutron spectrum, irradiation,

and decay scenarios. As discussed, any single radiological quantity does not give a clear picture of material damage, therefore, in addition to calculating the effect of spatial variation of neutron spectrum, the ECF/ICF should also contain information regarding all the concerned radiological quantities. Hence to achieve a complete optimization, ECF/ICF should be evaluated for all the radiological quantities at each mesh point rather than providing the minimum value of the radiological quantity at any single location.

This would mean that an innovative method needs to be developed that would integrate the ECF/ICF methodology to the multipoint activation calculation to include the effect spatial and temporal variation of the neutron spectrum and radiological quantities. The composition thus calculated should incorporate the contribution factors of parents from various radiological quantities like activity, gamma dose rate, helium production, decay heat generation, and radwaste index and their spatial and temporal variation for the entire material.

5.2 Material optimization formalization based on multiple radiological quantities and their Spatial and Temporal variation in a device

Traditionally, the principle adopted to reduce the amount of activation in a material is by substitution of elements that are particularly susceptible to activation, with chemically similar elements with lower susceptibility to activation [86, 87, 92, 96, 97, 99, 100, 101]. As mentioned in section 5.1, ECF/ICF identifies such elements by quantifying their response towards the radiological quantities. However, the formalization discussed in section 5.1 cannot be directly implemented to encompass the spatial and temporal variation of multiple radiological quantities over the material, during its lifetime. For example, if we directly adopt the methodology it would predict different compositions for each mesh

point according to equation 5.12. This happens because ECF is a strong function of the neutron energy spectrum. A material with different compositions at each mesh point is meaningless. This implies that a careful strategy is required for multiple parameter optimization.

The derivation of the multi-parameter optimization scheme is given below. New reduced radiological quantity for single neutron flux at a particular time step is given by the equation: 5.11. Now, the total reduced radiological quantity at multiple mesh points can be written as:

$$R_{tot} = \sum_k R_k^{'} = \sum_k (R_k(1 + \sum_e (ECF_{ke}\delta_{ke}))) \tag{5.13}$$

Where R_k is the radiological quantity at mesh point 'k', ECF_{ke} is the ECF calculated at mesh point 'k' for element 'e' and δ_{ke} is the change in elemental composition calculated for mesh point 'k' and element 'e'. To overcome the problem of the generation of multiple compositions, a common Δ_e is defined that is independent of mesh points, such that the total reduced radiological response for all the mesh points remains the same. The Δ_e is obtained in the following steps:

$$\begin{aligned} R_{tot} = \sum_k R_k^{'} &= \sum_k (R_k(1 + \sum_e (ECF_{ke}\Delta_e))) \\ &= \sum_k R_k + \sum_k R_k(\sum_e (ECF_{ke}\Delta_e)) \\ &= \sum_k R_k + \sum_e \Delta_e(\sum_k (R_k ECF_{ke})) \end{aligned} \tag{5.14}$$

Equating equation: 5.13 and equation: 5.14, Δ_e can be written as:

$$\Delta_e = \frac{\sum_k (R_k ECF_{ke}\delta_{ke})}{\sum_k (R_k ECF_{ke})} \tag{5.15}$$

As discussed above, one radiological quantity does not give a complete picture of the damage to the materials. For example, long-lived nuclides produce radwaste, short-lived nuclides affect the dose rates during periods of maintenance and very short-lived acti-

vation products produce risks during an accident scenario. Thus, a truly low activation material should have a low activation profile for short, medium and long-lived nuclides. Unfortunately, achieving this goal in entirety is not possible [95]. However, a calculation of 'Effective material composition' for all the radiological quantities could help towards achieving this goal. As discussed in section 5.1, the minimization of parent elements/isotopes of highest ECF/ICF values at any given flux or irradiation scenario would imply a reduced radiological response for that particular flux value and that particular irradiation. From equation: 5.15 we can calculate the optimized material composition for a single radiological quantity. Hence an effective Δ_e, for all the radiological quantities 'j' at all spatial location 'k' where the material is located can be derived similarly to the equation: 5.14, and is given below:

$$\Delta_e = \frac{\sum_j \sum_k (R_{jk} ECF_{jke} \delta_{jke})}{\sum_j \sum_k (R_{jk} ECF_{jke})} \tag{5.16}$$

During the activation process, the neutron energy spectrum encountered by the material would be different at each irradiation time and zero at each shutdown time. This would also lead to a difference in radiological quantities and subsequent ECF values. Hence, Δ_e should include the effects of the irradiation scenario 'i' on the material. This improved Δ_e can be written as:

$$\Delta_e = \frac{\sum_j \sum_k \sum_i (R_{ijk} ECF_{ijke} \delta_{ijke})}{\sum_k \sum_j \sum_i (R_{ijk} ECF_{ijke})} \tag{5.17}$$

Equation 5.17 gives the optimized material composition considering multiple radiological quantities and their spatial and temporal variation. This, however, is incomplete. The optimization for a set of points where the material is located should be considered from a reactor point of view, for example in the event of the formation of hot-spots or localized regions of high radiological response, the optimization solution should lead to an overall decrease in the responses. This is achieved by introducing location sensitivity coefficients α_k. The optimization scheme should also include the importance of different radiological

responses given by the radiological parameter coefficients β_j. It is defined for each radiological quantity like activity, dose rate, gamma spectrum, radwaste index, decay heat, and helium production. β_j acts as the weight function for each radiological quantity and is defined for each time step. It should be noted that $\sum_j \beta_j = 1.0$. This provides better control of the optimization process and gives the freedom to optimize the radiological quantity for any particular system or material located at different places in a reactor. For example, gas production is a dominating quantity during the irradiation process, as most of the gas is produced by (n, He) reaction, so during cooling times ($\phi = 0$), β_j for gas production should be considered to be zero. Or in case of port plugs of ITER where constant maintenance is required, minimizing dose rate and gamma spectrum are important and hence β_j for dose rate and gamma spectrum should be higher. Furthermore, the optimization process is carried out only when the time step coefficient γ_i is equal to unity. This modified Δ_e including all the above coefficients are written as:

$$\Delta_e = \frac{\sum_k \alpha_k (\sum_j \beta_j (\sum_i (\gamma_i (R_{ijk} ECF_{ijke} \delta_{ijke}))))}{\sum_k \alpha_k (\sum_j \beta_j (\sum_i (\gamma_i (R_{ijk} ECF_{ijke}))))} \tag{5.18}$$

Δ_e in the equation: 5.18 gives the change in the weight fraction of each element that would produce a material with least radiological responses for a particular spatial and temporal variation of the neutron energy spectrum. The Δ_e is optimized within the closed range provided as input and this flexibility would help material developers to achieve a more realistic composition. This optimization scheme is included in the multi-point activation code ACTYS-1-GO for practical application purposes.

5.2.1 Implementation of Optimization Procedure in ACTYS-1-GO

ACTYS-1-GO performs activation calculation at each time step, for each mesh location where the material is located. From the input file, ACTYS-1-GO reads all the coefficients(α_k, β_j and γ_i) for the optimization scheme. For every time step during the

activation calculation, with $\gamma_i = 1$, a record of dominating isotopes and their parents are kept. These dominating parents are for radiological quantities with non zero β_j. At the end of each inventory calculation for any given irradiation scenario, ECF for various parent isotopes is evaluated. Based on these ECF values, the program then suggests the necessary elimination or reduction of elements in order to minimize the radiological quantities, $\delta_i jke$. This process is repeated for all the time steps in the irradiation scenario and mesh points where the material is located, thus including the change in radiological quantities with the temporal and spatial variation of the neutron energy spectrum. At the end of activation run the optimized composition is predicted based on the equation: 5.18 and new reduced radiological quantities are calculated and presented. The change in the weight fraction of the elements is done in a closed range provided as input to ensures that the predicted material composition is realistic. These upper and lower limits to $\delta_i jke$ should be provided by the experts, based on material properties. The basic outline for the working ECF/ICF subroutine is given in algorithm 3:

Data: λ,σ,Φ_k,material composition, irradiation scenario, and geometry details
while *j<# materials* **do**
  Data: N is the number of mesh
  initialization;
  while *i<n* **do**
    For **Time(t)**;
    Call chain solver using multipoint activation algorithm;
    Save the final inventory of the isotopes created from activation;
    Calculate of N(t),Activity(t),Dose rate(t), Nuclear Heat(t), Radwaste, Helium production;
    Sort and saving Dominant Radionuclides of each radiological quantity;
    Find the parent isotopes using pathway analysis;
    Assign separate ECF/ICF values to each parent for each radiological response;
    Calculate δ_{ijke} based on all the radiological responses at the particular time 't';
    For each irradiation and decay step update Δ_e, according to equation 5.18
  end
end

Algorithm 3: Algorithm for multi-parameter optimization technique considering temporal and spatial variation in nuclear response of materials

The weights α_k, γ_j and β_i, as mentioned in equation 5.18, are chosen based on material response and sensitivity of the parameters. These coefficients are variable and can be

provided in the input file by the user or default values built-in the code can be used.

Since the optimization scheme makes use of the data already generated by the code like the radiological quantities at the end of each time step and pathways during the inventory calculation, no extra computational time is required in its implementation. The accuracy and the speed of the multipoint code ACTYS-1-GO remain the same.

5.3 Effectiveness of material optimization using multi-parameter ECF

To demonstrate the capabilities and the usefulness of the tool, the 'ITER Shutdown Dose Rate Benchmarking problem' is used as the reference model [75, 102]. Using the default setting mentioned in section 5.2, the composition of stainless steel (SS316) is optimized and the radiological quantities produced by the optimized material are compared with that of original material. The flux and energy spectrum for ITER- Shutdown Benchmark model is evaluated using deterministic neutron transport code, ATTILA. A detailed description of the problem is given in section 3.2.2. A detailed figure with geometric details and material specification is given below for quick reference:

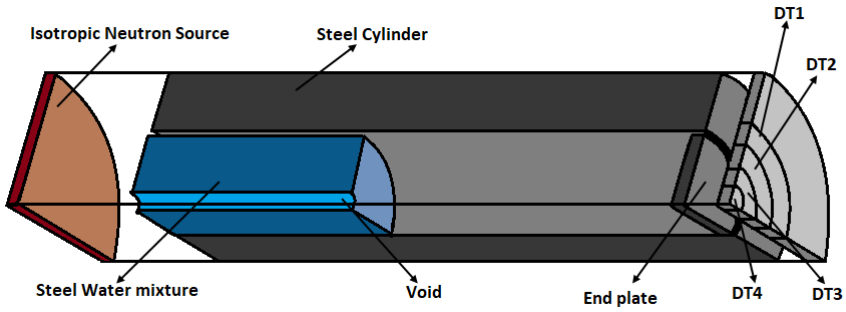

Figure 5.1: Quarter geometry of the model for ITER Shutdown Dose Rate Benchmark Study that is used for flux generation and activation calculation.

In the previous chapter, the details of neutron transport calculation using ATTILA is given. The transport calculation yields 175 group neutron spectrum at each 2085 mesh locations

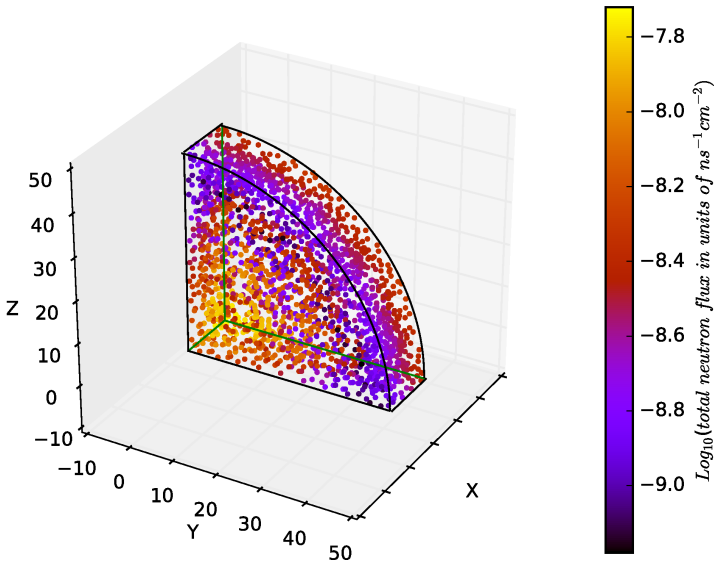

Figure 5.2: Total neutron flux at each 2085 mesh points of the endplate for a unit source strength of neutrons represented in log_{10} scale.

in the endplate. The total flux at each mesh point for unit source strength of neutrons is given in figure:5.2. The activation calculation is performed using ACTYS-1-GO at the endplate consists of 2085 mesh points using the SA2 irradiation scenario given in table 5.2 and for cooling time steps given in table 5.3, with material composition given in table 5.1. The actual neutron flux and spectrum at any time step is obtained by multiplying the neutron spectrum generated by unit neutron source with the corresponding source strength given in table 2.4.

The optimized composition is obtained from the multi-parameter optimization technique considering temporal and spatial variation in nuclear response of stainless steel at 2085 mesh points of the endplate and is given table:5.1 along with the original composition. The optimized material composition is calculated based on the equation:5.18 and the upper and lower limits to material composition provided in the input file, given in column 'Range' in the table: 5.1. 'Range' is the limit within which the material composition is optimized. To achieve a realistic optimized composition this 'range' should be an input derived from material properties and thermo-mechanical constraints. The 'range' used

in this exercise is just for demonstrating the capabilities of the optimization scheme. To minimize the hazardous short-lived and long-lived isotopes simultaneously, ECF/ICF calculation is done at 3 different time steps, first with the highest fluence, second just after shutdown and third at 100 years after shutdown. The coefficient α_k is taken as unity as there are no identified hot-spots in the example program. The upper and lower limits taken for the material in this exercise, are just educated guesses based on all the ferritic, martensitic and austenitic steel compositions used in ITER. Since it is not always possible to change the composition of crucial alloying elements, the upper and lower limits to material composition largely dictate the optimization process. Therefore, one should be very careful using the tool and the acceptable optimization should only be done with realistic values.

The above-optimized composition is given in the table: 5.1, is to demonstrate the capability of the code and does not explicitly suggest any new material. Eurofer is a Reduced Activation Ferritic-Martensitic (RAFM steel) which is used here as a reference material [96, 101, 103, 19, 104]. The elements having the highest ECF values for the optimization scheme given by the equation: 5.18 that are optimized by ACTYS-1-GO is also zero in Eurofer. This demonstrates the capability and effectiveness of a multi-parameter optimization scheme. The elements that have a higher concentration in Eurofer might have been added to enhance the thermo-mechanical properties of the material. The above discrepancy can be overcome by carefully defining the upper and lower limits of material weight fraction, within which the optimization process is performed.

The relative difference between the total radiological quantities like activity, gamma dose rate, decay heat, calculated for the entire endplate with the optimized material composition and the original material composition is given in table 5.2, 5.3. The table shows a decrease in values of radiological quantities at almost each time step and a decrease of more than 99% after 50 years of cooling time.

Also, the radiological quantities at each mesh location, obtained from the above opti-

Table 5.1: Elemental composition in weight fraction of stainless steel (SS316), Eurofer and the optimized material generated from the material optimization scheme in ACTYS-1-GO

Elements	SS316 composition	Range	Optimized material Composition	Eurofer composition
B	5.14E-03	(1.00E-03 - 5.14E-03)	1.00E-03	5.00E-03
C	1.04E-01	(3.00E-02 - 1.10E-01)	9.96E-02	1.10E-01
N	2.78E-01	(3.00E-02 - 2.78E-01)	3.00E-02	3.00E-02
O	6.95E-03	(0.00E+00 - 6.95E-03)	0.00E+00	0.00E+00
Al	1.03E-01	(0.00E+00 - 1.03E-01)	0.00E+00	0.00E+00
Si	9.89E-01	(5.00E-02 - 9.89E-01)	5.00E-02	5.00E-02
P	4.48E-02	(0.00E+00 - 4.48E-02)	0.00E+00	0.00E+00
S	1.30E-02	(0.00E+00 - 1.30E-02)	0.00E+00	0.00E+00
K	7.10E-04	(0.00E+00 - 7.10E-04)	6.43E-04	0.00E+00
Ti	1.74E-01	(0.00E+00 - 1.74E-01)	1.58E-01	0.00E+00
V	4.36E-03	(0.00E+00 - 2.50E-01)	2.26E-01	2.50E-01
Cr	1.87E+01	(8.50E+00 - 1.87E+01)	1.69E+01	8.50E+00
Mn	1.82E+00	(5.00E-01 - 1.82E+00)	5.00E-01	5.00E-01
Fe	6.44E+01	(6.44E+01 - 8.95E+01)	8.10E+01	8.95E+01
Co	4.71E-02	(0.00E+00 - 5.00E-02)	0.00E+00	0.00E+00
Ni	1.16E+01	(0.00E+00 - 1.23E+01)	0.00E+00	0.00E+00
Cu	2.62E-01	(0.00E+00 - 3.00E-01)	0.00E+00	0.00E+00
Zr	1.22E-03	(0.00E+00 - 1.22E-03)	0.00E+00	0.00E+00
Nb	5.98E-03	(0.00E+00 - 1.00E-02)	0.00E+00	0.00E+00
Mo	1.45E+00	(0.00E+00 - 2.50E+00)	0.00E+00	0.00E+00
Sn	9.36E-04	(0.00E+00 - 9.36E-04)	0.00E+00	0.00E+00
Ta	3.07E-03	(3.07E-03 - 8.00E-02)	7.24E-02	8.00E-02
W	3.02E-04	(0.00E+00 - 1.00E+00)	9.05E-01	1.00E+00
Pb	2.14E-04	(0.00E+00 - 2.14E-04)	0.00E+00	0.00E+00
Bi	2.13E-04	(0.00E+00 - 2.13E-04)	0.00E+00	0.00E+00

mization scheme, show a considerable decrease in value as compared to the radiological quantities obtained from the original material composition at each mesh point. For example, the contact dose rate after 50 years of shutdown, calculated at each 2085 mesh point with the original material composition and the optimized material composition for SA2 irradiation scenario is given in figure:5.3. It can be clearly seen from the figure: 5.3a that the dose rate is two orders higher for the original material composition in comparison to the optimized material composition. Also, at this time step the contact dose rate has reached the background level for the optimized material. This means that the optimized material is not producing any long-lived isotopes that would contribute to rad-waste. This

plot shows that at each 2085 mesh points in the endplate the contact dose rate produced by optimized composition is at least 99% less than that produced by the original material composition.

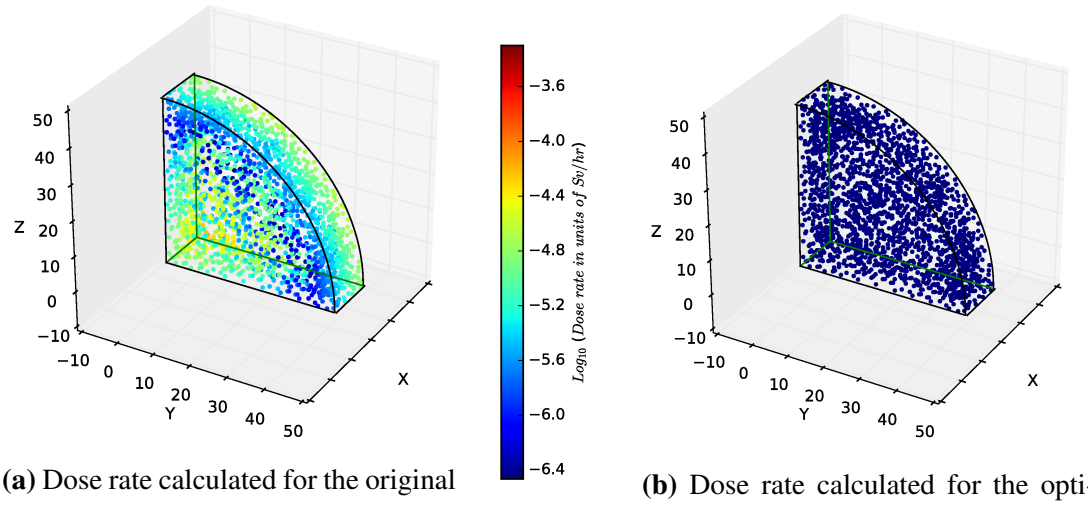

(a) Dose rate calculated for the original material composition

(b) Dose rate calculated for the optimized material composition

Figure 5.3: Dose rate at every 2085 meshes calculated using the original material composition and optimized material composition. The values are plotted in log-scale with background radiation level ($3.7X10^{-7}$ Sv/hr) as the lowest value.

5.4 Chapter Summary

In this chapter, a novel method is developed to predict the elemental composition of a material such that the resulting material is less susceptible to neutron damage. The methodology for quantifying the contribution from each parent element to the total radiological response is discussed. The contributing factors called ECF for elements and ICF for isotopes are defined. A multi-parameter composition optimized based on ECF or ICF is developed. The optimization scheme encompasses the effects of spatially and temporally varying neutron spectrum in fusion reactor like device. The method also provides coefficients to give weight to spatial location, radiological quantity, and time step. This ensures more freedom in the optimization process and allows for a better analysis. The developed method is written into an algorithm and is incorporated in the multipoint ac-

tivation code, ACTYS-1-GO. The usefulness of the scheme is demonstrated by taking Stainless steel(SS316) used in the ITER shutdown benchmark study as an example problem. For SS316 the optimized composition calculated by ACTYS-1-GO yields all radiological quantities reduced by more than 99% after 50 years of shutdown. The contents of this chapter are published in article ***Nucl Fusion*** **2018;58(12)**.

Table 5.2: Relative difference between the total radiological quantities produced from Actual material and optimized material composition with SA2 Irradiation scenario for the 2085 mesh point at the endplate of the ITER ShutDown Benchmark Study.

Irradiation Time				
Time Step	Time(s)	Activity	Dose rate	Decay heat
1	6.31E+07	-23.49%	-15.42%	-14.87%
2	3.15E+08	-14.60%	-14.34%	-15.06%
3	2.11E+07	1.24%	-60.33%	-60.56%
4	4.18E+07	-17.94%	-9.54%	-9.46%
5	3.92E+03	-19.49%	-20.50%	-18.40%
6	4.00E+02	-24.40%	-27.18%	-26.70%
7	3.92E+03	-19.00%	-18.85%	-16.61%
8	4.00E+02	-24.08%	-26.55%	-26.09%
9	3.92E+03	-18.67%	-17.72%	-15.41%
10	4.00E+02	-23.87%	-26.10%	-25.67%
11	3.92E+03	-18.47%	-16.94%	-14.62%
12	4.00E+02	-23.73%	-25.78%	-25.37%
13	3.92E+03	-18.34%	-16.40%	-14.08%
14	4.00E+02	-23.64%	-25.55%	-25.16%
15	3.92E+03	-18.26%	-16.02%	-13.70%
16	4.00E+02	-23.59%	-25.38%	-25.01%
17	3.92E+03	-18.21%	-15.76%	-13.44%
18	4.00E+02	-23.55%	-25.27%	-24.91%
19	3.92E+03	-18.18%	-15.57%	-13.26%
20	4.00E+02	-23.53%	-25.18%	-24.83%
21	3.92E+03	-18.17%	-15.43%	-13.13%
22	4.00E+02	-23.52%	-25.12%	-24.78%
23	3.92E+03	-18.17%	-15.34%	-13.04%
24	4.00E+02	-23.51%	-25.08%	-24.74%
25	3.92E+03	-18.17%	-15.27%	-12.97%
26	4.00E+02	-23.51%	-25.05%	-24.71%
27	3.92E+03	-18.18%	-15.23%	-12.93%
28	4.00E+02	-23.51%	-25.03%	-24.69%
29	3.92E+03	-18.19%	-15.20%	-12.90%
30	4.00E+02	-23.52%	-25.02%	-24.68%
31	3.92E+03	-18.20%	-15.17%	-12.88%
32	4.00E+02	-23.52%	-25.01%	-24.67%
33	3.92E+03	-18.21%	-15.16%	-12.86%
34	4.00E+02	-23.53%	-25.00%	-24.66%
35	3.92E+03	-18.22%	-15.15%	-12.86%
36	4.00E+02	-23.53%	-24.99%	-24.66%
37	3.92E+03	-18.23%	-15.15%	-12.85%
38	4.00E+02	-23.54%	-24.99%	-24.66%
39	3.92E+03	-18.25%	-15.15%	-12.85%
40	4.00E+02	-24.60%	-26.03%	-25.74%

Table 5.3: Relative difference between the total radiological quantities produced from Actual material and optimized material composition with SA2 Irradiation scenario for the 2085 mesh point at the endplate of the ITER ShutDown Benchmark Study. [Cont.]

Irradiation Time				
Time Step	Time(s)	Activity	Dose rate	Decay heat
41	3.92E+03	-17.77%	-13.11%	-10.94%
42	4.00E+02	-24.28%	-25.22%	-25.02%
43	3.92E+03	-17.45%	-11.79%	-9.70%
44	4.00E+02	-24.06%	-24.65%	-24.52%
45	3.92E+03	-17.25%	-10.92%	-8.88%
46	4.00E+02	-23.92%	-24.25%	-24.16%
Cooling Time				
Time Step	Cumulative Time(s)	Activity	Dose rate	Decay heat
47	1.36E-01	-23.68%	-24.17%	-24.06%
48	6.49E+03	-18.11%	-13.92%	-11.62%
49	4.96E+04	-22.56%	-66.14%	-66.17%
50	3.09E+05	-19.65%	-72.51%	-73.45%
51	6.54E+05	-19.00%	-72.00%	-72.91%
52	1.00E+06	-18.62%	-71.61%	-72.54%
53	1.58E+09	-97.69%	-99.99%	-99.59%
54	3.16E+09	-99.31%	-99.32%	-96.55%

Chapter 6

Radiation Response Diagrams

The radiological response of materials in a neutron environment plays a key role in the sustainability of fusion devices. Thus representation and visualization of large sets of complex activation data and related radiological quantities, in an easily understandable format is a requirement for material selection and analysis. For this purpose, a set of new visualization techniques using ECF/ICF formalization are developed. This technique helps to identify parent which would produce isotopes responsible for radiological quantities in the material. Some of the early results of the technique are reported in the article: [105].

In literature, there are already some techniques developed for visualizing inventory data like (a) importance diagrams, which are a neutron spectrum independent representation of the dominant nuclides that contribute more than 50% to the activity of an irradiated material and (b) nuclide maps, which allow the concentrations or activity contributions from all nuclides in the inventory to be displayed and also for the variation to be traced in time under a specific irradiation scenario [88, 89, 106, 107, 108]. These graphs are useful for activation analysis however they provide an incomplete picture for material optimization purposes. The isotopes producing radiological quantities are daughter products of initial parents in the material. These radioisotopes can be produced from many different

parents. Moreover, each parent would also be producing other radioisotopes. This creates a complicated activation tree with branching, loops and cross-linking as discussed in section 2.2.2. Because of this, the evaluation of the exact contribution from parents to dominating isotopes is done via pathway analysis. Hence, for composition optimization first, the radioisotopes contributing most towards any radiological quantity are identified then using complex pathway analysis parents of these radioisotopes are discovered. These parent isotopes are then replaced in the initial material composition with isotopes that are less susceptible to neutron irradiation, ie produce low radioactive or short-lived isotopes. This process is very cumbersome and time-consuming. ECF formulation provides an easy way to identify and eliminate these parent isotopes that are responsible for radiotoxicity in the irradiated material. ECF/ICF gives a direct correlation between the contributing parent and the dominating isotopes, which gives a quick insight into ways to optimize material. The details of the material optimization scheme based on ECF are discussed in sections: 5.2 and 5.1. This implies that a visualization technique using the quantification of radiation response of parent elements/isotopes would give a comprehensive picture of material optimization without doing a cumbersome pathway analysis. Thus, a series of spectrum independent graphs using ECF/ICF is created to give an effect of parent elements/isotopes on various radiological quantities over time and, is named as Radiation Response Diagrams (RRD). Such a graph could be very useful as a first approximation for material design and selection purposes. In this chapter, the construction of RRDs is discussed in section 6.1, and various kinds of RRDs are given in sections 6.1.1, 6.1.2, 6.1.3 and 6.1.4.

6.1 Construction of Radiation Response Diagrams

Radiation Response Diagrams are constructed by performing activation calculations with total neutron flux concentrated at a single group and repeating the calculation for each neutron energy group thus creating a spectrum independent diagram. In the construction

of RRD, instead of plotting dominating isotopes with respect to time, the parents with the highest ECF values are plotted with cooling time. This gives a clear picture of the effect of parents on the radiological quantity and variation of contributing parents with cooling time.

To illustrate the importance and construction of RRD's, as an example, stainless steel (SS316L(N)) is irradiated for 2 years with a maximum flux of $1.0E12\ n/cm^2$ followed by a cooling period of $10^{10}\ s$ (317.09 years) divided into 100 equal intervals. RRD is constructed from results obtained from each activation run for neutron flux of $1.0E12\ n/cm_2$ concentrated at each neutron energy group. A separate PYTHON program is written to construct the RRD. The python program calls ACTYS-1-GO sequentially for activation calculation at each neutron energy group, Vitamin-J energy group is used for this example [49]. For each activation run, parents with the highest EC and ECF values for each radiological quantities are listed and stored in a matrix along with the allowable margin for change in concentration of each element. After all the activation runs, 175 in this case, the entire information, the parents with the highest EC and ECF values at each energy group for all the cooling time steps are used to construct RRDs for every radiological quantity. There are 4 kinds of RRD given in figure 6.1, 6.2, 6.3 and 6.4. The color scheme used for each element in the stainless steel composition is given below:

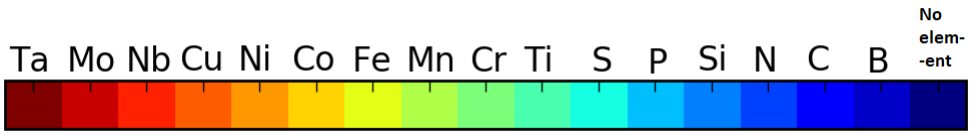

6.1.1 RRD based on Elemental contribution

This RRD, given in figure:6.1, shows parents with the highest elemental contribution (EC) towards activity, contact dose rate, decay heat, and IRAS Index as a function of cooling time. Daughters of these parents would produce maximum radiological quantity at that particular cooling time. If some parent is abundant in the material, this RRD would show would those parents as the major contributor. For example, for almost all the radiological quantities iron(Fe) has the highest EC values, as it is in most abundance in stainless steel composition. In most cases, the most abundant parent might not be producing the most

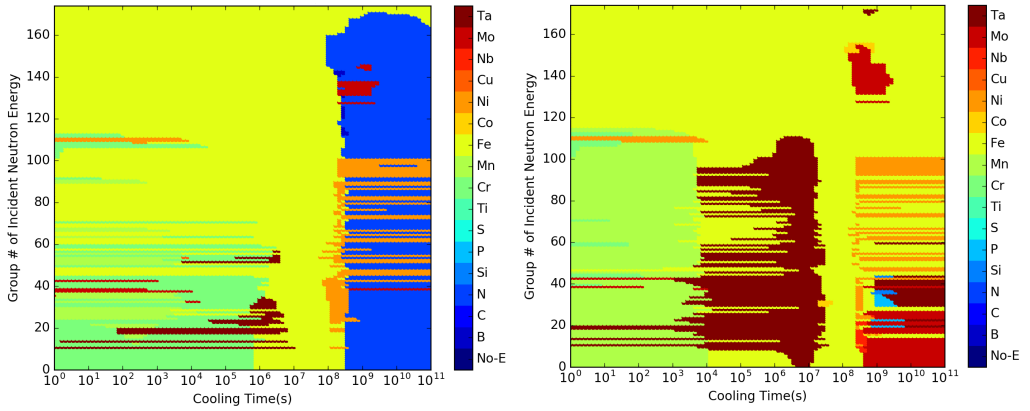

(a) Parents with highest EC values for activity

(b) Parents with highest EC values for dose rate

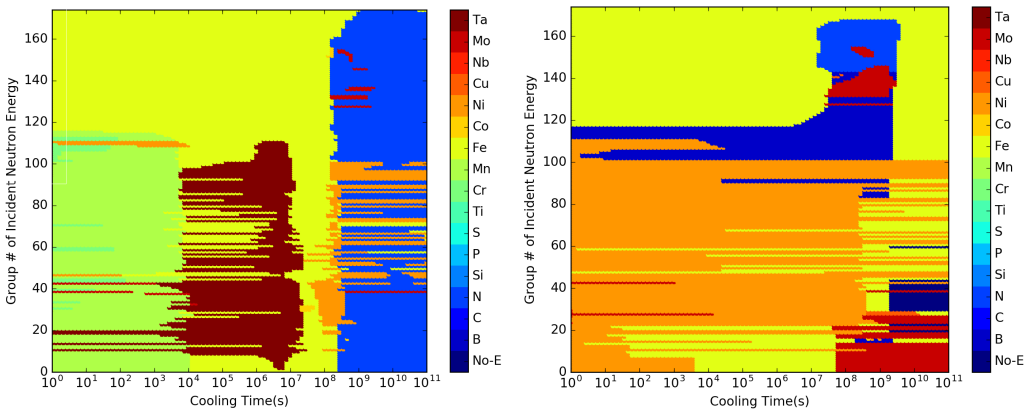

(c) Parents with highest EC values for decay heat

(d) Parents with highest EC values for IRAS Index

Figure 6.1: Variation of parents with highest EC values with cooling time

dangerous elements per weight fraction of the composition. To visualize this we need to plot parents with the highest ECF values.

6.1.2 RRD based on Elemental contribution Factor

The second RRD in figure:6.2 shows parents with the highest ECF as a function of cooling time. ECF is a measure of contribution per gram of a parent element towards the radiological quantity and hence determines the impact of the reduction of the element on the total radiological quantity. In this RRD, for all radiological quantities, it becomes evident that parents present in small amounts are actually contributing more per weight towards any radiological quantities. Hence reducing these elements will be helpful in minimizing the radiological quantity. Parents with the highest ECF may not have the margins to reduce

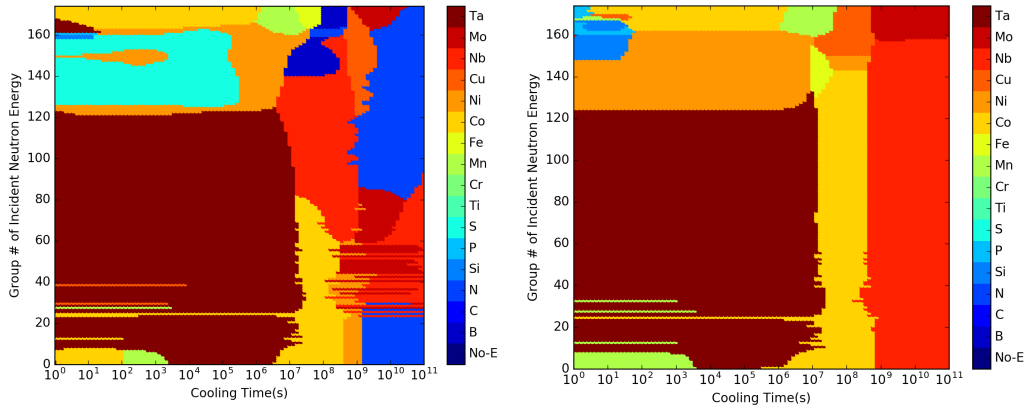

(a) Parents with highest ECF values for activity

(b) Parents with highest ECF values for dose rate

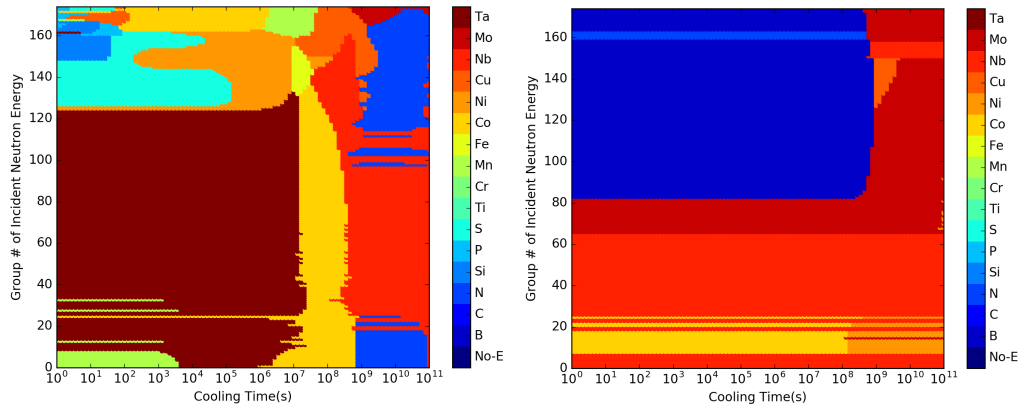

(c) Parents with highest ECF values for decay heat

(d) Parents with highest ECF values for IRAS Index

Figure 6.2: Variation of parents with highest ECF values with cooling time

them. Hence another RRD is required that would give the product of ECF and range for optimization.

6.1.3 RRD based on Elemental contribution Factor and Delta

The third RRD in the figure:6.3 represents the elements with the highest allowable range for tailoring that also have high ECF values.

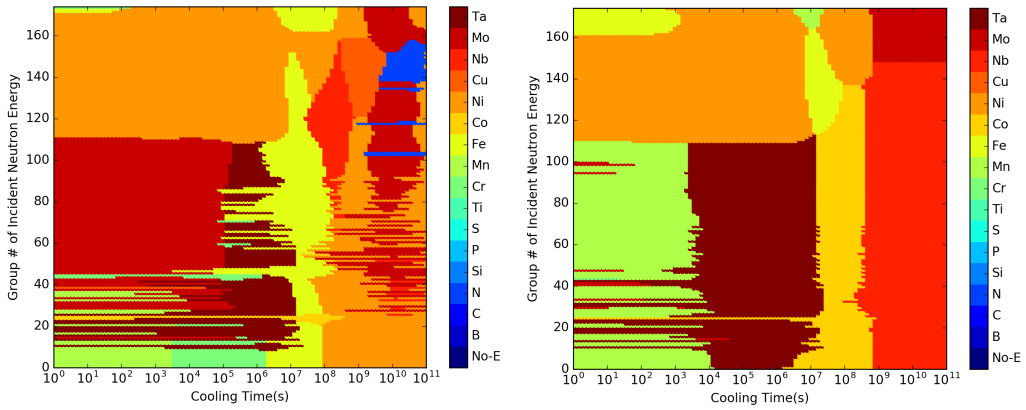

(a) Parents with highest ECF*wf values for activity

(b) Parents with highest ECF*wf values for dose rate

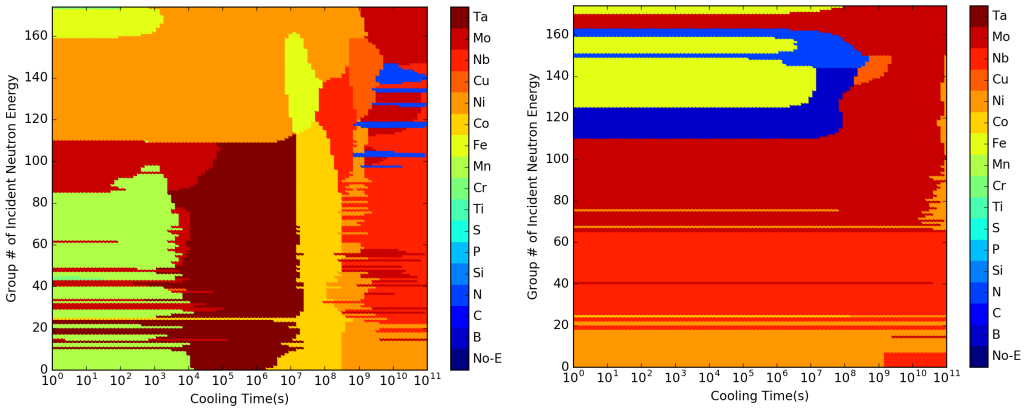

(c) Parents with highest ECF*wf values for decay heat

(d) Parents with highest ECF*wf values for IRAS index

Figure 6.3: Variation of parents with highest ECF*wf values with cooling time

Similar graphs can be generated with IC and ICF to find isotopes whose daughter products would contribute towards radiological quantities. These RRDs can then be used for isotopic tailoring to obtain low activation material. Instead of reducing the concentration of element altogether, isotopic enrichment could be used for material optimization using the IC and ICF RRDs.

6.1.4 Spectrum dependent RRD

All the above graphs represent parents with the highest values of EC or ECF. In a realistic scenario, some parents could have EC or ECF very next to each other and thus, minimizing the highest contributor would not make a substantial difference. In such cases, the fourth RRD given in figure:6.4 becomes very important. This plot is spectrum dependent ECF response of each element with respect to cooling time. This irradiation graph thus provides a complete understanding of contributing elements for a specific activation problem.

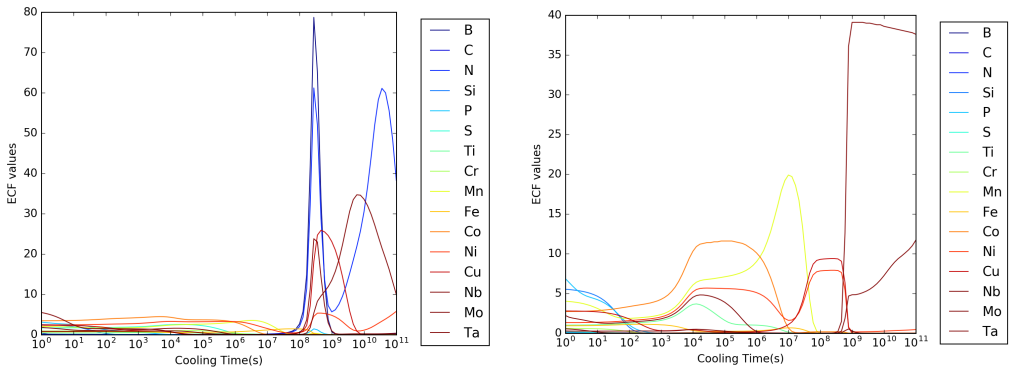

(a) Evolution element's ECF values for activity with cooling time

(b) Evolution element's ECF values for dose rate with cooling time

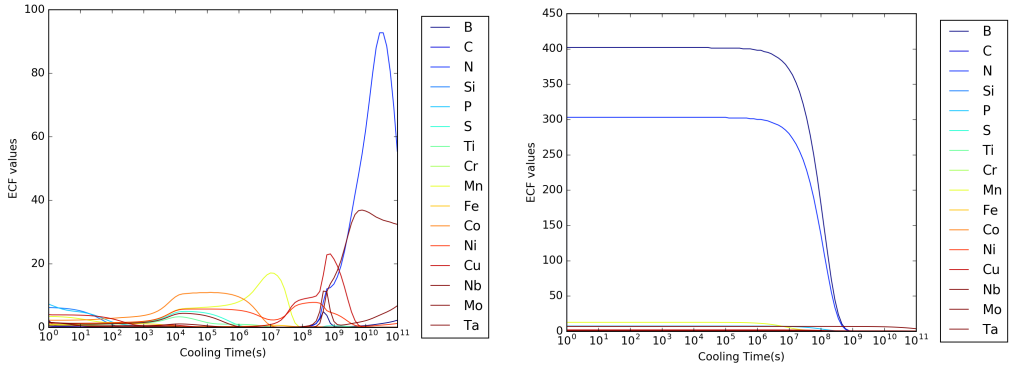

(c) Evolution element's ECF values for decay heat with cooling time

(d) Evolution element's ECF values for IRAS index with cooling time

Figure 6.4: Variation in ECF values of parents with cooling time for delta flux at group 167 or in energy range 13.8 MeV - 14.2 MeV

6.2 Chapter Summary

In this chapter various Radiation Response Diagrams are developed. These diagrams provide key information regarding material optimization. All the four RDDs when viewed in a sequential form, provide information: 1) the elements contributing most to the radiological quantity, 2) the elements whose reduction would affect the overall radiological quantity, 3) the elements which would affect the radiological quantity the most and have the most flexibility in the reduction of their concentration and 4) how each element contributes to the dose over cooling periods, for a specific spectrum. The four graphs together can provide an enhanced knowledge of how each parent (elements/isotopes) behave in a neutron environment and how they contribute to the radiological responses of the material. The contents of this chapter are published in article ***Nucl Fusion* 2018;58(12)**.

APPENDIX-A

Derivation of chain solution for Bateman Equation

The Bateman equation can be derived from the radioactive decay law in the following manner. For a radioactive isotope, **A** with initial concentration $N_A(0)$ decaying to isotope **B** with decay constant λ_{AB} and initial concentration $N_B(0) = 0.0$, the Bateman equation is given as:

$$\frac{dA}{dt} = -\lambda_{AB}A \tag{7.1}$$

The solution of the above equation is :

$$N_A(t) = e^{-\lambda_{AB}t}N_A(0) \tag{7.2}$$

Likewise, if isotope **B** is also radioactive and would decay into isotope **C**, with decay constant λ_{BC} and initial concentration $N_C(0) = 0.0$, the rate of decay of isotope **B** will be given as:

$$\frac{dB}{dt} = \lambda_{AB}A - \lambda_{BC}B \tag{7.3}$$

The concentration of isotope B as a function of time can be written as:

$$N_B(t) = \lambda_{AB}N_A(0)\left[\frac{e-\lambda_{AB}t}{\lambda_{BC}-\lambda_{AB}} + \frac{e-\lambda_{BC}t}{\lambda_{AB}-\lambda_{BC}}\right] \tag{7.4}$$

Hence for a chain of 'n' isotopes the rate equation of each isotope 'i' can be written as:

$$\frac{dN_i}{dt} = \lambda_{i-1} N_{k-1} - \lambda_i N_i \tag{7.5}$$

where, λ_i is the decay constant of the i^{th} nuclide, and N_i is the number of atoms of isotope at time 't', with the assumption that $N_i(0) = 0.0$. Now, the concentration of n^{th} isotope can be written as:

$$N_n(t) = \frac{N_1(0)}{\lambda_n} \sum_{i=1}^{n} \lambda_i \alpha_i exp[-\lambda_i t] \tag{7.6}$$

where

$$\alpha_i = \prod_{j=1, j\neq i}^{n} \frac{\lambda_j}{(\lambda_j - \lambda_i)} \tag{7.7}$$

The equation 7.6 can be arranged in a recursive algorithm and is used to calculate the isotopic inventory at any time 't' for a given neutron spectrum. To accommodate the neutron-induced reactions $\sigma_i j * \phi$ is added to the decay constant λ_i. ACTYS solves this equation based on the analytical linear chain solution method forming progressively growing linear continuous-time Markov chains starting from each parent nuclide and solving them as they grow in length with careful checks for termination. It follows that each parent and its subsequent linear chain development is completely independent of other parent nuclides in the material. This is a direct outcome due to the inherent property of a nuclide's decay and transmutation in nature. Special routines are written in the program to take care of loop formation, chain termination, and chain weighing. The details of the chain solving algorithm and various chain termination techniques can be found in the article [48].

Bibliography

[1] A. D. Pasternak, "Global energy futures and human development: A framework for analysis," Lawrence Livermore National Laboratory, Tech. Rep., 2000, uCRL-ID-140773. [Online]. Available: https://e-reports-ext.llnl.gov/pdf/239193.pdf

[2] J. P. Freidberg, *Plasma Physics and Fusion Energy*. Cambridge University Press, 2007.

[3] "Eia projects nearly 50% increase in world energy usage by 2050, led by growth in asia," https://www.eia.gov/todayinenergy/detail.php?id=41433.

[4] B. W. Brook, A. Alonso, D. A. Meneley, J. Misak, T. Blees, and J. B. van Erp, "Why nuclear energy is sustainable and has to be part of the energy mix," *Sustainable Materials and Technologies*, vol. 1-2, pp. 8 – 16, 2014. [Online]. Available: http://www.sciencedirect.com/science/article/pii/S2214993714000050

[5] "Report of the working group r&d sector," Eleventh Plan Proposals by Government of India Department of Atomic Energy and Atomic Energy Regulatory Board.

[6] S. Zinkle and G. Was, "Materials challenges in nuclear energy," *Acta Materialia*, vol. 61, no. 3, pp. 735 – 758, 2013, the Diamond Jubilee Issue. [Online]. Available: http://www.sciencedirect.com/science/article/pii/S1359645412007987

[7] P. Kaw and I. Bandyopadhyay, *Fusion Physics, CHAPTER 1: THE CASE FOR FUSION*. INTERNATIONAL ATOMIC ENERGY AGENCY, 2012, ch. 1,

pp. 1–58. [Online]. Available: http://www-pub.iaea.org/books/IAEABooks/8879/Fusion-Physics

[8] S. Deshpande and P. Kaw, "Fusion research programme in india," *Sadhana, Indian Academy of Sciences*, vol. 38, no. 5, pp. 839–848, 10 2013. [Online]. Available: https://www.ias.ac.in/article/fulltext/sadh/038/05/0839-0848

[9] J. Ongena and Y. Ogawa, "Nuclear fusion: Status report and future prospects," *Energy Policy*, vol. 96, pp. 770 – 778, 2016. [Online]. Available: http://www.sciencedirect.com/science/article/pii/S0301421516302658

[10] Ongena, J., "Fusion: A true challenge for an enormous reward," *EPJ Web of Conferences*, vol. 98, p. 05004, 2015. [Online]. Available: https://doi.org/10.1051/epjconf/20159805004

[11] S. K. Malhotra, "Establishment of the iter (international thermo-nuclear experimental reactor) international fusion energy organization for the joint implementation of the iter project (21-november-2006)," http://www.dae.in/node/66, 11 2006.

[12] F. Dobran, "Fusion energy conversion in magnetically confined plasma reactors," *Progress in Nuclear Energy*, vol. 60, pp. 89 – 116, 2012. [Online]. Available: http://www.sciencedirect.com/science/article/pii/S0149197012000765

[13] M. Gilbert, S. Dudarev, D. Nguyen-Manh, S. Zheng, L. Packer, and J.-C. Sublet, "Neutron-induced dpa, transmutations, gas production, and helium embrittlement of fusion materials," *Journal of Nuclear Materials*, vol. 442, no. 1âĂŞ3, Supplement 1, pp. S755 – S760, 2013. [Online]. Available: http://www.sciencedirect.com/science/article/pii/S0022311513005886

[14] J. Knaster, A. Moeslang, and T. Muroga, "Materials research for fusion," *Nature Physics*, vol. 12, pp. 424–434, 2016. [Online]. Available: http://dx.doi.org/10.1038/nphys3735

[15] M. J. Loughlin, P. Batistoni, C. Konno, U. Fischer, H. Iida, L. Petrizzi, E. Polunovskiy, M. Sawan, P. Wilson, and Y. Wu, "Iter nuclear analysis strategy and requirements," *Fusion Science and Technology*, vol. 56, no. 2, pp. 566–572, 2009.

[16] L. EL-Guebaly, L. Mynsberge, C. Martin, D. Henderson, and A.-A. Team, "Activation and environmental aspects of aries-act1 power plant," *Fusion Science and Technology*, vol. 67, no. 1, pp. 179–192, 2015.

[17] G. Butterworth and L. Giancarli, "Some radiological limitations on the compositions of low-activation materials for power reactors," *Journal of Nuclear Materials*, vol. 155-157, pp. 575 – 580, 1988. [Online]. Available: http://www.sciencedirect.com/science/article/pii/0022311588903741

[18] K. Nordlund, S. J. Zinkle, A. E. Sand, F. Granberg, R. S. Averback, R. E. Stoller, T. Suzudo, L. Malerba, F. Banhart, W. J. Weber, F. Willaime, S. L. Dudarev, and D. Simeone, "Primary radiation damage: A review of current understanding and models," *Journal of Nuclear Materials*, vol. 512, pp. 450 – 479, 2018. [Online]. Available: http://www.sciencedirect.com/science/article/pii/S002231151831016X

[19] S. J. Zinkle, "Fusion materials science: Overview of challenges and recent progress," *Physics of Plasmas*, vol. 12, no. 5, p. 058101, 2005. [Online]. Available: https://doi.org/10.1063/1.1880013

[20] U. Fischer, "Computational methods, tools, and data for nuclear analyses of fusion technology systems," in *International Conference Nuclear Energy for New Europe*. Association FZK-Euratom, Forschungszentrum Karlsruhe Hermann-von-Helmholtz-Platz 1, D- 76344 Eggenstein-Leopoldshafen, Germany: Nuclear Society of Slovenia, 9 2006.

[21] E. Cheng, R. Forrest, and A. Pashchenko, "Report on the second international activation calculation benchmark comparision study," International Atomic Energy

Agency, IAEA Nuclear Data Section, Wagramerstrasse 5, A-1400 Vienna, Tech. Rep., 2 1994.

[22] J. E. Martin, *Physics for Radiation Protection*. Wiley-VCH, 4 2013.

[23] W. M. Stacey, *Nuclear Reactor Physics*. Wiley-YCH, 6 2007.

[24] T. Hamacher, R. Korhonen, K. Aquilonius, H. Cabal, B. Hallberg, Y. LechÃşn, S. Lepicard, R. SÃąez, T. Schneider, and D. Ward, "Radiological impact of an intense fusion economy," *Fusion Engineering and Design*, vol. 58-59, pp. 1037 – 1042, 2001. [Online]. Available: http://www.sciencedirect.com/science/article/pii/S0920379601005440

[25] D. Keefe, "Inertial confinement fusion," *Annual Review of Nuclear and Particle Science*, vol. 32, no. 1, pp. 391–441, 1982. [Online]. Available: https://doi.org/10.1146/annurev.ns.32.120182.002135

[26] Y. Xu, "A general comparison between tokamak and stellarator plasmas," *Matter and Radiation at Extremes*, vol. 1, no. 4, pp. 192 – 200, 2016. [Online]. Available: http://www.sciencedirect.com/science/article/pii/S2468080X16300322

[27] P. Helander, C. D. Beidler, T. M. Bird, M. Drevlak, Y. Feng, R. Hatzky, F. Jenko, R. Kleiber, J. H. E. Proll, Y. Turkin, and P. Xanthopoulos, "Stellarator and tokamak plasmas: a comparison," *Plasma Physics and Controlled Fusion*, vol. 54, no. 12, p. 124009, 2012. [Online]. Available: http://stacks.iop.org/0741-3335/54/i=12/a=124009

[28] "Iter: The way to new energy," https://www.iter.org/mach.

[29] V. Shafranov, "Stellarators," *Nuclear Fusion*, vol. 20, no. 9, p. 1075, 1980. [Online]. Available: http://stacks.iop.org/0029-5515/20/i=9/a=005

[30] Y. Shimomura, R. Aymar, V. Chuyanov, M. Huguet, R. Parker, and I. J. C. Team, "ITER overview," *Nuclear Fusion*, vol. 39, no. 9Y, pp. 1295–1308, sep 1999. [Online]. Available: https://doi.org/10.1088%2F0029-5515%2F39%2F9y%2F307

[31] G. Federici, C. Bachmann, L. Barucca, W. Biel, L. Boccaccini, R. Brown, C. Bustreo, S. Ciattaglia, F. Cismondi, M. Coleman, V. Corato, C. Day, E. Diegele, U. Fischer, T. Franke, C. Gliss, A. Ibarra, R. Kembleton, A. Loving, F. Maviglia, B. Meszaros, G. Pintsuk, N. Taylor, M. Tran, C. Vorpahl, R. Wenninger, and J. You, "Demo design activity in europe: Progress and updates," *Fusion Engineering and Design*, vol. 136, pp. 729 – 741, 2018, special Issue: Proceedings of the 13th International Symposium on Fusion Nuclear Technology (ISFNT-13). [Online]. Available: http://www.sciencedirect.com/science/article/pii/S0920379618302898

[32] G. Federici, W. Biel, M. Gilbert, R. Kemp, N. Taylor, and R. Wenninger, "European DEMO design strategy and consequences for materials," *Nuclear Fusion*, vol. 57, no. 9, p. 092002, jun 2017. [Online]. Available: https://doi.org/10.1088%2F1741-4326%2F57%2F9%2F092002

[33] S. J. Zinkle, "Advanced materials for fusion technology," *Fusion Engineering and Design*, vol. 74, no. 1, pp. 31 – 40, 2005, proceedings of the 23rd Symposium of Fusion Technology. [Online]. Available: http://www.sciencedirect.com/science/article/pii/S0920379605004060

[34] L. A. El-Guebaly, A. Team, and F. Team, "Nuclear assessment to support aries power plants and next-step facilities: Emerging challenges and lessons learned," *Fusion Science and Technology*, vol. 74, no. 4, pp. 340–369, 2018. [Online]. Available: https://doi.org/10.1080/15361055.2018.1494946

[35] T. Allen, J. Busby, M. Meyer, and D. Petti, "Materials challenges for nuclear systems," *Materials Today*, vol. 13, no. 12, pp. 14 – 23, 2010. [Online]. Available: http://www.sciencedirect.com/science/article/pii/S1369702110702200

[36] A. Ciampichetti, P. Rocco, and M. Zucchetti, "Accidental and long-term safety assessment of fission and fusion power reactors," *Fusion Engineering and Design*, vol. 63âĂŞ64, pp. 229 – 234, 2002. [Online]. Available: http://www.sciencedirect.com/science/article/pii/S0920379602002442

[37] S. J. Zinkle and J. T. Busby, "Structural materials for fission and fusion energy," *Materials Today*, vol. 12, no. 11, pp. 12 – 19, 2009. [Online]. Available: http://www.sciencedirect.com/science/article/pii/S1369702109702949

[38] P. V. Subhash, G. Indauliya, S. C. Tadepalli, P. Kanth, S. Jakhar, S. Varshney, S. Kumar, R. Krishna, N. Bhaliya, S. Mishra, P. Shrishail, and V. Kumar, "Activation and radioactive waste analysis for survey x-ray crystal spectrometer of iter," *Fusion Science and Technology*, vol. 71, no. 2, pp. 215–224, 2017.

[39] B. Colling, T. Eade, M. J. Joyce, R. Pampin, F. Seyvet, A. Turner, and V. Udintsev, "Neutronics analysis for integration of iter diagnostics port ep10," *Fusion Engineering and Design*, vol. 109 - 111, Part B, pp. 1109 – 1113, 2016, proceedings of the 12th International Symposium on Fusion Nuclear Technology-12 (ISFNT-12). [Online]. Available: http://www.sciencedirect.com/science/article/pii/S0920379616300126

[40] L. Greenwood, "Neutron interactions and atomic recoil spectra," *Journal of Nuclear Materials*, vol. 216, pp. 29 – 44, 1994. [Online]. Available: http://www.sciencedirect.com/science/article/pii/0022311594900043

[41] X.-. M. C. Team, *MCNP - A General Monte Carlo N-Particle Transport Code, Version 5, Volume I: Overview and Theory*, Los Alamos National Laboratory, 4 2003.

[42] *Attila User's Manual*, Transpire, Inc., 6659 Kimball Drive, Suite E-502 Gig Harbor, WA 98335-5142, 5 2012.

[43] T. A. Wareing, J. M. McGhee, J. E. Morel, and S. D. Pautz, "Discontinuous finite element sn methods on three-dimensional unstructured grids," *Nuclear Science and Engineering*, vol. 183, no. 3, pp. 256–268, 2001.

[44] P. V. Subhash, R. Feder, S. Jakhar, S. Thomas, and D. Aggarwal, "Iter related neutronics calculations with attila computer code, invited," *Transactions of the American Nuclear Society*, vol. 109, no. 2, pp. pp–1149, 2013.

[45] H. Bateman, Ed., *Solution of a system of differential equations occurring in the theory of radioactive transformations*, vol. 15. Proceedings of Cambridge Philosophical Society, Mathematics and Physical Sciences, 1910, pages 423-427.

[46] R. A. Forrest, *FISPACT-2007:User manual*, Culham Science Centre, EURATOM/UKAEA Fusion Association, Culham Science Centre, Abingdon, Oxfordshire OX14 3DB, UK, 3 2007.

[47] J. Cetnar, "General solution of bateman equations for nuclear transmutations," *Annals of Nuclear Energy*, vol. 33, no. 7, pp. 640 – 645, 2006. [Online]. Available: http://www.sciencedirect.com/science/article/pii/S0306454906000284

[48] S. C. Tadepalli, P. Kanth, G. Indauliya, I. Saikia, S. P. Deshpande, and P. V. Subhash, "Development and validation of actys, an activation analysis code," *Annals of Nuclear Energy*, vol. 107C, pp. 71–81, 2017.

[49] H. WIENKE, "A study into the reliability of collapsing sand-ii 640 multigroup data into vitamin-j 175 multigroup cross section," International Atomic Energy Agency, IAEA Nuclear Data Section, Wagramerstrasse 5, A-1400 Vienna, Tech. Rep., 7 1995.

[50] M. Pusa and J. Leppanen, "Computing the matrix exponential in burnup calculations," *Nuclear Science and Engineering*, vol. 164, no. 2, pp. 140–150, 2010.

[51] M. Wagner and HLVonach, Eds., *Neutron Activtaion cross section for fission and fusion energy applications*. ARCONNE NATIONAL LABORATORY and OECD NUCLEAR ENERGY AGENCY, 9 1989.

[52] C. Moler and C. V. Loan, "Nineteen dubious ways to compute the exponential of a matrix, twenty-five years later," *SIAM Review*, vol. 45, no. 1, pp. 3–49, 2003. [Online]. Available: http://dx.doi.org/10.1137/S00361445024180

[53] A. G. Croff, *ORIGEN2-A Revised and Updated Version of the Oak Ridge Isotope Generation and Depletion Code*, Oak Ridge National Laboratory, ORNL, Oak Ridge, Tennessee, 7 1980.

[54] P. P. Wilson, "Alara: Analytic and laplacian adaptive radioactive analysis," Ph.D. dissertation, University of Wisconsin, Fusion Technology Institute, University of Wisconsin, Madison Wisconsin, 4 1999.

[55] J. Zhang, Y. Ma, Y. Peng, and Y. Chen, "Aburn: A material activation calculation code based on cram method," *Fusion Engineering and Design*, vol. 125, pp. 659 – 663, 2017. [Online]. Available: http://www.sciencedirect.com/science/article/pii/S0920379617305331

[56] M. Pusa and J. LeppÃd'nen, "Computing the matrix exponential in burnup calculations," *Nuclear Science and Engineering*, vol. 164, no. 2, pp. 140–150, 2010. [Online]. Available: https://doi.org/10.13182/NSE09-14

[57] P. P. Wilson and D. L. Henderson, "Alara: Analytic and laplacian adaptive radioactivity analysis. a complete package for analysis of induced activation volume i technical manual," Fusion Technology Institute, University of Wisconsin, Tech. Rep., 1 1998.

[58] J.-C. Sublet, J. Eastwood, J. Morgan, M. Gilbert, M. Fleming, and W. Arter, "Fispact-ii: An advanced simulation system for activation, transmutation

and material modelling," *Nuclear Data Sheets*, vol. 139, pp. 77 – 137, 2017, special Issue on Nuclear Reaction Data. [Online]. Available: http://www.sciencedirect.com/science/article/pii/S0090375217300029

[59] A. Davis and R. Pampin, "Benchmarking the mcr2s system for high-resolution activation dose analysis in iter," *Fusion Engineering and Design*, vol. 85, no. 1, pp. 87 – 92, 2010. [Online]. Available: http://www.sciencedirect.com/science/article/pii/S0920379609002518

[60] S. Rosanvallon, D. Torcy, J. Chon, and A. Dammann, "Waste management plans for iter," *Fusion Engineering and Design*, vol. 109-111, pp. 1442 – 1446, 2016, proceedings of the 12th International Symposium on Fusion Nuclear Technology-12 (ISFNT-12). [Online]. Available: http://www.sciencedirect.com/science/article/pii/S0920379615303860

[61] M. Zucchetti, L. D. Pace, L. El-Guebaly, B. N. Kolbasov, V. Massaut, R. Pampin, and P. Wilson, "The back end of the fusion materials cycle," *Fusion Science and Technology*, vol. 55, no. 2, pp. 109–139, 2009. [Online]. Available: https://doi.org/10.13182/FST09-12

[62] U. Fischer, M. Angelone, M. Avrigeanu, V. Avrigeanu, C. Bachmann, N. Dzysiuk, M. Fleming, A. Konobeev, I. Kodeli, A. Koning, H. Leeb, D. Leichtle, F. Ogando, P. Pereslavtsev, D. Rochman, P. Sauvan, and S. Simakov, "The role of nuclear data for fusion nuclear technology," *Fusion Engineering and Design*, vol. 136, pp. 162 – 167, 2018, special Issue: Proceedings of the 13th International Symposium on Fusion Nuclear Technology (ISFNT-13). [Online]. Available: http://www.sciencedirect.com/science/article/pii/S0920379618300541

[63] H. Lemmel, "Nuclear data for science & technology: Centres for development," International Atomic Energy Agency (IAEA), Tech. Rep., 1996, june 1996

IAEA Bulletin. [Online]. Available: https://www.iaea.org/sites/default/files/38205383438.pdf

[64] M. of the Cross Sections Evaluation Working Group, *ENDF-6 Formats Manual Data Formats and Procedures for the Evaluated Nuclear Data File ENDF/B-VI and ENDF/B-VII*, Brookhaven National Laboratory, 6 2009.

[65] "Evaluated nuclear data library descriptions," https://www.oecd-nea.org/dbdata/data/ndsevallibs.htm.

[66] M. A. Kellett, O. Bersillon, and R. W. Mills, "The jeff-3.1/-3.1.1 radioactive decay data and fission yields sub-libraries," NUCLEAR ENERGY AGENCY, Tech. Rep., 2009, iSBN 978-92-64-99087-6. [Online]. Available: http://www.oecd-nea.org/dbdata/nds_jefreports/

[67] R. G. Jaeger, *Engineering Compendium on Radiation Shielding*. Springer-Verlag Berlin Heidelberg, 1968.

[68] H. Allen, "Iter tfa radwaste management plan," iter, Tech. Rep., 6 2014, iTER D AUBYHS v1.1.

[69] R. Pampin, A. Davis, J. Izquierdo, D. Leichtle, M. Loughlin, J. Sanz, A. Turner, R. Villari, and P. Wilson, "Developments and needs in nuclear analysis of fusion technology," *Fusion Engineering and Design*, vol. 88, no. 6âĂŞ8, pp. 454 – 460, 2013, proceedings of the 27th Symposium On Fusion Technology (SOFT-27); Liege, Belgium, September 24-28, 2012. [Online]. Available: http://www.sciencedirect.com/science/article/pii/S0920379613003438

[70] P. W. Humrickhouse and B. J. Merrill, "Aries-act1 safety design and analysis," *Fusion Science and Technology*, vol. 67, no. 1, pp. 167–178, 2015.

[71] R. Pampin, S. Zheng, S. Lilley, B. Na, M. Loughlin, and N. Taylor, "Activation analyses updating the iter radioactive waste assessment," *Fusion Engineering*

and Design, vol. 87, no. 7âĂŞ8, pp. 1230 – 1234, 2012, tenth International Symposium on Fusion Nuclear Technology (ISFNT-10). [Online]. Available: http://www.sciencedirect.com/science/article/pii/S0920379612001846

[72] R. Pampin, "Update of iter radioactive waste analysis: Activation and waste classification final report," iter, Tech. Rep., 6 2012, (ITER D 656CRV v2.0).

[73] M. E. Sawan, "Fendl activation benchmark: Specifications for calculation for the calculation activtaion benchmark," International Atomic Energy Agency, IAEA Nuclear Data Section, Wagramerstrasse 5, A-1400 Vienna, Tech. Rep., 12 1994.

[74] "Fendl-2 benchmarks sublibrary," https://www-nds.iaea.org/fendl2/validation/benchmarks/wisconsin/.

[75] M. Loughlin, "Conclusion of shutdown dose rate benchmark study," ITER, 6th ITER Neutronics Meeting,Hefei, China, Tech. Rep., 2011, june 17-24.

[76] Y. Chen and U. Fischer, "Rigorous mcnp based shutdown dose rate calculations: computational scheme, verification calculations and application to iter," *Fusion Engineering and Design*, vol. 63 - 64, pp. 107 – 114, 2002. [Online]. Available: http://www.sciencedirect.com/science/article/pii/S0920379602001448

[77] S. Lilley, T. Eade, and F. Fox, "Iter nbi nuclear analysis phase 2 deliverable 5: Final report," iter, Tech. Rep., 1 2015, (ITER D Q73NR8 v1.0).

[78] J. Knaster, A. Moeslang, and T. Muroga, "Materials research for fusion," *Nat Phys*, vol. 12, no. 5, pp. 424–434, nature Publishing Group. [Online]. Available: http://dx.doi.org/10.1038/nphys3735

[79] J. P. Catalan, P. Sauvan, and J. Sanz, "Shutdown dose rate assessment for a dcll blanket-based reactor: Application of the r2s-uned approach," *Fusion Engineering and Design*, vol. 88, no. 9, pp. 2088 – 2091, 2013, proceedings of the 27th Symposium On Fusion Technology (SOFT-27); LiÃĺge, Belgium, September

24-28, 2012. [Online]. Available: http://www.sciencedirect.com/science/article/pii/S0920379613003918

[80] M. Majerle, D. Leichtle, U. Fischer, and A. Serikov, "Verification and validation of the r2smesh approach for the calculation of high resolution shutdown dose rate distributions," *Fusion Engineering and Design*, vol. 87, no. 5, pp. 443 – 447, 2012, tenth International Symposium on Fusion Nuclear Technology (ISFNT-10). [Online]. Available: http://www.sciencedirect.com/science/article/pii/S0920379611006417

[81] I. Palermo, R. Villari, and A. Ibarra, "Shutdown dose rate assessment with the advanced d1s method for the european dcll demo," *Fusion Engineering and Design*, 2017. [Online]. Available: http://www.sciencedirect.com/science/article/pii/S0920379617307986

[82] P. Kanth, S. C. Tadepalli, R. Srinivasan, and P. Subhash, "Actys-1-go: A faster and accurate algorithm for multipoint nuclear activation calculations," *Fusion Engineering and Design*, vol. 122, pp. 154 – 162, 2017. [Online]. Available: http://www.sciencedirect.com/science/article/pii/S0920379617307998

[83] P. Sauvan, J. P. Catalan, F. Ogando, R. Juarez, and J. Sanz, "Development of the r2suned code system for shutdown dose rate calculations," *IEEE Transactions on Nuclear Science*, vol. 63, no. 1, pp. 375–384, Feb 2016.

[84] A. M. Ibrahim, D. E. Peplow, J. L. Peterson, and R. E. Grove, "Novel hybrid monte carlo/deterministic technique for shutdown dose rate analyses of fusion energy systems," *Fusion Engineering and Design*, vol. 89, no. 9, pp. 1933 – 1938, 2014, proceedings of the 11th International Symposium on Fusion Nuclear Technology-11 (ISFNT-11) Barcelona, Spain, 15-20 September, 2013. [Online]. Available: http://www.sciencedirect.com/science/article/pii/S0920379614001938

[85] A. D. R. PAMPIN, "Novel tools for estimation of activation dose: Description, preliminary comparison and nuclear data requirements," EURATOM/UKAEA Fusion Association, EURATOM/UKAEA Fusion Association Culham Science Centre Abingdon Oxfordshire OX14 3DB United Kingdom, Tech. Rep. 549, 7 2008, uKAEA FUS 549.

[86] G. Butterworth, "Objectives and prospects for low-activation materials," *Journal of Nuclear Materials*, vol. 179-181, pp. 135 – 142, 1991. [Online]. Available: http://www.sciencedirect.com/science/article/pii/0022311591900286

[87] K. Ehrlich, E. Bloom, and T. Kondo, "International strategy for fusion materials development," *Journal of Nuclear Materials*, vol. 283-287, pp. 79 – 88, 2000, 9th Int. Conf. on Fusion Reactor Materials. [Online]. Available: http://www.sciencedirect.com/science/article/pii/S0022311500001021

[88] Gilbert, Mark R., Fleming, Michael, and Sublet, Jean-Christophe, "Inventory simulation tools: Separating nuclide contributions to radiological quantities," *EPJ Web Conf.*, vol. 146, p. 09017, 2017. [Online]. Available: https://doi.org/10.1051/epjconf/201714609017

[89] M. Gilbert, S. Dudarev, S. Zheng, L. Packer, and J.-C. Sublet, "An integrated model for materials in a fusion power plant: transmutation, gas production, and helium embrittlement under neutron irradiation," *Nuclear Fusion*, vol. 52, no. 8, p. 083019, 2012. [Online]. Available: http://stacks.iop.org/0029-5515/52/i=8/a=083019

[90] T. Noda, M. Fujita, and M. Okada, "Transmutation and induced radioactivity of w in the armor and first wall of fusion reactors," *Journal of Nuclear Materials*, vol. 258-263, pp. 934 – 939, 1998. [Online]. Available: http://www.sciencedirect.com/science/article/pii/S0022311598000889

[91] T. Tanno, A. Hasegawa, J. He, M. Fujiwara, M. Satou, S. Nogami, K. Abe, and T. Shishido, "Effects of transmutation elements on the microstructural evolution

and electrical resistivity of neutron-irradiated tungsten," *Journal of Nuclear Materials*, vol. 386-388, pp. 218 – 221, 2009, fusion Reactor Materials. [Online]. Available: http://www.sciencedirect.com/science/article/pii/S0022311508008453

[92] A. Moslang, E. Diegele, M. Klimiankou, R. LÃd'sser, R. Lindau, E. Lucon, E. Materna-Morris, C. Petersen, R. Pippan, J. Rensman, M. Rieth, B. van der Schaaf, H.-C. Schneider, and F. Tavassoli, "Towards reduced activation structural materials data for fusion demo reactors," *Nuclear Fusion*, vol. 45, no. 7, p. 649, 2005. [Online]. Available: http://stacks.iop.org/0029-5515/45/i=7/a=013

[93] M. Gilbert and J.-C. Sublet, "Neutron-induced transmutation effects in w and w-alloys in a fusion environment," *Nuclear Fusion*, vol. 51, no. 4, p. 043005, 2011. [Online]. Available: http://stacks.iop.org/0029-5515/51/i=4/a=043005

[94] M. E. Sawan, "Transmutation of tungsten in fusion and fission nuclear environments," *Fusion Science and Technology*, vol. 66, no. 1, pp. 272–277, 2014. [Online]. Available: https://doi.org/10.13182/FST13-717

[95] L. Morgan, J. Shimwell, and M. Gilbert, "Isotopically enriched structural materials in nuclear devices," *Fusion Engineering and Design*, vol. 90, pp. 79 – 87, 2015. [Online]. Available: http://www.sciencedirect.com/science/article/pii/S0920379614006395

[96] R. Kurtz, A. Alamo, E. Lucon, Q. Huang, S. Jitsukawa, A. Kimura, R. Klueh, G. Odette, C. Petersen, M. Sokolov, P. Spatig, and J.-W. Rensman, "Recent progress toward development of reduced activation ferritic/martensitic steels for fusion structural applications," *Journal of Nuclear Materials*, vol. 386-388, pp. 411 – 417, 2009, fusion Reactor Materials. [Online]. Available: http://www.sciencedirect.com/science/article/pii/S002231150800891X

[97] P. Hosemann, D. Frazer, M. Fratoni, A. Bolind, and M. Ashby, "Materials selection for nuclear applications: Challenges and opportunities," *Scripta*

Materialia, vol. 143, pp. 181 – 187, 2018. [Online]. Available: http://www.sciencedirect.com/science/article/pii/S1359646217302038

[98] S. C. Tadepalli, P. Kanth, and P. V. Subhash, "Parent isotopic and elemental contributing factors to minimize nuclear radiological responses and optimize material composition," *Nuclear Science and Engineering*, vol. 188, no. 03, pp. 282–293, 2017. [Online]. Available: http://www.tandfonline.com/doi/abs/10.1080/00295639.2017.1367570

[99] H. Tanigawa, E. Gaganidze, T. Hirose, M. Ando, S. Zinkle, R. Lindau, and E. Diegele, "Development of benchmark reduced activation ferritic/martensitic steels for fusion energy applications," *Nuclear Fusion*, vol. 57, no. 9, p. 092004, 2017. [Online]. Available: http://stacks.iop.org/0029-5515/57/i=9/a=092004

[100] D. Harries, G. Butterworth, A. Hishinuma, and F. Wiffen, "Evaluation of reduced-activation options for fusion materials development," *Journal of Nuclear Materials*, vol. 191-194, pp. 92 – 99, 1992, fusion Reactor Materials Part A. [Online]. Available: http://www.sciencedirect.com/science/article/pii/S0022311509800159

[101] A. Kohyama, A. Hishinuma, D. Gelles, R. Klueh, W. Dietz, and K. Ehrlich, "Low-activation ferritic and martensitic steels for fusion application," *Journal of Nuclear Materials*, vol. 233-237, pp. 138 – 147, 1996. [Online]. Available: http://www.sciencedirect.com/science/article/pii/S0022311596003273

[102] P. Kanth and P. V. Subhash, "Actys-asg, tool for coupling actys-1-go with attila," *Fusion Engineering and Design*, vol. 129, pp. 196 – 201, 2018. [Online]. Available: http://www.sciencedirect.com/science/article/pii/S0920379618302011

[103] Q. Huang, N. Baluc, Y. Dai, S. Jitsukawa, A. Kimura, J. Konys, R. Kurtz, R. Lindau, T. Muroga, G. Odette, B. Raj, R. Stoller, L. Tan, H. Tanigawa, A.-A. Tavassoli, T. Yamamoto, F. Wan, and Y. Wu, "Recent progress of r&d activities on reduced activation ferritic/martensitic steels," *Journal of Nuclear Materials*, vol.

442, no. 1, Supplement 1, pp. S2 – S8, 2013, fIFTEENTH INTERNATIONAL CONFERENCE ON FUSION REACTOR MATERIALS. [Online]. Available: http://www.sciencedirect.com/science/article/pii/S0022311512006964

[104] R. Klueh and A. Nelson, "Ferritic/martensitic steels for next-generation reactors," *Journal of Nuclear Materials*, vol. 371, no. 1, pp. 37 – 52, 2007, nuclear Fuels and Structural Materials 1. [Online]. Available: http://www.sciencedirect.com/science/article/pii/S0022311507007398

[105] P. Kanth, "Visualization technique for nuclear materials using actys," in *DAE Symposium on Nuclear Physics*, vol. 62, 2017, pp. 1042–1043.

[106] R. Forrest, "Importance diagrams - a novel presentation of the response of a material to neutron irradiation," *Fusion Engineering and Design*, vol. 43, no. 2, pp. 209 – 235, 1998. [Online]. Available: http://www.sciencedirect.com/science/article/pii/S0920379698004189

[107] M. Gilbert and R. Forrest, "Comprehensive handbook of activation data calculated using easy-2003," *Fusion Engineering and Design*, vol. 81, no. 8, pp. 1511 – 1516, 2006, proceedings of the Seventh International Symposium on Fusion Nuclear Technology. [Online]. Available: http://www.sciencedirect.com/science/article/pii/S0920379605006915

[108] M. Gilbert, L. Packer, J.-C. Sublet, and R. A. Forrest, "Inventory simulations under neutron irradiation: Visualization techniques as an aid to materials design," *Nuclear Science and Engineering*, vol. 177, pp. 291–306, 07 2014.

[109] S. C. Tadepalli and P. Subhash, "Simplified recursive relations for the derivatives of bateman linear chain solution and their application to sensitivity and multi-point analysis," *Annals of Nuclear Energy*, vol. 121, pp. 479 – 486, 2018. [Online]. Available: http://www.sciencedirect.com/science/article/pii/S030645491830416X

Thesis Highlight

Name of the Student: Priti Kanth

Name of the CI/OCC: Institute for Plasma Research, Gandhinagar

Enrolment No.: ENGG06201504009

Thesis Title: Nuclear Activation Studies in Fusion Systems: New Methods and Algorithms

Discipline: Engineering Sciences **Sub-Area of Discipline**: Nuclear Science

Date of viva voce: 20th August, 2020

In the present thesis, various methods and algorithms are developed to simulate neutron interaction with the material and evaluate the nuclear response of the material in spatially and temporally varying neutron fields. The main works carried out during my Ph.D. are listed below:

1. Development of methods to evaluate radiological quantities like activity, biological dose rate, decay heat, and radwaste classification. It includes extracting data from standard nuclear data libraries, processing the data and creating computational algorithms to evaluate these quantities. These methods are implemented in the code ACTYS and successfully benchmarked against standard benchmarking exercises given by IAEA.
2. To reduce the time of multipoint activation calculation in complex geometries, the concept of Superlist is developed. This captures the essence of an entire material placed at multiple locations and experiencing different neutron spectrums in a small set of isotopes called the superlist. Activation calculation performed on this list alone yields radiological quantities with 99% accuracy in just 1.5% computation time as compared to other conventional methods.
3. This concept of superlist is implemented in code ACTYS-1-GO for performing activation in large and complex fusion reactors. Successful benchmarking of the above formulation is performed using standard benchmarking exercises given by IAEA and with ITER radial buildup model.
4. Developed tool for coupling activation solver with external neutron transport code to evaluate the biological dose rate produced by the decay gammas that are emitted from the activated materials.
5. Various tools are developed to visualize the large amount of data produced during multipoint activation calculation. These plots as given in Figure: 1, help to identify radiation hotspots in the geometry. These plots also show time evolution of radiological within the device.

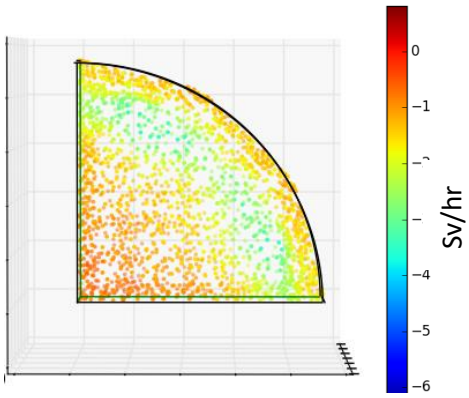

Figure 1: Total contact doserate in log scale at 2085 mesh locations in stainless steel plate

6. Low activation materials are pre-requisite for fusion reactor development. No tools were available in the literature to directly evaluate the best material composition based on nuclear responses of the material. Hence, composition optimization scheme for materials, based on various radiological responses and experiencing a spatial and temporal variation of the neutron spectrum is developed.